**Electrocaloric Properties of PVDF-HFP Composites
for Cooling Systems**

Ahamad Salea

**A Thesis Submitted in Fulfillment of the Requirements for the
Doctor of Philosophy in Physics (International Program)
Prince of Songkla University
2020**

**Electrocaloric Properties of PVDF-HFP Composites
for Cooling Systems**

Ahamad Salea

**A Thesis Submitted in Fulfillment of the Requirements for the
Doctor of Philosophy in Physics (International Program)
Prince of Songkla University
2020**

Thesis Title   Electrocaloric Properties of PVDF-HFP Composites for Cooling Systems
Author   Mr. Ahamad Salea
Major Program   Physics (International Program)

_____

Major Advisor   **Examining Committee :**

....
(Assoc. Prof. Dr. Chatchai Putson)

....Chairperson
(Assoc. Prof. Dr. Chesta Ruttanapun)

....Committee
(Assoc. Prof. Dr. Nantakan Muensit)

....Committee
(Assoc. Prof. Dr. Sumetha Suwanboon)

....Committee
(Asst. Prof. Dr. Paphavee van Dommelen)

....Committee
(Asst. Prof. Dr. Chalongrat Daengngam)

....Committee
(Assoc. Prof. Dr. Chatchai Putson)

        The Graduate School, Prince of Songkla University, has approved this thesis as fulfillment of the requirements for the Doctor of Philosophy Degree in Physics (International Program).

....
(Prof. Dr. Damrongsak Faroongsarng)
Dean of Graduate School

This is to certify that the work here submitted is the result of the candidate's own investigations. Due acknowledgement has been made of any assistance received.

....Signature
(Assoc. Prof. Dr. Chatchai Putson)
Major Advisor

....Signature
(Mr. Ahamad Salea)
Candidate

I hereby certify that this work has not been accepted in substance for any degree, and is not being currently submitted in candidature for any degree.

....Signature
(Mr. Ahamad Salea)
Candidate

ชื่อวิทยานิพนธ์	ศึกษาสมบัติอิเล็คโทรแคลอริคของวัสดุคอมโพสิธพอลิไวนิลิดีฟลูออไรด์
	โคเฮกซะฟลูออโรโพรพิลีนสำหรับระบบทำความเย็น
ผู้เขียน	นายอาหะมัด สาและ
สาขา	ฟิสิกส์
ปีการศึกษา	2562

บทคัดย่อ

เทคโนโลยีทำความเย็นอิเล็คโทรแคลอริคมีความสำคัญในการพัฒนาเทคโนโลยีที่เป็นมิตรกับสิ่งแวดล้อมโดยลดสารซีเอฟซีและเพิ่มประสิทธิภาพความเย็นให้สูงขึ้น   เทคโนโลยีดังกล่าวได้ถูกประยุกต์ใช้ในหลายด้าน เช่น อาหาร เครื่องยนต์ ที่พักอาศัย หรือโรงงานอุตสาหกรรม ปรากฏการณ์อิเล็คโทรแคลอริคเป็นการคายและดูดความร้อนในวัสดุเฟอโรอิเล็คทริคเมื่อมีการเพิ่มหรือลดสนามไฟฟ้าภายนอกตามความสัมพันธ์แมกส์เวลล์   งานวิจัยที่ผ่านมาได้มีรายงานการพัฒนาการณ์ต่อเนื่องในหลายวิธีเพื่อเพิ่มประสิทธิภาพ   งานวิจัยนี้มีวัตถุประสงค์เพื่อลดอุณหภูมิคูรี (Curie temperature) และเพิ่มการเปลี่ยนแปลงอุณหภูมิ (temperature change) บนพอลิเมอร์พอลิไวนิลิดีนฟลูออไรด์โคเฮกซะฟลูออโรโพรพิลีนด้วยวิธีอันตรชั้นเฟสวิศวกรรม   (interfacial phase engineering) เช่น สารตัวเติมอนุภาคนาโน (filler nanocomposites) และเทคนิคการยืดสองแกน (biaxial stretch technique) ผลการศึกษาพบว่าการเพิ่ม ลด และรักษาไว้ของผลึกดั้งเดิม (ordinary crystallization) มีผลต่อการเพิ่มขึ้นของการเปลี่ยนแปลงอุณหภูมิบนพอลิเมอร์   ความแข็งแรงบนอันตรกริยาระหว่างสารตัวเติมและพอลิเมอร์มีผลต่อการลดลงของอุณหภูมิคูรี   ซึ่งขึ้นกับชนิดของสารตัวเติม   ความสัมพันธ์ระดับโครงสร้างวัสดุของการลดอุณหภูมิคูรีและการเพิ่มการเปลี่ยนแปลงอุณหภูมิบนพอลิเมอร์สามารถคาดการณ์ประสิทธิผลของเทคโนโลยีอิเล็คโทรแคลอริคในอนาคต

Thesis Title   Electrocaloric Properties of PVDF-HFP Composites for Cooling Systems

Author   Mr. Ahamad Salea

Major Program   Physics

Academic Year   2019

ABSTRACT

Electrocaloric cooling technologies play an important role in the development of environmentally-friendly technology of zero-CFCs waste gas with greater cooling efficiency. They are applied in several fields such as cooling for meals, automobiles, residences, and industrial environments. The electrocaloric effect is the exothermal and endothermal on ferroelectric material when it was applied/ejected external electric field, according to Maxwell's relation. In the electrocaloric literature, it has spread developed in several approaches. This study is aimed to reduce Curie temperature and enhance temperature change on electrocaloric PVDF-HFP by interfacial phase engineering such as filler nanocomposites and biaxial stretch technique. Three PVDF-HFP behaviors of induced, reduced, and kept the ordinary crystallization, affected temperature change enhancement. The effect of how strong boding interaction on interfacial filler-polymer was noticed on Curie temperature reduction, depending on filler types. The deep-understanding of Curie temperature reduction and temperature change enhancement by tailored microstructure can extrapolate electrocaloric performance for the novel electrocaloric cooling technology in the future.

ACKNOWLEDGEMENTS

CONTENTS

CONTENTS (cont.)

CONTENTS (cont.)

CONTENTS (cont.)

LIST OF TABLES

LIST OF FIGURES

LIST OF ABBREVIATIONS AND SYMBOLS

A Electrode area (m^2)

A_α Absorbance's wavenumber at 767 cm^{-1}

A_β Absorbance's wavenumber at 837 cm^{-1}

ε_0 Dielectric permittivity of free space (8.853 x 10^{-12} F m^{-1})

ε_r Dielectric constant

$\varepsilon_r^{''}$ Dielectric loss

C   Electrical capacity

C_E Heat capacity

d Sample thickness (m)

Dy   Dysposium

DMF   N, N-dimethylformamide

DI water   Deionized water

DSC   Differential Scanning Calorimetry

ΔE   Eelectric Field

EC   Electricaloric

ECE   Electrocaloric effect

Er   Erbium

f Frequency

F(β)   Fraction of β phase

FTIR   Fourier Transform Infrared Spectrophotometer

GPN   Graphene nanoplatelet

LIST OF ABBREVIATIONS AND SYMBOLS (cont.)

GCNs	Graphitic Carbon Nanomaterials
ΔH_m	Melting enthalpy change
ΔH_m^0	The melting enthalpy of 100% crystalline PVDF-HFP (104.6 J g^{-1})
$\emptyset$	The weight fraction of filler
$I_{\beta(20.5)}\big/I_{\alpha(18.3)}$	The crystal β phase ratio
K_α	The α coefficient (6.1×10^4 cm^2 mol^{-1})
K_β	The β coefficient (7.7×10^4 cm^2 mol^{-1})
η	Energy storage efficiency
NST	non-stretching
P_+	positive-dipole
P_-	anti-dipole
P	Polarization
P_r	Remnant polarization
P_{max}	Maximum polarization
ρ	Density
PVDF	Polyvinylidene fluoride
PVDF-HFP	Polyvinylidene fluoride-co-hexafluoropropylene
p	Pyroelectric coefficient
PE loop	Polarization-Electric field loop
ΔQ	Heat transfer
RE	Rare-earth
RT	Room temperature

LIST OF ABBREVIATIONS AND SYMBOLS (cont.)

σ_{ac}	AC electrical conductivity
SEM	Scanning Electron Microscopy
ST	Stretching
ΔS	entropy-change
ΔT	adiabatic temperature-change
T	Temperature
T_m	Melting temperature
T_c	Curie temperature
τ	Torque polarization
TEM	Transmission Electron Microscopy
U_e	Recoverable energy density
U_l	Unrecoverable energy density
X_c	Crystallinity
XRD	X-Ray Diffraction

CHAPTER 1

INTRODUCTION

1.1 Background and Motivation of the Thesis

Novel cooling technologies have to produce a greater energy conversion efficiency with environmentally-friendly and green technology as zero-CFCs waste gas. It can apply for routine cooling of meals, automobiles, residences, or industrial environments, deserving for future growing world energy consumption [1]. The current cooling technology of vapor-compression technology is limiting of energy efficiency improvement. This is an opportunity for alternative technology as non-vapor-compression with greater efficiency and zero-hazardous-gases releasing. Caloric technology is a great candidate, providing advanced efficiency of about 60-70% [2-8] compared with other cooling technologies. Among caloric technologies, electrocaloric is the most suitable research for the commercial market. For examples of limited-space and lighter weight of voltage are included.

The electrocaloric effect is effect producing/absorbing temperature after applied/ejected external electric field, following Maxwell's relation [9]. This effect has changed the dipole moment in ferroelectric material by the electric field (ΔE). Consequently, entropy-change (ΔS) and adiabatic temperature-change (ΔT, ΔQ constant) have occurred following the second law of thermodynamic; $\Delta Q = T\Delta S$. Electrocaloric cycle is explained in **Figure 1** (a). Firstly, dipole moments are rearranged by applying ΔE with decreasing ΔS, resulting in T increase (T+ΔT_{ad}, exothermal material, stage 4 to 1). Afterward, the hotter temperature was released (stage 1 to 2). Secondly, dipole moments are reversed to usual random by ejecting ΔE with

increasing ΔS, resulting in T reduction (T-ΔT_{ad}, endothermal material, stage 2 to 3). Finally, the cooler temperature was consumed (stage 3 to 4).
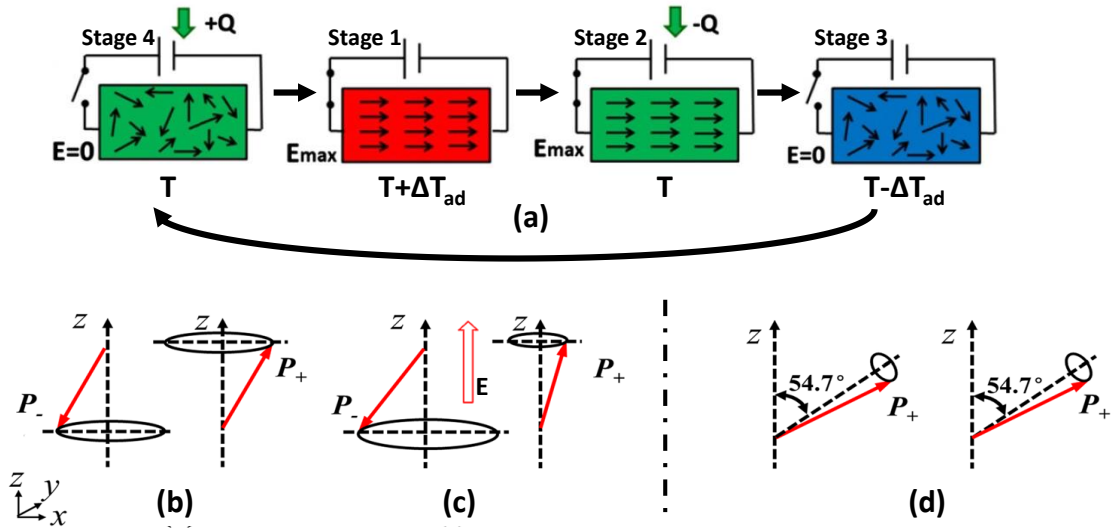
Figure 1 (a) Electrocaloric cycle in ferroelectric materials (adapted from the prior study [10]), negative ECE behavior of AFE phase (a) without E and (b) with E, compared with the normal ferroelectric phase (adapted from the prior studies [11, 12]).

The ferroelectric materials have a large change of dipole moment at the phase transition temperature, and the enormous change is often found at ferroelectric-paraelectric transition or Curie temperature (T_c). The high T_c on many ferroelectric materials has to reduce the nearer room temperature. Moreover, a great ΔT and low applied ΔE are also considering for electrocaloric strength ($\Delta T/\Delta E$) development.

There is negative electrocaloric (negative ECE) that behaved in the opposite of positive electrocaloric (positive ECE), with producing the endothermal before exothermal. According to Geng's theory, the dipole moment direction of negative ECE is opposite pair dipoles as shown in the antiferroelectric phase without E in Figure 1 (b).

This anti-dipole (P_-) tries to rearrange in the same direction with E, by changing to be a wider angle while P_+ changing to be a narrower angle (Figure 1 (c)), compared with normal ferroelectric (Figure 1 (d)). This behavior produces the ΔS enlargement, resulting in adiabatic cooler temperature in beginning. Most of the negative ECE behaved as the asymmetry ferroelectric structure as called antiferroelectric.

The negative ECE was found in anti-ferroelectric materials. For examples of negative ECE materials were $(Pb_{0.88}Sr_{0.08})[Nb_{0.08}(Zr_{0.53}Ti_{0.47})_{0.92}]O_3$ with $\Delta T = -0.38$ K (1.5 MV/m) [13], NBT with $\Delta T = -1.6$ K (7 MV/m) [14], $Pb_{0.97}La_{0.02}(Zr_{0.80}Sn_{0.14}Ti_{0.06})O_3$ with $\Delta T = -5.5$ K (11 MV/m) [15]. For examples of positive ECE materials were $BaTiO_3$ with $\Delta T = 1.6$ K (1 MV/m) [16], $Pb_{0.97}La_{0.02}(Zr_{0.66}Sn_{0.23}Ti_{0.11})O_3$ with $\Delta T = 0.6$ K (30 MV/m) [17], etc.. Those ceramics have some drawbacks of the less flexible, difficulty in fabrication, and high weight, and low electrical breakdown strength. The distinct disadvantage of low electrical breakdown strength on ECE ceramic has limited for producing a great ΔT at high E, excepting PVDF polymer.

Polyvinylidene fluoride (PVDF) is the great ferroelectric polymer with semi-crystalline polymer, discovering the giant ΔT in the years of 2008 [18]. There are Fluorine (F), Hydrogen (H), and Carbon (C) backbone in the units $(-C_2H_2F_2-)_n$. The direction in the opposition between F and H produced a large dipole moment, calling β phase (TTT conformation). PVDF molecules with several phases are polarized by E, providing ΔT respectively. Polyvinylidene fluoride-co-hexafluoropropylene (PVDF-HFP) is one of PVDF copolymer in the units $(-CH_2CF_2-)_x[-CF_2CF(CF_3)-]_y$. which has low cost and more flexibility. There are many techniques for PVDF polarization. For examples of Tailored polarization by electron-beam or gamma irradiation [19-21], self-rearranged polarization by electrospinning [22, 23], rearranged

polarization by poling [24], modified crystal structure by stretching technique at a given temperature [25], are included for polarization improvement. The combination of stretching technique and polymer composite by adding filler are interesting to study.

PVDF molecules are simply polarized when adding a conducting-filler nanocomposite. The research has successfully found that filler-nanocomposite improved not only ΔT enlargement but also T_c reduction effectively. The detailed filler-nanocomposite information is extremely discussed in Chapter 2; related to electrocaloric material literature. For example, Ca doped $BaTi_{0.975}(Nb_{0.5}Yb_{0.5})_{0.025}O_3$ was included [26]. The diffusion of Ca in $BaTi_{0.975}(Nb_{0.5}Yb_{0.5})_{0.025}O_3$ can reconstruct the original phase transition to lower temperature, resulting in T_c reduction. According to a prior study [27], the Rare-earth elements powerfully induced dielectric polarization on PVDF, resulting in great dielectric properties. The stronger interaction of rare-earth filler nanocomposite in PVDF polymer is challenging to further ECE study.

In addition, many researchers have less focused on filler size effect in microstructural PVDF polarization. C. Putson and coworkers studied the effect of filler size on the dielectric polymer.[28] They highlighted that a stronger electrostatic force on a smaller filler size had potentially improved dielectric performance. Besides copper powder, a nanopowder of gold nanoparticles (AuNPs) is interesting in this field. M. Kushwah and colleagues tried to study the effect of AuNPs concentration in PVDF.[29] They found that the increasing concentration improved PVDF chain polymer by electrostatic force, resulting in greater dielectric properties. The synthesis of conductive AuNPs was reported by G. Frens as a well-known citrate reduction procedure.[30] AuNPs have formed in different sizes by the amount of citrate reduction

solution.[31] So far the different sizes of AuNP in PVDF polymer are interesting to study the relationship between dielectric and electrocaloric performances.

1.2 The Purposes of Thesis

In response to the general electrocaloric relationships, the main objectives of this research are as follows:

1) to reduce the Curie temperature of PVDF-HFP.

2) to promote the temperature change of PVDF-HFP.

There are several aims for each paper, follows; two sub-main objectives were accomplished as follows:

The strategy I: different graphene contents with biaxial stretch on ECE PVDF-HFP was studied in Paper I, for improving ΔT by both filler and stretching effects.

Strategy II: different rare-earth contents with two electronegativities on ECE PVDF-HFP was observed in Paper II, for reducing T_c by the advanced filler.

1.3 Thesis Organization

Chapter 1 starts to explain the motivation of this thesis. Some literature reviews are small discussed. The concept of ECE and thermodynamic theory is deeply explained following the highlights in this thesis.

Chapter 2 has the most references because of concentrating on detailed information on the literature review. Most of the review topic covers and relates to this research.

Chapter 3 explains the main materials, preparation, and dielectric and electrocaloric characterizations. All detailed electrical characterizations are explained in this chapter.

Chapter 4 expresses the results and discussion of the ECE effects of PVDF-HFP based on different graphene contents with biaxial stretch. Many contents of this chapter were published in the Journal of Cleaner Production (Appendix A). I added some detailed information and extra discussion to fulfill the content.

Chapter 5 expresses the results and discussion of the ECE effects of PVDF-HFP based on different rare-earth contents with two electronegativities. Many contents of this chapter are revised in the Journal of Materials Science; Materials in Electronics (Appendix B) with major revision. I added some detailed information and extra discussion to fulfill the content.

Chapter 6 summarizes all content in this thesis. It consists of conclusions, limitations, and recommendations for future work.

After Chapter 6, Bibliography was shown, as well as Appendices before finalizing with my updated Vitae.

1.4 Concept of EC and Thermodynamic Theory

The external electric field polarizes dipole moment in ferroelectric material following electric field direction. As a result, entropy change (ΔS) and adiabatic temperature change (ΔT) are increased to hotter material (exothermic), following the second law of thermodynamic

$$\Delta Q = T\Delta S, \qquad (1)$$

After removing the hotter temperature out of the material for a moment, the field is ejected with increasing ΔS of random dipole moment. As a result, ΔT decreases to cooler material (endothermic), as shown in Figure 1.

According to Gibbs free energy (G) equation, dielectric relation is determined as Equation (2),

$$G = U - TS - Xx - ED, \tag{2}$$

and thus,

$$dG = -SdT - xdX - DdE, \tag{3}$$

the derivative of Gibb free energy,

$$S = -\left(\frac{\partial G}{\partial T}\right)_{E,X}, D = -\left(\frac{\partial G}{\partial E}\right)_{X,T}, \tag{4}$$

where U, T, S, X, x, E, and D, are internal energy of the system, temperature, entropy, stress, strain, electric field, and electric displacement, respectively

Because the EC effect is thermodynamically equivalent to the pyroelectric effect, using Maxwell's relation, it is then given by

$$\left(\frac{\partial S}{\partial E}\right)_{T,X} = \left(\frac{\partial D}{\partial T}\right)_{E,X} = p_E, \tag{5}$$

where p_E is the definition pyroelectric coefficient

and thus, using differential equation integration,

$$\Delta S = \int_{E_1}^{E_2} \left(\frac{\partial D}{\partial T}\right)_E dE, \tag{6}$$

where E_1 and E_2 are the initial and final applied electric field, respectively. For heat capacity definition; $C = T(\partial S / \partial T)$, the adiabatic temperature change (ΔT) can describe the EC effect as follow:

$$\Delta T = -\frac{T}{C} \int_{E_1}^{E_2} \left(\frac{\partial D}{\partial T}\right)_E dE, \tag{7}$$

when C independent of E

Besides, Landau's theory widely uses to demonstrate macroscopic phenomena that occur near their phase transition temperature in polar materials e.g. ferroelectric properties including EC materials. Using the general form of the Landau-phenomenological theory

$$G = \frac{1}{2}g_1 D^2 + \frac{1}{2}g_2 D^2 + \frac{1}{2}g_3 D^2 - EP, \tag{8}$$

because of $g_1 = \beta(T - T_C)$ and $\frac{\partial G}{\partial T} = -\Delta S$

and thus,

$$\Delta S = -\frac{1}{2}\beta \Delta D^2, \tag{9}$$

$$\Delta T = \frac{1}{2C}\beta T \Delta D^2, \tag{10}$$

where g and β is the Landau coefficient, and D is equal to polarization (P) in ferroelectric materials.

The equation (10) is the final term of the EC effect. P is one of the main factors that can improve ΔT. In addition, to improve EC materials, pyroelectric factors are also interesting as well. It may also increase EC coefficient because both two effects are thermodynamically equivalent as described in the equation (5). As the definition pyroelectric coefficient is p_E as $p = \left(\frac{\partial D}{\partial T}\right)_{E,X}$ then given by:

$$p = \left(\frac{\partial D}{\partial T}\right)_{E,X} = \left(\frac{\partial D}{\partial T}\right)_{E,X} + \left(\frac{\partial D}{\partial x}\right)_{E,T}\left(\frac{\partial x}{\partial T}\right)_{E,X}, \tag{11}$$

Because the equation (12) compose of two parts of pyroelectric; primary coefficient (p_{pr}) and secondary coefficient (p_{sc}),

$$P = P_s + E\varepsilon, \tag{12}$$

Because P_s is the saturated polarization and ε is the multiplying of $\varepsilon_0\varepsilon_r$ as shown in the equation (13), so the primary coefficient can rearrange as the equation (14)

$$D = \varepsilon E = \varepsilon_0 E + P = \varepsilon_0 E + \varepsilon_0\varepsilon_r E \tag{13}$$

where D is the electric displacement field, ε_0 is the permittivity of vacuum

$$p_{pr} = \left(\frac{\partial D}{\partial T}\right)_{E,X} = \left(\frac{\partial P_s}{\partial T}\right)_{E,X} + E\left(\frac{\partial \varepsilon}{\partial T}\right)_{E,X}, \tag{14}$$

From the equation (14), it can confirm that EC coefficient was improved with increasing three factors in primary pyroelectric coefficient; the saturated polarization of materials (P_s), the dielectric constant of materials (ε_r) and external electric filed (E). Also, in the secondary coefficient, it improves the EC coefficient although its impact is less than the first one. It can expend equations as equation (15). There are three factors of secondary pyroelectric coefficient; Piezoelectric coefficient (d), Young's modulus (c), and thermal expansion coefficient (α).

$$p_{sc} = \left(\frac{\partial D}{\partial x}\right)_{E,T}\left(\frac{\partial x}{\partial T}\right)_{E,X} = \left(\frac{\partial D}{\partial X}\right)_{E,X}\left(\frac{\partial X}{\partial x}\right)_{E,T}\left(\frac{\partial x}{\partial T}\right)_{E,X} = dc\alpha, \tag{15}$$

Curie-Weiss has found ferroelectric-paraelectric transition in ferroelectric materials, calling Curie temperature (T_c). The highest polarization of ferroelectric material is found on this Tc, following the Equation (16)

$$\varepsilon - \varepsilon_0 = \frac{C}{T - T_c}, \tag{16}$$

where T_c is Curie temperature, ε_0 is initially dielectric constant and C is the heat capacity. This equation (16) is similarly with the Landau coefficient of $\beta = g/(T - T_C)$. Equation (16) explains that the greatest polarization ensures to occur when ferroelectric material reaches the temperature at T_c. Different ferroelectric materials

produced different T_c position. Some of them have a small phase transitions such as PMN-PT single crystal [32]. Many studies have reduced the T_c to lower temperature [26], discussing in Chapter 2.

1.5 Highlights

This work has successfully studied the effects on the T_c reduction and ΔT enlargement of PVDF-HFP, via tuning chemical filler nanocomposite and biaxial stretch techniques. The effect of the stronger bonding interaction of rare-earth (RE) fillers has powerfully reduced Curie temperature of electrocaloric PVDF-HFP. The great ΔT enhancement was devoted to the filler nanocomposite that kept the ordinary crystallization of PVDF-HFP. the induced and reduced the ordinary crystallization decreased ΔT, by biaxial stretch and strong bond RE filler, respectively. Only a few filler contents of 1 wt% promoted the best electrocaloric effect on PVDF-HFP. The detailed highlights were showed in each specific topic.

CHAPTER 2

RELATED ELECTROCALORIC MATERIAL LITERATURE

2.1 The Effect of Curie Temperature by Filler Composition

The general strategy is to induce transition region or Curie temperature (T_c) near room temperature (RT) to improve the EC effect and expand its operating temperature.

2.1.1 Reduction of T_c by Filler Composition

One of the most appropriate strategies is adding filler for a polarizing microstructural phase in the main matrix. Some research reported that this strategy increased T_c [33-36], while the others reported that the filler can induce T_c to lower temperature [37-39]. For example, Weihua Wang and coworkers prepared Yb doped in $PbZrO_3$ from 0 to 3.0 mol% [40]. They found that T_c was decreased with Yb content. The suitable Yb content is 1.0 mol% with ΔT of -12.01 K at 70 °C of E = 800 kV/cm. The ΔT also was improved with Yb content. K. Co and colleagues [41] found that the addition of Zr in $BaZr_xTi_{(1-x)}O_3$ (BZT) of $0 < x < 0.30$ can reduce the T_c nearer RT with increasing Zr content. As a result, the ΔT of 1.25 °C had reported the maximum value for an electric field of 100 kV/cm when x = 0.20. They confirmed that a small amount of Zr ($0 < x < 0.15$) can transform $BaTiO_3$ from cubic paraelectric phase to tetragonal, orthorhombic, and rhombohedral phase, while the large amount ($x > 0.15$) can transform from cubic paraelectric phase to the rhombohedral phase and the sole ferroelectric phase. This is the typical phenomenon of diffused phase transition [42]. For example, In^{3+} cations substituted $Ba(Ti_{1-x}In_x)O_{3-x/2}$ (x = 0.01, 0.03, and 0.05) ceramics

can transform phase transition temperature, resulting in T_c reduction due to the parameter of c/a reduction with the In^{3+} content [43]. $Ba(Ti_{0.99}In_{0.05})O_{2.975}$ produced ΔT of 0.42 K under an E of 36 kV/cm. In addition, Jankowska-Sumara and coworkers reported that just 0.2 % of Cr ions doping in $Pb_5Ge_3O_{11}$ significantly reduced T_c from 453 K to 431 K with enhancing ΔT [44].

2.1.2 Increase of T_c by Filler Composition

However, some studies reported that the T_c was increased with filler content. The example of $(1-x)Pb(Mg_{1/3}Nb_{2/3})O_3-xPbTiO_3$ with x = 0, 0.05, and 0.10 was included [33]. The T_c increased with $PbTiO_3$ content. However, ΔT and $\Delta T/\Delta E$ were increased with the $PbTiO_3$ content. In the worst case, the filler content can both increase T_c and keep ΔT constant at high filler content. For example of $(Ba_{0.85}Ca_{0.15})(Ti_{0.9}Zr_{0.1-x}Sn_x)O_3$ with x = 0.00, 0.02, 0.04, 0.06 was included [36]. The x = 0.06 seemed to increase the T_c and kept ΔT constant. The increase of cation and/or anion filler in the BZT structure has an important role in improving the ECE. According to [34], the increase of Ba and Ti content in $(Ba_{0.85}Sr_{0.15})(Zr_{0.15}Ti_{0.85})O_3$, significantly enhanced T_c and ΔT, resulting in the greater $\Delta T/\Delta E$. The increase of T_c and ΔT with Ba content was matched with the prior study [35].

2.1.3 Hit a Peak of T_c by Filler Composition

Some research has hit a peak filler content for T_c reduction [45-47]. For example, $(Bi_{0.5}Na_{0.5})_{0.92}Ba_{0.08-3x/2}La_xTiO_3$ lead free ceramics with $x = 0$, 0.01, 0.02, and 0.03 was included [48]. Only at x = 0.01 strongly reduced T_c to the lowest temperature from

115 °C to 50 °C before increasing back to 115 °C on x = 0.03. As a result, the ΔT of

0.95 K was reported at T_c the nearest RT with E=50 kV/cm. It is possible that

the position of the hit a peak of T_c was in-between an increase and a reduction of T_c by

the suitable content of filler composition. The phase transition reduction via the amount

of filler content has limited. The too much filler content might increase the possibility

of the rapid phase transition, instead of gradually changing phase.

2.1.4 Curie Temperature Reduction by Other Strategies

There was evidence of T_c reduction by applying high external electric fields.

For example, the negative ECE of $Pb_{0.97}La_{0.02}(Zr_{0.80}Sn_{0.14}Ti_{0.06})O_3$ reduced T_c by

enhancing the external electric field [15]. The T_c was linearly decreased from 210 °C to

30 °C by enhancing E from 20 kV/cm to 110 kV/cm.

The temperature-pressure and temperature-electric field phase diagrams on

composite also affect the Tc reduction as well. An example of $K_{0.5}Na_{0.5}NbO_3$ was

included [49]. The increased hydrostatic pressure linearly reduced T_c from 700 K to

300 K with the pressures of 0 GPa to 7 GPa, respectively.

Ceramic composite's theory of electrocaloric development made an impact on

materials physic researcher for easily predictable the Tc and ΔT. However, the less

crystallinity of flexible PVDF polymer is more challenging because of the easy

fabrication, light-weight, flexible, and acidic resistance.

2.2 Ferroelectricity in Polyvinylidene fluoride (PVDF) Polymers

PVDF is one of the great dielectric properties with exposing strongly ferroelectric-electrocaloric behavior. A simple PVDF molecule is composed of H and F bonding with C back-bone, $-[C_2H_2F_2]_n-$. PVDF polymer present in five different phases conformations, such as α phase (TGTG′), β phase (TTTT), γ (T3GT3G′), and δ (TGTG′). The highest and the second-highest of net dipole moment are devoted to β and α phase, respectively, due to the highest orderly phase conformation in all PVDF molecules, showing in **Figure 2** [50]. Those phases are discriminated by the FTIR technique [51]. PVDF polymer exists semi-crystalline, having 50−70% crystallinity [52], based on different binary copolymers such as PVDF−TrFE, PVDF−HFP, PVDF−CTFE, and terpolymers such as P(VDF−TrFE−CTFE). Thus, those phases on the crystalline region (crystalline phases) in spherulite are also distinguished by the XRD technique [53]. According to the PVDF review [54], there are several procedures of the β-phase of PVDF polymers, such as poling, quenching, and stretching techniques. However, there are a few increases in β-phase nucleation.
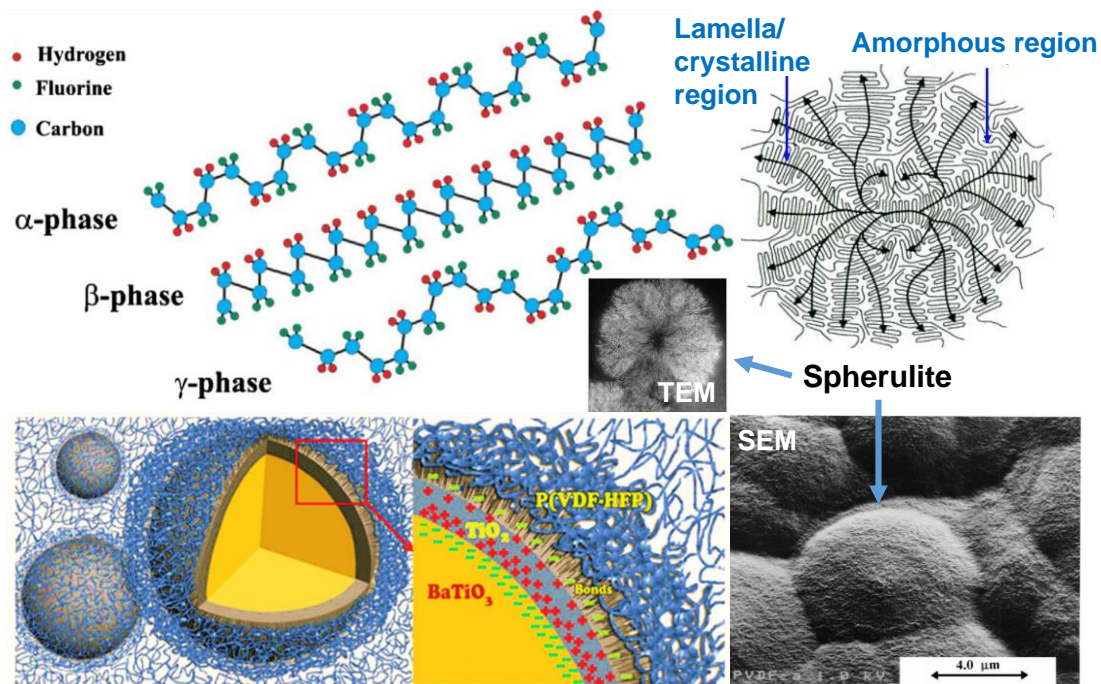
Figure 2 Electroactive phases of PVDF with SEM image of the crystalline and amorphous regions on spherulite PVDF structure, and the structure of PVDF based on BaTiO₃ filler nanocomposite (adapted from prior studies[50, 55]).

2.3 Interfacial Coupling in PVDF Based-Filler Nanocomposites

Nonconducting fillers are one of the interesting fillers for β-phase nucleation. For examples of ZnO [56], PZT [57], BaTiO$_3$ [58], KNaNbO [59], BNT-based ternary lead-free [60], Clay montmorillonite [61], SiO$_2$ [62], were included. However, conducting fillers-based PVDF nanocomposites play the most important role in the development of β-phase of PVDF polarization. For examples of Graphitic Carbon Nanomaterials (GCNs); Carbon Nanotube [63-72], Graphene Nanoplatelets [73-75], Graphene Oxide [76-82], metal nanopowders; Ag [83-85], Cu [86, 87], Fe [88], and Au [89], and Rare-earths (RE); La [90], Er [88, 91], Gd [91], Ce [27], and Y [27], were included. Most of conducting fillers induced the β-phase on PVDF molecule greater than the nonconducting fillers because

of the stronger H-bonding interactions (dipole-dipole interactions/ electrostatic force). Despite the H bonding, ion-dipole interactions show the stronger force in PVDF based filler nanocomposites [92], resulting in greater polarization and dielectric properties. It seemed that the conducting fillers-based PVDF nanocomposites are challenging and promising for further development to polarize dipole moment in effectively under electrocaloric performance.

2.4 The Performance of PVDF Based-Filler Nanocomposites

2.4.1 The Performance Level of PVDF among Ceramics

Figure 3 (a) showed the electrocaloric performance and efficiency energy density on PVDF among several ceramic composites [15]. According to the previous studies, research has found that great electrical breakdown strength of PVDF has resulted in the greatest ΔT among the ceramics. On the reason behind this is probably the amorphous region of PVDF, resulting in less $\Delta T/\Delta E$ compared with ceramics. The advanced electrocaloric on PVDF further developed. Research has found that there is mostly an increase in efficiency energy density by adding filler nanocomposites (Figure 3 (b)) [93]. Therefore, the addition of filler nanocomposite might polarize the dipole moment on the PVDF molecule for the electrocaloric performance in excellently. A great polarized on PVDF molecule by GCNs filler nanocomposites was reported in the previous literature [63-75][76-82], resulting in great dielectric constant (Figure 3 (c) [72]). The amount of filler nanocomposite is limited by the percolation threshold (the insulator-conductor transition), resulting in lower electrical breakdown strength [54]. The filler nanocomposites have increased $\Delta T/\Delta E$ on PVDF (Figure 3 (d)

[94]. For example, the $\Delta T/\Delta E$ of 0.10 K m MV^{-1} to 0.22 K m MV^{-1} was included when adding BZT in PVDF terpolymer. It seems that this technique can improve $\Delta T/\Delta E$ on PVDF nearer ceramic performance as PZT and BST.

2.4.2 Advanced ΔT on PVDF Based-Filler Nanocomposites

Many researchers had found that filler nanocomposites are an important role in the enhancement of PVDF electrocaloric. Lu Yang and colleagues reported graphene nanoplatelet doped in stretched blended polymer from 0.5, 0.7, and 1.0 wt% [95]. As a result, ΔT increased from 2.5 K for 0 wt% to 5.2 K for 1.0 wt% at RT with a small E of 40 MV m^{-1}. They found that the ΔT increased with graphene content. Moreover, Yuqi Chen and coworkers found that BiFeO$_3$ nanoparticles in Ba(Zr$_{0.21}$Ti$_{0.79}$)O$_3$ nanofibers doped in PVDF-TrFE-CFE [94]. Consequently, the ΔT of PVDF improved from 8 K to 14 K with E of 75 MV m^{-1} at 30 °C. They also found that the volume fraction of the filler was hit a peak at 30 vol% before drop ΔT at 50 vol%. Some had successfully increased ΔT in an effective idea such as designed the advanced fiber-filler form. For instance, the nanofiber of BaTi$_{0.89}$Sn$_{0.11}$O$_3$ doped in P(VDF-TrFE-CFE) from 2.5 vol% to 10.0 vol% [96]. Consequently, 7.5 vol% of fiber-filler produced the highest ΔT of 9.08 K with kept T$_c$ constant at RT (E = 1000 kV/cm). Furthermore, Jianfeng Qian reported that P(VDF-TrFE-CFE) was changed to nanofiber form by electrospinning and doped with Ba(Zr$_{0.21}$Ti$_{0.79}$)O$_3$ nanofibers [97] from 0 to 10 vol%. As a result, ΔT increased with Ba(Zr$_{0.21}$Ti$_{0.79}$)O$_3$ filler content. For example, at an electric field of 200 MV m^{-1} at 30 °C, ΔT increased from 21 K of pure P(VDF-TrFE-CFE) to 44.3 K of 10 vol% filler.

This is the typical phenomenon of filler/polymer interfaces according to Maxwell-Wagner-Sillars (MWS) effect [98]. It can explain that these fillers can promote interfacial surface charges or interfacial coupling polarization at phase boundaries between dipoles across the polymer-filler interfaces.

2.4.3 An Advanced ΔT on PVDF by the Other Strategies

Besides the fiber-filler form, PVDF-TrFE-CFE was changed from thin film to nanowire by anodic aluminum oxide (AAO) [99]. As a result, ΔT increased from 0.55 K to 2.5 K at RT with 50 MV m^{-1}. The $\Delta T/\Delta E$ was increased about three times. The high cost of relaxor PVDF-TrFE-CTFE polymer with the great $\Delta T/\Delta E$ [100] has led to research in normal-relaxor transformation on PVDF. They tried to improve normal PVDF to be the relaxor PVDF. Similarly with the prior study [101], they can add copolymer PVDF-TrFE in terpolymer PVDF-TrFE-CFE in the volume ratio of 3/7 to produce ΔT of 45.4K at an electric field of 100 MV/m at 85 °C. The increase in copolymer content increased T_c.

In PVDF based-filler nanocomposites, there is less research on the technique of T_c reduction near RT. Most of them successfully improved the temperature-change enhancement for electrocaloric efficiency only as shown in Figure 3.
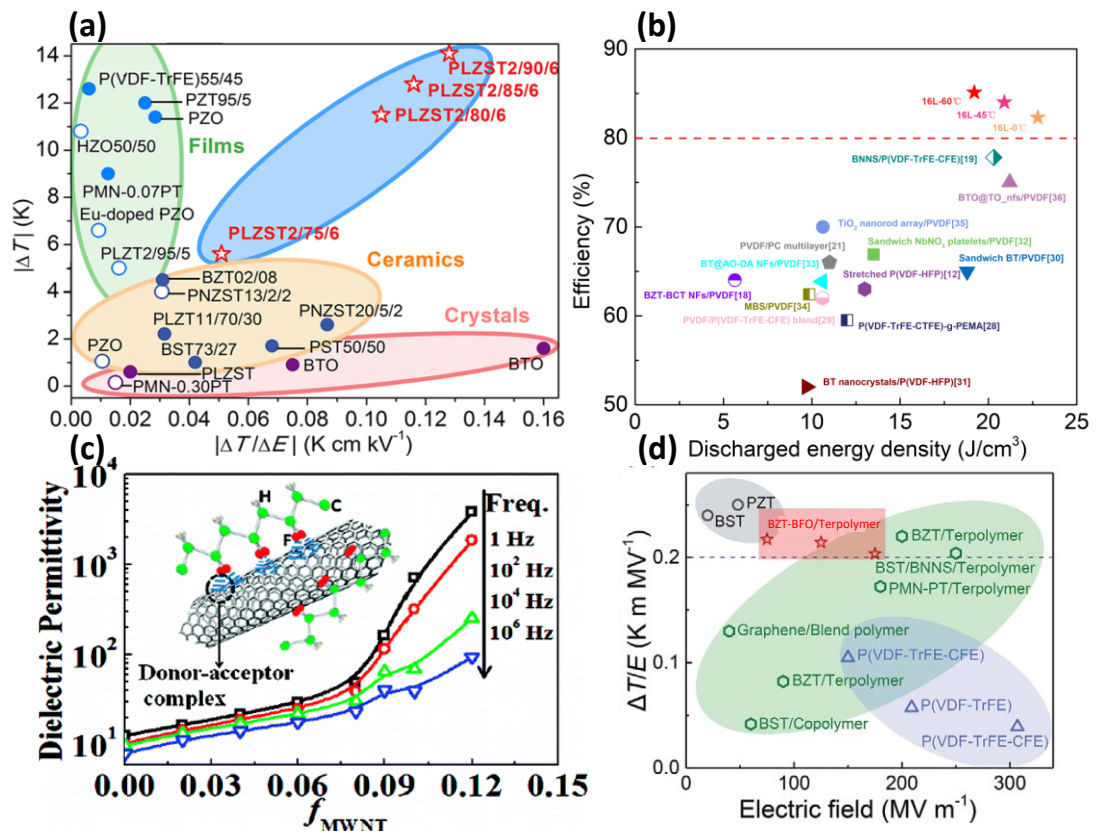
Figure 3 Electrocaloric performance and energy density efficiency of PVDF based on filler nanocomposite, (a) electrocaloric PVDF performance among ceramics [15], (b) energy density efficiency [93], (c) dielectric constant of PVDF based on GCNs filler nanocomposites [72], and (d) the electrocaloric enhancement of PVDF based on filler nanocomposite [94].

2.5 Strengths and Weaknesses of Indirect and Direct ECE Measurements

The direct measurement is a method for detecting the endothermal/exothermal in directly on materials. Many researchers have tried to directly measure ΔT in precisely. The invented ECE setup has to effort to make a precise in every single position, according to several ECE setup patents. The difficulty of direct measurement [102] occurred when the sample had a small transformation. As a result, some researchers

decided to adjust the high-price apparatus as DSC for the applied external electric field [26].

The indirect measurement is the transformation technique by using Maxwell's relation. The PE loops are measured by applying a constant external electric field for finding $\frac{\partial P}{\partial T}$ in each temperature interval, depending on accurate data. The indirect measurement has resulted in relative ΔT. The relative ΔT awareness might not really 100% the same with real ΔT. Many researchers tried to figure out the differentiated on two measurements. They reported that both measurements have not significantly different [103, 104]. Matching with the prior study[26], the electrocaloric performance on the indirect method is the same as the direct DSC method. The result also showed that T_c from the indirect method is more accurate. The DSC direct method has a drawback of less accuracy in T_c. Just a few research reported that the indirect seem larger than direct [105], and vice visa[106]. Even though the ΔT from the indirect method is still called relative ΔT, the T_c from the indirect method is more precise than the direct method.

CHAPTER 3

MATERIALS, PREPARATION, AND CHARACTERIZATIONS

3.1 Materials

- Polyvinylidene fluoride-hexafluoropropylene PVDF-HFP (Solef 11010/1001, Solvay Solexis, Belgium)

- *N, N*-dimethylformamide with ≥ 99% purity (DMF, RCI Labscan, Thailand)

- Graphene nanoplatelets (806633 ALDRICH, Sigma-Aldrich Ltd, Singapore)

- Erbium (III) nitrate pentahydrate ($Er(NO_3)_3 \cdot 5H_2O$, 298166 ALDRICH, Sigma-Aldrich Ltd, Singapore)

- Dysprosium (III) nitrate hydrate ($Dy(NO_3)_3 \cdot xH_2O$, 298158 ALDRICH, Sigma-Aldrich Ltd, Singapore)

3.2 Preparation

3.2.1 Polyvinylidene fluoride (PVDF-HFP) Thin Film with Filler Nanocomposite

Polyvinylidene fluoride-hexafluoropropylene (PVDF-HFP) powder was purchased from Solvay Solexis, Belgium, having 10 wt. % HFP (Solef 11010/1001). Every filler powder was sonicated in the solvent of N, N-dimethylformamide (DMF, purchased from RCI Labscan, Thailand) for well dispersion by ultra-sonicator 200 W for 20 minutes. Afterward, PVDF-HFP was gradually mixed and stirred at 30 °C for 12 hours. This homogeneous solution was then cast on a glass plate by a tape casting technique with an adjustable film applicator (Sheen S/N 102503/2, lncl, Shims). The DMF in this film had to remove by drying evaporation at 80 °C for 12 hours in

the oven (Asset positively identifiable T410353 Binder). This final film was peeled off from the plate by dropping a few DI water for preventing the film crack formation. Neat PVDF-HFP was prepared as the control case to compare with these composite thin films.

3.3 Dielectric and Electrocaloric Characterizations

3.3.1 Dielectric measurement

The LCR meter (LCR meter, IM 3533 HIOKI, Japan) measured dielectric properties such as dielectric constant (ε_r), loss tangent or dielectric loss ($\varepsilon_r^{''}$), and electrical conductivity (σ_{ac}) at various frequencies from 1 Hz to 10^5 Hz. The thin film was applied with 1 V_{ac} voltage across the sample by two parallel electrodes for measuring the capacitance of surface charge (C, in F) and $\varepsilon_r^{''}$. The ε_r, and σ_{ac} were calculated by using Equation (17), and (18), respectively.

$$\varepsilon_r = Cd/\varepsilon_0 A \tag{17}$$

$$\sigma_{ac} = 2\pi f \varepsilon_0 \varepsilon_r \varepsilon_r^{''} \tag{18}$$

Here, d refers to sample thickness (m) with 100 μm, A is electrode area (m^2) with 5 mm diameter, and ε_0 (8.853 x 10^{-12} F m^{-1} [107-110]) is the free space permittivity. f is the ac frequency in Hz.

3.3.2 Electrocaloric characterization with Maxwell relation

Ferroelectric Polarization Loop Test System (P-E analyzer, PK-CPE1701, USA) measured polarization and electric field loop (P-E loop) on thin films by applying

40 MV/m electric field (Trek model 610E) at 10 Hz frequency. In this measurement, two electrodes on thin-film (30 µm) were sputtered by Sputter Coater (SPI-MODULE, Structure Probe, Inc, West Chester, PA, USA).

Remnant polarization (P_r, µC/cm^2) was recorded from the previous measurement at various temperatures from 30 °C to 140 °C (1 °C interval) in a controllable oven. The adiabatic temperature change (ΔT) was further calculated by using Maxwell relations [9] as **Equation (19)**.

$$\Delta T = -\frac{1}{\rho C_E} \int_{E_1}^{E_2} T \left(\frac{\partial P}{\partial T}\right) dE \tag{19}$$

Here, ρ is density, C_E refers to specific PVDF-HFP heat capacity, T is temperature, E is an electric field, and $\frac{\partial P}{\partial T}$ is the gradient between P_r and T. The ΔT calculation was explained in Appendix E.

CHAPTER 4

ECE IN PVDF COMPOSITES BASED ON DIFFERENT GRAPHENE CONTENTS WITH BIAXIAL STRETCH

4.1 Highlights

- PVDF-HFP blends with graphene nanoplatelets.

- Stretched composites improve crystallinity.

- Stretched composites improve dielectric and ferroelectric performances.

- Negative electrocaloric performance is decreased by increasing crystallinity.

4.2 Introduction

There were many techniques for an advanced PVDF polarization to polarize following the direction of the external electric field. For examples of electrical poling with temperature [24], nano-spider by electrospinning [22, 23], and tailored polarization by electron/gamma irradiation [19-21], are included. The fascinating on the modified crystallinity by biaxial stretching with a given temperature was reported [25]. However, the effect on biaxial stretch-induced crystallization of PVDF has less focused on electrocaloric performance. In this work, the graphene nanoplatelet (GPN) filled in stretched PVDF-HFP thin film was observed on the electrocaloric effect. The thin film preparation of PVDF-HFP based on graphene filler nanocomposite was studied in stretched and unstretched techniques for electrocaloric behavior.

4.3 Experimental Details

4.3.1 Stretched PVDF-HFP Thin Film - based on Graphene Filler Nanocomposite Preparation

Graphene nanoplatelet powder was purchased from Sigma-Aldrich Ltd, Singapore, having 12.01 g/mol (806633 ALDRICH). This filler was introduced to study the stretching effect with graphene filler contents of 1, 2, 3, 4, and 5 wt% in PVDF-HFP. The stretching samples were labeled GPN1ST, GPN2ST, GPN3ST, GPN4ST, and GPN5ST, respectively, similarly without stretching samples labeling GPN1NST, GPN2NST, GPN3NST, GPN4NST, and GPN5NST. The pure ST and pure NST were labeled for neat PVDF-HFP in with and without stretching as the control cases.

In this work, some PVDF-HFP was stretched for changing the macroscopic structure. The original length (L_o) started from 20 mm to 80 mm elongation length (L). This process controlled 2.5 mm/min of stretching rate by adjustable step motor in the oven 100 °C. The final thickness is 30 µm from 100 µm. This technique had been improved PVDF-HFP crystallinity for dielectric properties [111].

4.3.2 Thermal Analysis

Differential Scanning Calorimeter (DSC, STA8000, Perkin Elmer, USA) analyzed the amount of crystallinity (X_c) of thin films by applying the heat in ambient air with a 10.00 °C/min heating rate from 120 °C to 180 °C. The X_c was calculated from the melting enthalpy change (ΔH_m, J g^{-1}) as Equation (20).

$$X_c(\%) = \frac{\Delta H_m}{(1 - \emptyset)\Delta H_m^0} \times 100 \qquad (20)$$

where ΔH_m is the observed melting enthalpy, ΔH_m^0 (104.6 J g^{-1} [112]) is the melting enthalpy of 100% crystalline PVDF-HFP, and $\emptyset$ is the weight fraction of filler.

4.3.4 Ferroelectric Energy Efficiency Measurement

Ferroelectric Polarization Loop Test System (P-E analyzer, PK-CPE1701, USA) measured polarization and electric field loop (P-E loop) on thin films by applying 40 MV/m electric field (Trek model 610E) at 10 Hz frequency.

The integrated area of the loop was considered in this work. According to the hysteresis loops[93, 113-116], the equation of energy storage efficiency was defined as the Equation (21).

$$\eta\,(\%) = \frac{U_e}{U_e + U_l} \times 100 \tag{21}$$

where η is the energy storage efficiency of the material, U_e is recoverable energy density (charging area), U_l is an unrecoverable energy density (charging-discharging area or closed area of the hysteresis loops). Here, the well-known equation recoverable energy denoted to $U_e = \int_{P_r}^{P_{max}} EdP$. In this measurement, two electrodes on thin-film were sputtered by Sputter Coater (SPI-MODULE, Structure Probe, Inc, West Chester, PA, USA).

4.3.3 Dielectric and Electrocaloric Characterizations

The dielectric and electrocaloric characterizations were examined, as presented in **Chapter 3**.

4.4 A Brief of Results and Discussion

The stretched PVDF-HFP was a more translucent thin film. This is because of the biaxial stretch-induced crystallization of PVDF-HFP. The crystallite size also decreased, as shown in Appendix A. **Figure 4** (a) confirmed the increase of crystallinity (X_c) on stretched film. The non-stretched film had not significantly changed with GPN contents. However, the X_c was suddenly reduced at 5 wt% GPN of the stretched film. The larger interfacial gap on exceeding GPN content might occur after stretching, resulting in sudden X_c reduction. In addition, the T_m on stretched film was a fluctuated reduction compared with non-stretched film, due to the interfacial gap after stretching.

Figure 4 (b) showed the gradual increase of dielectric constant and conductivity with GPN content. This is because of the enhancement of interfacial polarization at phase boundaries of GPN-PVDF-HFP, according to Maxwell-Wagner-Sillars (MWS) effect [98]. Biaxial stretch-induced crystallization of PVDF-HFP promoted the dielectric properties as well, due to the greater polarization on crystallinity region. The biaxial stretch-induced crystallization had resulted in the great ferroelectric properties as Figure 4 (c). The lower Remnant polarization (P_r) from the slimmer PE loop was showed on stretched film, resulting in greater energy density efficiency. This is because the smaller crystallite size on stretched film (as showed in Appendix A) can easily polarize.

Figure 4 (d) showed a sharp increase of $\left| \Delta T_{max} \right|$ at 1 wt% GPN and a gradual decrease when the GPN >1 wt%. The effect of biaxial stretch-induced crystallization can reduce $\left| \Delta T_{max} \right|$. It is possible that the induced crystallization on PVDF-HFP is the abnormal crystallinity with unnatural polarization, resulting in the electrocaloric

performance reduction. This was confirmed on stretched film at 5 wt% that the sudden X_c reduction promoted $\left| \Delta T_{max} \right|$. In addition, the GPN filler nanocomposite in PVDF-HFP had the potential to change the phase transition to lower temperatures slightly. The suitable on GPN nanoplatelet form might effectively tailor structural phase PVDF-HFP. However, another negative effect on the biaxial stretch-induced crystallization is that an increase in T_c in PVDF-HFP go to higher temperature again. In this work, the negative effect of biaxial stretch-induced crystallization of PVDF-HFP was successfully reported. The stretching technique on PVDF-HFP might inappropriate process to maximize electrocaloric performance.
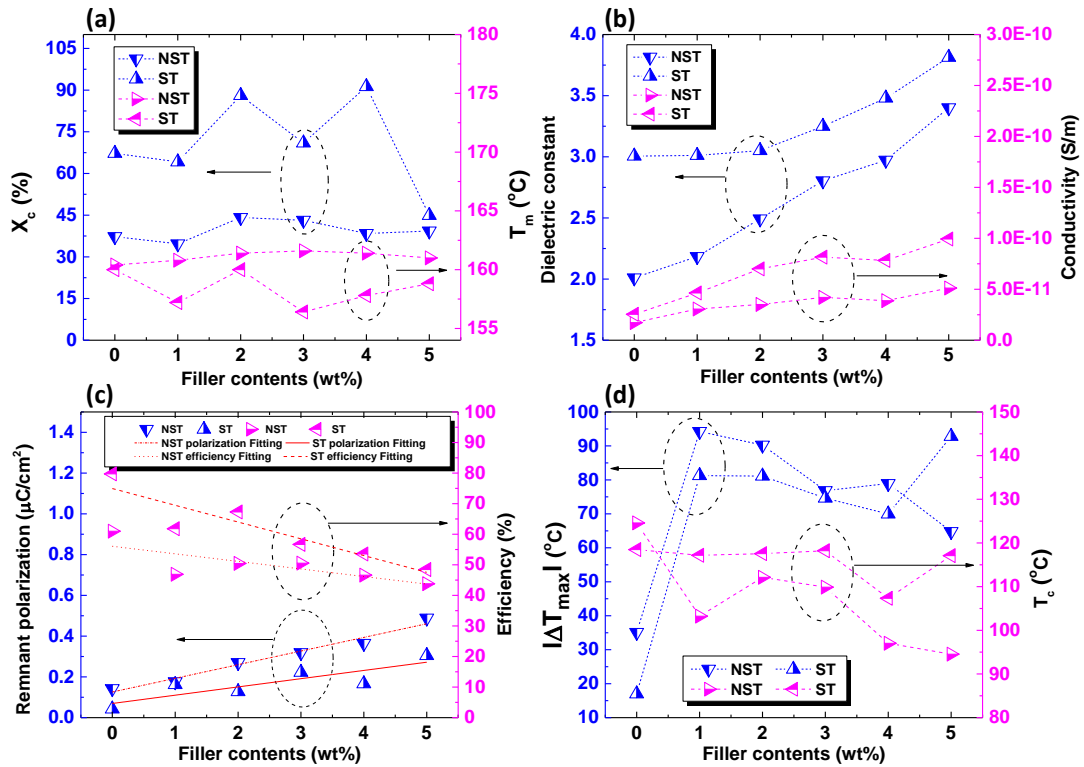
Figure 4 The stretched and GPN filler nanocomposite effects on PVDF-HFP thin film, (a) crystallinity enhancement melting temperature reduction, (b) the increases of dielectric constant and conductivity, (c) ferroelectric performance, and (d) electrocaloric performance.

4.5 Conclusion

Graphene powders were blended with thin-film PVDF-HFP by solution casting technique. This composite film was stretched in the biaxial stretching technique. The comparison between stretching and non-stretching was studied. As a result, the unchanged of PVDF-HFP by non-stretching technique with GPN contents increased ΔT, while the induced-X_c of PVDF-HFP by stretching technique decreased ΔT. Moreover, the interfacial bonding of GPN-PVDF-HFP as dipole-dipole interaction can

slightly reduce T_c. However, the stretching improved dielectric properties and energy storage efficiency due to the induced-X_c. The best negative ΔT_{max} was devoted to 1 wt% GPN without stretching with T_c reduction to a lower temperature by 20 °C.

CHAPTER 5

ECE IN PVDF COMPOSITES BASED ON DIFFERENT RARE-EARTH CONTENTS WITH TWO ELECTRONEGATIVITIES

5.1 Highlights

- Polyvinylidene fluoride hexafluoropropylene blended with Er/Dy rare-earths fillers.

- The rare-earth fillers suddenly decreased Curie temperature (T_c) by 40 °C.

- Stronger EN of Er induced T_c and β phase on crystalline region better than Dy.

- Stronger EN filler decreased crystalline along with dielectric properties.

5.2 Introduction

The availability of materials with high electrocaloric strengths is critical to improve. Many studies had tried to reduce a high T_c, which is inappropriate the daily devices, shifted from a high temperature to RT via filler nanocomposite, advanced material preparation, etc. (as discussed in Topic 2.1). As PVDF based on filler nanocomposite literature review (as explained in the topic 2.2), many of them with high interfacial bonding significantly promoted PVDF polarization, especially the RE element in nitrate tetrahydrate [92]. The high conductive RE and strong bonding of ion-dipole interaction might powerfully reduce T_c on PVDF-HFP. The two different electronegativities (EN) of Dy and Er is an important role to figure out high electrocaloric strengths. In this work, the PVDF-HFP thin film was blended with RE fillers of Er and Dy.

5.3 Experimental Details

5.3.1 PVDF-HFP-based on RE fillers nanocomposite preparation

Erbium (III) nitrate pentahydrate ($Er(NO_3)_3 \cdot 5H_2O$) and Dysprosium (III) nitrate hydrate ($Dy(NO_3)_3 \cdot xH_2O$), were purchased from Sigma-Aldrich Ltd, Singapore, having 99.9% purity (298166 ALDRICH, and 298158 ALDRICH). The fillers used to study the effect of the RE filler on PVDF-HFP in-between Er and Dy fillers with contents of 1, 5, 10, and 20 wt% in PVDF-HFP. The Er contents are here labeled PEr1, PEr5, PEr10, and PEr20, respectively. Similarly, the cases with Dy contents are labeled as PDy1, PDy5, PDy10, and PDy20, respectively. The pure PVDF-HFP was labeled for neat PVDF-HFP and it was used as the control cases.

5.3.2 FTIR spectra

Fourier-transform infrared spectroscopy (FTIR, VTR, Vertex70, Bruker, Germany) was used to characterize functional groups of the sample's light absorption from 400 cm^{-1} to 1350 cm^{-1} with 4 cm^{-1} of resolution. This work focused on the absorption of two electroactive phases of α phase and β phase because of the two highest net polarization. The β phase (TTTT) produces the highest net polarization compared with α (TGTG') and γ (TTTGTTTG') phases. The second highest α phase is detected at several peaks [22, 117], for example, 484, 534, 613, **767**, 795, and 976 cm^{-1}, while the first highest β phase is noticed at 511, **837**, 1234, and 1275 cm^{-1} [22, 117], as shown in **Table 1**. According to the relative fraction of the β phase [118], Gregorio et al.

used Lambert-Beer law to calculates the β phase fraction comparing with α phase as shown in Equation (22).

$$F(\beta) = \frac{A_\beta}{\frac{K_\beta}{K_\alpha}A_\alpha + A_\beta} \times 100 \qquad (22)$$

where, K_α (6.1×10^4 cm^2 mol^{-1}) and K_β (7.7×10^4 cm^2 mol^{-1}) represent the coefficients, and A_α (767 cm^{-1}) and A_β (837 cm^{-1}) are the absorbance of wavenumbers [109, 119]. The electroactive β phase on PVDF-HFP was measured in both amorphous and crystalline regions.

Table 1 Divergence in the absorption FTIR of typical bands characteristics of PVDF phases [50, 51].

	Wavenumber (cm^{-1})
α	408, 484, 534, 613, **767**, 795, 855, and 976
β	511, **837**, 1234, and 1275
γ	431,512, 776, 812, 833, 840, and 1234

5.3.3 XRD diffraction

In this work, an X-ray diffractometer (XRD, X'Pert MPD, Philips, Netherlands, PANalytical, Empyrean, Netherlands), was used to identify the crystal phase diffraction on semi-crystalline PVDF material. This wok focused on the crystalline α and β phases. According to prior related works [50, 51], the strongest dipole β phase is observed at 2θ = 20.5° with (110)/(200) crystallographic planes, while the α phase is diffracted

at $2\theta = 18.3°$ with the (020) plane [120], as presented in **Table 2**. The diffraction peak was observed from $2\theta = 10°$ to $2\theta = 40°$, with $0.05°$ s^{-1} scanning rate. The Cu-Kα_1 radiation with 0.15406 nm wavelength was applied at 40 kV, 30 mA. The crystal β phase ratio was evaluated by the ratio of $I_{\beta(20.5)}/I_{\alpha(18.3)}$ as shown Equation (23), when the $2\theta = 20.5°$ and $18.3°$ referred to β and α phases, respectively.

$$\text{The crystal } \beta \text{ phase ratio} = \frac{I_{\beta(20.5)}}{I_{\alpha(18.3)}} \tag{23}$$

Table 2 Divergence in the diffraction XRD of angle and crystal planes of crystalline PVDF phases [50, 51]

	2θ (°) with Crystallographic plane
α	17.66 (1 0 0), **18.30** (0 2 0), 19.90 (1 1 0), and 26.56 (0 2 1)
β	**20.5** (1 1 0)/(2 0 0)
γ	18.5 (0 2 0), 19.2 (0 0 2), and 20.04 (1 1 0)

5.3.4 Thermal Analysis

The DSC characterization was examined, as presented in **Chapter 4**.

5.3.5 Dielectric and Electrocaloric Characterizations

The dielectric and electrocaloric characterizations were examined, as investigated in **Chapter 3**.

5.4 A Brief of Results and discussion

The increase of RE filler suddenly improved β phase in whole PVDF-HFP polymer, with insignificantly different on both Er and Dy (**Figure 5** (a)). The two RE elements showed a significant difference when measuring the crystal β phase ratio on the crystalline region of PVDF-HFP. It can be seen that the stronger EN of Er had the potential to induced the crystal β phase ratio more than Dy, especially at high filler content. The crystal β phase ratio of both Er and Dy hits a peak at 5 wt% before reducing at 10 and 20 wt% respectively. It is possible that the crystalline region on the whole PVDF-HFP was decreased with RE content.

Matching with Figure 5 (b), the crystallinity of PVDF-HFP was gradually reduced with RE content. The stronger EN of Er had more potential to reduce the crystalline region than those Dy. The lower crystallinity region of PVDF-HFP by Er had resulted in a lower dielectric constant compared with Dy. The schematic of PVDF-HFP based on RE filler nanocomposite (Figure 5 (c)) showed the strong bonding interaction (dipole-dipole interaction) and the strongest bonding interaction (dipole-dipole interaction) on PVDF-HFP molecule via RE element. The crystalline region reduction on PVDF-HFP also significantly expressed at ≥10 wt%, affecting crystal β phase reduction. Predictably, the increase of filler nanocomposite often increased dielectric constant (Figure 5 (b)) because of the interfacial-polarization enlargement with filler content [98].

The electrocaloric performance showed in Figure 5 (d) (as showed detailed information was shown in detail in Appendix B). The RE filler had successfully reduced T_c on PVDF-HFP by 40 °C. For example, the reduction of 118.47 °C (pure PVDF-HFP)

to 94.71 °C (PDy5) and 91.84 °C (PEr5) was reported. The T_c was further reduced to 83.42 °C and 77.38 °C when adding RE content of 1 wt%. The too much filler content in PVDF-HFP might split and suddenly change phase transition, resulting in an increase of T_c at too high filler content [26]. It matched with prior reports [45-48] that the T_c was hit a peak by filler composition before gradual increased, reviewed in **The topic 2.1.3**. Moreover, Figure 5 (d) showed a gradual decrease in $\left|\Delta T_{max}\right|$ with RE content. It is possible that the PVDF polarization was effectively polarized on a great ordinary crystalline. This was matched with the crystalline reduction with RE content as shown in Figure 5 (b), which is in the same reason on the greater $\left|\Delta T_{max}\right|$ on Dy than Er. The best performance of Curie temperature reduction was found with 1 wt% Er filler. The Curie temperature reduction was related to micro-phase structure and interfacial charge mobility for future electrocaloric cooling technology.
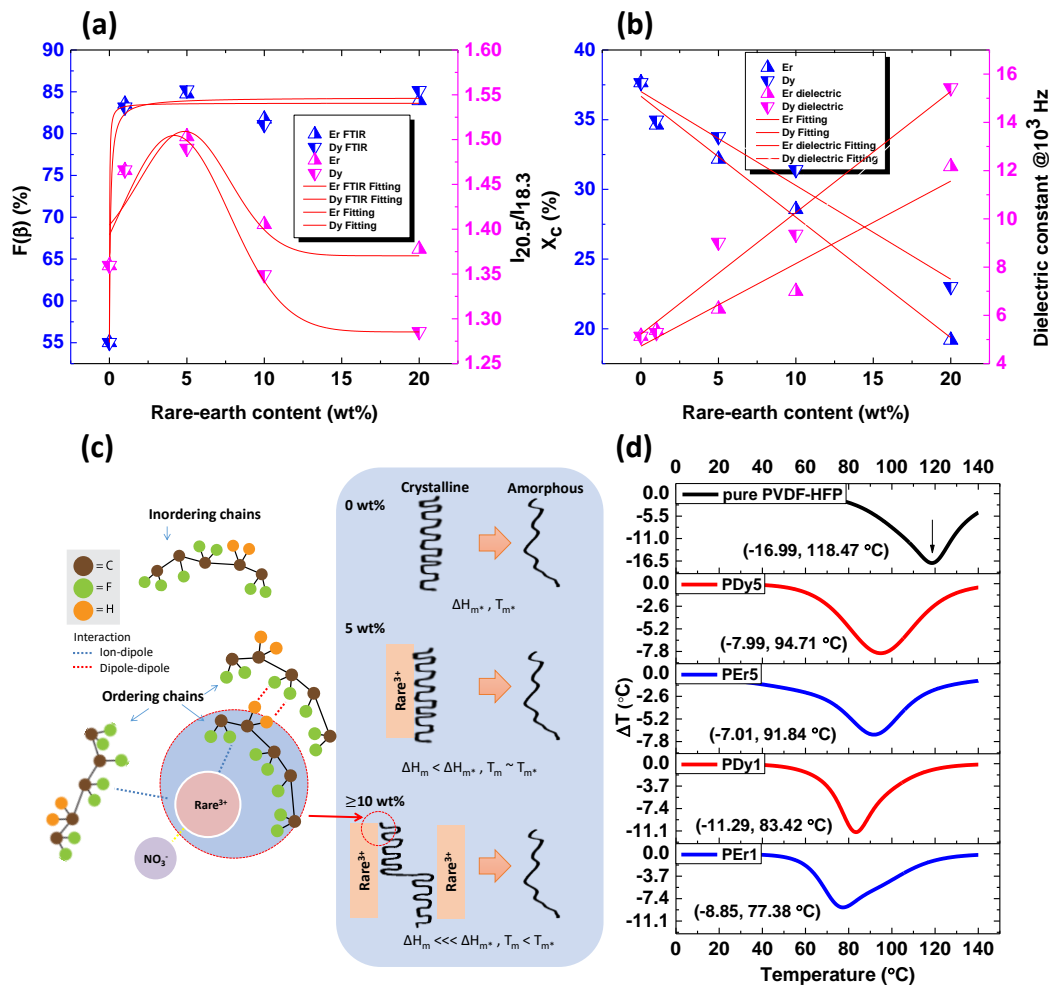
Figure 5 The RE filler nanocomposite effect, (a) β phase and crystal β behaviors, (b) crystallinity region and dielectric constant, (c) the structural schematic of PVDF-HFP based on RE filler, and (d) electrocaloric behaviors.

5.5 Conclusion

In this work, RE filler of Er and Dy were blended with thin-film PVDF-HFP by solution casting technique. The two EN differences between Er and Dy were considered in this work. As a result, the reduced-X_c of PVDF-HFP by RE fillers decreased ΔT. However, the strongest interfacial bonding of RE-PVDF-HFP as ion-dipole interaction can powerfully reduce the T_c. The best ΔT_{max} was devoted to 1 wt% Er with T_c

reduction to a lower temperature by 40 °C. The stronger EN of Er had more potential to reduce Xc on PVDF-HFP, resulting in lower dielectric properties compared with Dy. However, these fillers had successfully reduced T_c to lower temperatures from 120 °C to 77-83 °C.

CHAPTER 7

SUMMARY

7.1 Conclusions

This work is aimed to develop both ΔT enhancement and T_c reduction of PVDF-HFP based on filler nanocomposite for applications in the electrocaloric cooling. The thin film of PVDF-HFP based on filler nanocomposites was successfully fabricated by tape casting method. The negative result of biaxial stretching crystallization on PVDF-HFP was also noticed. This work was divided into two main results; the approach on ΔT enhancement, and the tactic on T_c reduction.

Firstly, the approach in ΔT enhancement was observed, depending on PVDF-HFP crystallization. The great ΔT enhancement was noticed for the filler nanocomposite that has the ability to keep the ordinary crystallinity constant. The small-changed-crystallization of PVDF-HFP enables to intensification ΔT by graphene nanoplatelet fillers. However, there were two effects of ΔT reduction; induced-crystallization, and reduced-crystallization. Two of them were raised from biaxial stretch technique and strong bonding interaction of RE filler.

Secondly, the access in T_c reduction was observed, depending on how strong bonding interaction. The great T_c reduction was noticed for the great interfacial filler-polymer composite. The strongest interfacial-bonding of ionic-dipole interaction produced the highest T_c reduction, observing in nitrate-hydrate RE filler such as Er and Dy. The stronger electronegativity of Er provided the greater T_c reduction. The second highest T_c reduction was devoted to the H-bonding of dipole-dipole interaction

(electrostatic charge), such as PVDF-HFP based on graphene nanoplatelet filler composite.

These two approaches of ΔT enhancement and T_c reduction are applicable for an advanced electrocaloric refrigerator with suitable energy storage efficiency in the future.

7.2 Limitations and Recommendations for Future Work

The graphene nanoplatelet and RE filler have to reduce content from 1 wt% of the best electrocaloric condition. A small content of <1wt% filler may show greater electrocaloric performance.

Normally, the ΔT from Maxwell relation is compared to the ΔT from direct measurement with high sensitivity of such as DSC. This work constrains the level of high accuracy equipment for detecting the ΔT in the current study. We had tried to detect ΔT directly with IR thermal camera. The IR camera cannot detect due to small sensitivity detection. To support our ΔT, the high accuracy DSC equipment may be additionally researched. Developing a new instrument to measure direct ΔT might an option to eliminate these limitations.

To improve the ΔT by adding larger E, this sample should be less conductive. The Silane coupling agent should continue to study to solve this problem by reducing the conductive of filler. The maximum silane content showed the result of the conductive filler type as shown in Appendix D.

BIBLIOGRAPHY

1.   William Goetzler*, et al.*, *Energy Savings Potential and RD&D Opportunities for Commercial Building HVAC Systems*. **2017**: US Department of Energy.

2.   Pakhomov, O.V.*, et al.*, *Thermodynamic estimation of cooling efficiency using an electrocaloric solid-state line.* Technical Physics, **2010**. 55(8): p. 1155-1160.

3.   Cui, J.*, et al.*, *Demonstration of high efficiency elastocaloric cooling with large ΔT using NiTi wires.* Applied Physics Letters, **2012**. 101(7): p. 073904.

4.   Kim, D.S.*, et al.*, *Solar refrigeration options – a state-of-the-art review.* International Journal of Refrigeration, **2008**. 31(1): p. 3-15.

5.   Snyder, G.J.*, et al.*, *Thermoelectric Efficiency and Compatibility.* Physical Review Letters, **2003**. 91(14): p. 148301.

6.   Backhaus, S.*, et al.*, *A thermoacoustic Stirling heat engine.* Nature, **1999**. 399: p. 335.

7.   Garrett, S.L., *Resource Letter: TA-1: Thermoacoustic engines and refrigerators.* American Journal of Physics, **2004**. 72(1): p. 11-17.

8.   Slaton, W.V.*, et al.*, *Theory of inert gas-condensing vapor thermoacoustics: Transport equations.* The Journal of the Acoustical Society of America, **2002**. 112(4): p. 1423-1430.

9.   Lines, M.E.*, et al.*, *Principles and Applications of Ferroelectrics and Related Materials*. **1977**: OUP Oxford.

10.   Valant, M., *Electrocaloric materials for future solid-state refrigeration technologies.* Progress in Materials Science, **2012**. 57(6): p. 980-1009.

11. Geng, W., *et al.*, *Giant Negative Electrocaloric Effect in Antiferroelectric La-Doped Pb(ZrTi)O₃ Thin Films Near Room Temperature.* Advanced Materials, **2015**. 27(20): p. 3165-3169.

12. Zhuo, F., *et al.*, *Coexistence of multiple positive and negative electrocaloric responses in (Pb, La)(Zr, Sn, Ti)O₃ single crystal.* Applied Physics Letters, **2016**. 108(8): p. 082904.

13. Chen, C., *et al.*, *Coexistence of negative and positive electrocaloric effect in Sr and Nb co-doped Pb(Zr,Ti)O₃ ferroelectric ceramics.* Materials Letters, **2017**. 189: p. 303-306.

14. Jiang, X., *et al.*, *Electrocaloric effect based on the depolarization transition in (1−x)Bi₀.₅Na₀.₅TiO₃–xKNbO₃ lead-free ceramics.* Ceramics International, **2014**. 40(2): p. 2627-2634.

15. Zhuo, F., *et al.*, *Giant Negative Electrocaloric Effect in (Pb,La)(Zr,Sn,Ti)O₃ Antiferroelectrics Near Room Temperature.* ACS Applied Materials & Interfaces, **2018**. 10(14): p. 11747-11755.

16. Bai, Y., *et al.*, *Entropy-change measurement of electrocaloric effect of BaTiO₃ single crystal.* physica status solidi (a), **2012**. 209(5): p. 941-944.

17. Zhuo, F., *et al.*, *Phase transformations, anisotropic pyroelectric energy harvesting and electrocaloric properties of (Pb,La)(Zr,Sn,Ti)O₃ single crystals.* Physical Chemistry Chemical Physics, **2017**. 19(21): p. 13534-13546.

18. Neese, B., *et al.*, *Large Electrocaloric Effect in Ferroelectric Polymers Near Room Temperature.* Science, **2008**. 321(5890): p. 821-823.

19. Parangusan, H., *et al.*, *Investigation on the effect of γ-irradiation on the dielectric and piezoelectric properties of stretchable PVDF/Fe–ZnO*

nanocomposites for self-powering devices. Soft Matter, **2018**. 14(43): p. 8803-8813.

20. Bauer, F., *Relaxor fluorinated polymers: novel applications and recent developments.* IEEE Transactions on Dielectrics and Electrical Insulation, **2010**. 17(4): p. 1106-1112.

21. Zhang, Q.M.*, et al.*, *Giant Electrostriction and Relaxor Ferroelectric Behavior in Electron-Irradiated Poly(vinylidene fluoride-trifluoroethylene) Copolymer.* Science, **1998**. 280(5372): p. 2101.

22. Parangusan, H.*, et al.*, *Stretchable Electrospun PVDF-HFP/Co-ZnO Nanofibers as Piezoelectric Nanogenerators.* Scientific Reports, **2018**. 8(1): p. 754.

23. Tohluebaji, N.*, et al.*, *High Electromechanical Deformation Based on Structural Beta-Phase Content and Electrostrictive Properties of Electrospun Poly(vinylidene fluoride- hexafluoropropylene) Nanofibers.* Polymers, **2019**. 11(11): p. 1817.

24. Sencadas, V.*, et al.*, *Characterization of poled and non-poled β-PVDF films using thermal analysis techniques.* Thermochimica Acta, **2004**. 424(1): p. 201-207.

25. Tan, S.*, et al.*, *Significantly improving dielectric and energy storage properties via uniaxially stretching crosslinked P(VDF-co-TrFE) films.* Journal of Materials Chemistry A, **2013**. 1(35): p. 10353-10361.

26. Zouari, I.*, et al.*, *Structural, dielectric, piezoelectric, ferroelectric and electro-caloric properties of $Ba_{1-x}Ca_xTi_{0.975}(Nb_{0.5}Yb_{0.5})_{0.025}O_3$ lead-free ceramics.* Ceramics International, **2018**. 44(7): p. 8018-8025.

27. Thakur, P*., et al.*, *The role of cerium(iii)/yttrium(iii) nitrate hexahydrate salts on electroactive β phase nucleation and dielectric properties of poly(vinylidene fluoride) thin films.* RSC Advances, **2015**. 5(36): p. 28487-28496.

28. Putson, C*., et al.*, *Effect of Micro- and Nano-Particle Fillers at Low Percolation Threshold on the Dielectric and Mechanical Properties of Polyurethane/Copper Composites.* Journal of Inorganic and Organometallic Polymers and Materials, **2012**. 22(6): p. 1300-1307.

29. Kushwah, M*., et al.*, *Dielectric, pyroelectric and polarization behavior of polyvinylidene fluoride (PVDF) - Gold nanoparticles (AuNPs) nanocomposites.* Vacuum, **2019**. 166: p. 298-306.

30. Frens, G., *Controlled Nucleation for the Regulation of the Particle Size in Monodisperse Gold Suspensions.* Nature Physical Science, **1973**. 241(105): p. 20-22.

31. Zhou, Y*., et al.*, *Selective and sensitive colorimetric sensor of mercury (II) based on gold nanoparticles and 4-mercaptophenylboronic acid.* Sensors and Actuators B: Chemical, **2014**. 196: p. 106-111.

32. Peräntie, J*., et al.*, *Electric-field-induced dielectric and temperature changes in a ⟨011⟩-oriented $Pb(Mg_{1/3}Nb_{2/3})O_3$-PbTiO$_3$ single crystal.* Physical Review B, **2010**. 82(13): p. 134119.

33. Fulanović, L*., et al.*, *Relation between dielectric permittivity and electrocaloric effect under high electric fields in the $Pb(Mg_{1/3}Nb_{2/3})O_3$-based ceramics.* Journal of Applied Physics, **2020**. 127(18): p. 184102.

34. Jian, X.-D., *et al.*, *Enhanced Electrocaloric Effect in Sr^{2+}-Modified Lead-Free BaZr$_x$Ti$_{1-x}$O$_3$ Ceramics.* ACS Applied Materials & Interfaces, **2019**. 11(22): p. 20167-20173.

35. Shan, D.L., *et al.*, *Large electrocaloric response over a broad temperature range near room temperature in Ba$_x$Sr$_{1-x}$TiO$_3$ single crystals.* Journal of Applied Physics, **2019**. 126(20): p. 204103.

36. Belkhadir, S., *et al.*, *Structural, dielectric and electrocaloric properties of (Ba$_{0.8}$5Ca$_{0.15}$)(Ti$_{0.9}$Zr$_{0.1-x}$Sn$_x$)O$_3$ ceramics elaborated by sol–gel method.* Journal of Materials Science: Materials in Electronics, **2019**. 30(15): p. 14099-14111.

37. Wang, H., *et al.*, *The primary and secondary electrocaloric effect at ferroelectric-ferroelectric transitions in lead-free ceramics.* Scripta Materialia, **2020**. 178: p. 150-154.

38. Zeng, S.-M., *et al.*, *Electrocaloric effect and pyroelectric properties in Ce-doped BaCe$_x$Ti$_{1-x}$O$_3$ ceramics.* Journal of Alloys and Compounds, **2019**. 776: p. 731-739.

39. Bao, Y., *et al.*, *The phase structure and dielectric properties around a new type of phase boundary in a lead ytterbium niobite based solid solution.* Dalton Transactions, **2019**. 48(47): p. 17644-17654.

40. Wang, W., *et al.*, *Tailoring the negative electrocaloric effect of PbZrO$_3$ antiferroelectric thin films by Yb doping.* Journal of Alloys and Compounds, **2020**. 830: p. 154581.

41. Co, K., *et al.*, *Electrocaloric and pyroelectric properties of barium zirconate titanate.* Journal of Applied Physics, **2020**. 127(17): p. 174102.

42. Shvartsman, V.V., *et al.*, *Diffuse phase transition in BaTi$_{1-x}$Sn$_x$O$_3$ ceramics: An intermediate state between ferroelectric and relaxor behavior.* Journal of Applied Physics, **2006**. 99(12): p. 124111.

43. Zhao, Y., *et al.*, *Effect of phase transition on electrocaloric effect in Indium substituted BaTiO$_3$ ceramics.* Journal of Alloys and Compounds, **2020**. 822: p. 153632.

44. Jankowska-Sumara, I., *et al.*, *Electrocaloric effect in pure and Cr doped lead germanate single crystals.* Materials Chemistry and Physics, **2020**. 242: p. 122494.

45. Wang, J., *et al.*, *Enhanced electrocaloric effect in a Si-doped PbZr$_{0.95}$Ti$_{0.05}$O$_3$ film deposited on FTO substrate.* Applied Physics Letters, **2019**. 115(5): p. 053901.

46. Turki, O., *et al.*, *Enhancement of dielectric, piezoelectric, ferroelectric, and electrocaloric properties in slightly doped (Na$_{0.5}$Bi$_{0.5}$)$_{0.94}$Ba$_{0.06}$TiO$_3$ ceramic by samarium.* Journal of Applied Physics, **2019**. 125(17): p. 174103.

47. Kumar, R., *et al.*, *Enhanced electrocaloric response and high energy-storage properties in lead-free (1-x) (K$_{0.5}$Na$_{0.5}$)NbO$_3$ - xSrZrO$_3$ nanocrystalline ceramics.* Journal of Alloys and Compounds, **2018**. 764: p. 289-294.

48. Mendez-González, Y., *et al.*, *Improved electrocaloric properties in La doped (Bi$_{0.5}$Na$_{0.5}$)$_{0.92}$Ba$_{0.08}$TiO$_3$ lead-free ceramics.* Applied Physics Letters, **2019**. 114(16): p. 162902.

49. Zhao, X., *et al.*, *A thermodynamic study of phase transitions and electrocaloric properties of K$_{0.5}$Na$_{0.5}$NbO$_3$ single crystals.* Applied Physics Letters, **2020**. 116(9): p. 092902.

50. Martins, P.*, et al.*, *Electroactive phases of poly(vinylidene fluoride): Determination, processing and applications.* Progress in Polymer Science, **2014**. 39(4): p. 683-706.

51. Cai, X.*, et al.*, *A critical analysis of the α, β and γ phases in poly(vinylidene fluoride) using FTIR.* RSC Advances, **2017**. 7(25): p. 15382-15389.

52. Ameduri, B., *From Vinylidene Fluoride (VDF) to the Applications of VDF-Containing Polymers and Copolymers: Recent Developments and Future Trends.* Chemical Reviews, **2009**. 109(12): p. 6632-6686.

53. Gregorio Jr., R., *Determination of the α, β, and γ crystalline phases of poly(vinylidene fluoride) films prepared at different conditions.* Journal of Applied Polymer Science, **2006**. 100(4): p. 3272-3279.

54. Prateek*, et al.*, *Recent Progress on Ferroelectric Polymer-Based Nanocomposites for High Energy Density Capacitors: Synthesis, Dielectric Properties, and Future Aspects.* Chemical Reviews, **2016**. 116(7): p. 4260-4317.

55. Gregorio, R.*, et al.*, *Effect of crystalline phase, orientation and temperature on the dielectric properties of poly (vinylidene fluoride) (PVDF).* Journal of Materials Science, **1999**. 34(18): p. 4489-4500.

56. Ruggiero, E.*, et al.*, *Structural and dielectric properties of hot-pressed poly(vinylidene fluoride)-based composites.* Journal of Composite Materials, **2017**. 0(0): p. 0021998317723967.

57. Pei, J.*, et al.*, *Effect of preparation techniques on structural and electrical properties of PZT/PVDF composites.* Materials Express, **2017**. 7(3): p. 180-188.

58. Meng, N.*, et al.*, *Crystallization kinetics and enhanced dielectric properties of free standing lead-free PVDF based composite films.* Polymer, **2017**. 121(Supplement C): p. 88-96.

59. Abdullah, I.Y.*, et al.*, *Enhancement piezoelectricity in poly(vinylidene fluoride) by filler piezoceramics lead-free potassium sodium niobate (KNN).* Optical and Quantum Electronics, **2016**. 48(2): p. 149.

60. Mahdi, R.I.*, et al.*, *Piezoelectric and pyroelectric properties of BNT-base ternary lead-free ceramic-polymer nanocomposites under different poling conditions.* RSC Advances, **2016**. 6(84): p. 81296-81309.

61. Gaur, A.*, et al.*, *Processing and nanoclay induced piezoelectricity in poly(vinylidene fluoride-co-hexafluoro propylene) nanohybrid for device application.* Polymer, **2016**. 97(Supplement C): p. 362-369.

62. Tiwari, V.K.*, et al.*, *Thin and surface adhesive ferroelectric poly(vinylidene fluoride) films with β phase-inducing amino modified porous silica nanofillers.* Journal of Polymer Science Part B: Polymer Physics, **2016**. 54(23): p. 2401-2411.

63. Guggilla, P.*, et al.*, *Dielectric Behavior of Lithium Tantalate (LiTaO$_3$)/Poly(vinylidene fluoride) (PVDF) Nanocomposites Doped with MWCNTs.* Advanced Science, Engineering and Medicine, **2017**. 9(3): p. 204-208.

64. Guggilla, P.*, et al.*, *Dielectric, Conductance and Pyroelectric Characterization of MWCNT: PVDF Nanocomposite Thin Films for Multiple Device Applications.* International Journal of Composite Materials, **2016**. 6(5): p. 145-151.

65.   Lim, J.Y., *et al.*, *Enhancement of the ferroelectricity of poly(vinylidene fluoride)/multiwalled carbon nanotube composite scaffolds and its effect on the cellular metabolic activity.* Polymer, **2016**. 97(Supplement C): p. 465-471.

66.   Matea, A., *et al.*, *Optical properties of single-walled carbon nanotubes highly separated in semiconducting and metallic tubes functionalized with poly(vinylidene fluoride).* Journal of Molecular Structure, **2017**. 1130(Supplement C): p. 38-45.

67.   Kumar, G.S., *et al.*, *High dielectric permittivity and improved mechanical and thermal properties of poly(vinylidene fluoride) composites with low carbon nanotube content: effect of composite processing on phase behavior and dielectric properties.* Nanotechnology, **2016**. 27(38): p. 385702.

68.   Qamar, Z., *et al.*, *Reinforcement of electroactive characteristics in polyvinylidene fluoride electrospun nanofibers by intercalation of multi-walled carbon nanotubes.* Journal of Polymer Research, **2017**. 24(3): p. 39.

69.   Hosseini, S.M., *et al.*, *Electrospun PVDF/MWCNT/OMMT hybrid nanocomposites: preparation and characterization.* Iranian Polymer Journal, **2017**. 26(5): p. 331-339.

70.   Sharma, M., *et al.*, *Outstanding dielectric constant and piezoelectric coefficient in electrospun nanofiber mats of PVDF containing silver decorated multiwall carbon nanotubes: assessing through piezoresponse force microscopy.* RSC Advances, **2016**. 6(8): p. 6251-6258.

71.   Kripotou, S., *et al.*, *Effects of CNT inclusions on structure and dielectric properties of PVDF/CNT nanocomposites.* Phase Transitions, **2016**. 89(7-8): p. 717-730.

72.   Yuan, J.-K.*, et al.*, *Giant Dielectric Permittivity Nanocomposites: Realizing True Potential of Pristine Carbon Nanotubes in Polyvinylidene Fluoride Matrix through an Enhanced Interfacial Interaction.* The Journal of Physical Chemistry C, **2011**. 115(13): p. 5515-5521.

73.   Kar, E.*, et al.*, *Poly(vinylidene fluoride)/submicron graphite platelet composite: A smart, lightweight flexible material with significantly enhanced β polymorphism, dielectric and microwave shielding properties.* European Polymer Journal, **2017**. 90(Supplement C): p. 442-455.

74.   Yang, D.*, et al.*, *Dielectric properties and thermal conductivity of graphene nanoplatelet filled poly(vinylidene fluoride) (PVDF)/poly(methyl methacrylate) (PMMA) blend.* Journal of Materials Science: Materials in Electronics, **2017**. 28(17): p. 13006-13012.

75.   Shang, J.*, et al.*, *Fabrication and enhanced dielectric properties of graphene-polyvinylidene fluoride functional hybrid films with a polyaniline interlayer.* Journal of Materials Chemistry A, **2013**. 1(3): p. 884-890.

76.   Alhusaiki-Alghamdi, H.M., *Thermal and electrical properties of graphene incorporated into polyvinylidene fluoride/polymethyl methacrylate nanocomposites.* Polymer Composites, **2016**: p. n/a-n/a.

77.   Wojtaś, M.*, et al.*, *Dielectric properties of graphene oxide doped P(VDF-TrFE) films.* Polymer Testing, **2017**. 60(Supplement C): p. 326-332.

78.   He, L.*, et al.*, *Enhanced β Crystalline Phase in Poly(vinylidene fluoride) via the Incorporation of Graphene Oxide Sheets assisted by Supercritical CO_2 Treatment.* Journal of Macromolecular Science, Part B, **2016**. 55(5): p. 503-517.

79. Fakhri, P.*, et al.*, *Improved electroactive phase content and dielectric properties of flexible PVDF nanocomposite films filled with Au- and Cu-doped graphene oxide hybrid nanofiller.* Synthetic Metals, **2016**. 220(Supplement C): p. 653-660.

80. Babu, K.F.*, et al.*, *Thermal actuation properties of bimorph based on PVDF/rGO composites.* Composites Science and Technology, **2016**. 122(Supplement C): p. 82-89.

81. Hu, Y.-C.*, et al.*, *Enhance the Pyroelectricity of Polyvinylidene Fluoride by Graphene-Oxide Doping.* Sensors, **2014**. 14(4): p. 6877.

82. Sabira, K.*, et al.*, *Impressive nonlinear optical response exhibited by Poly(vinylidene fluoride) (PVDF)/reduced graphene oxide (RGO) nanocomposite films.* Optics & Laser Technology, **2017**. 97(Supplement C): p. 77-83.

83. Paik, H.*, et al.*, *Effect of Ag nanoparticle concentration on the electrical and ferroelectric properties of Ag/P(VDF-TrFE) composite films.* Scientific Reports, **2015**. 5: p. 13209.

84. Huang, X.*, et al.*, *Ferroelectric polymer/silver nanocomposites with high dielectric constant and high thermal conductivity.* Applied Physics Letters, **2009**. 95(24): p. 242901.

85. Phromviyo, N.*, et al.*, *Enhanced dielectric permittivity with retaining low loss in poly(vinylidene fluoride) by incorporating with Ag nanoparticles synthesized via hydrothermal method.* Applied Surface Science, **2018**.

86. da Silva, A.B.*, et al.*, *Novel composites of copper nanowire/PVDF with superior dielectric properties.* Polymer, **2014**. 55(1): p. 226-234.

87. Santos, J.P.F.*, et al.*, *Nanofibers of poly(vinylidene fluoride)/copper nanowire: Microstructural analysis and dielectric behavior.* European Polymer Journal, **2018**. 101: p. 46-55.

88. Hoque, N.A.*, et al.*, *Er^{3+}/Fe^{3+} Stimulated Electroactive, Visible Light Emitting, and High Dielectric Flexible PVDF Film Based Piezoelectric Nanogenerators: A Simple and Superior Self-Powered Energy Harvester with Remarkable Power Density.* ACS Applied Materials & Interfaces, **2017**. 9(27): p. 23048-23059.

89. Tsutsumi, N.*, et al.*, *Nature of the Enhancement in Ferroelectric Properties by Gold Nanoparticles in Vinylidene Fluoride and Trifluoroethylene Copolymer.* ACS Applied Materials & Interfaces, **2016**. 8(26): p. 16816-16822.

90. Hassen, A.*, et al.*, *Dielectric relaxation and alternating current conductivity of polyvinylidene fluoride doped with lanthanum chloride.* Journal of Applied Physics, **2011**. 110(11): p. 114119.

91. El-Sayed, S.*, et al.*, *Dielectric properties of PVDF thin films doped with 3 wt.% of RCl_3 (R = Gd or Er).* AIP Advances, **2014**. 4(3): p. 037114.

92. Silva, M.C.*, et al.*, *Structural and spectroscopic characterization of poly(styrene sulfonate) films doped with neodymium ions.* Journal of Non-Crystalline Solids, **2008**. 354(52): p. 5496-5503.

93. Jiang, J.*, et al.*, *Ultrahigh discharge efficiency in multilayered polymer nanocomposites of high energy density.* Energy Storage Materials, **2019**. 18: p. 213-221.

94. Chen, Y.*, et al.*, *An All-Scale Hierarchical Architecture Induces Colossal Room-Temperature Electrocaloric Effect at Ultralow Electric Field in Polymer Nanocomposites.* Advanced Materials, **2020**. n/a(n/a): p. 1907927.

95. Yang, L., *et al.*, *Graphene enabled percolative nanocomposites with large electrocaloric efficient under low electric fields over a broad temperature range.* Nano Energy, **2016**. 22: p. 461-467.

96. Lu, Y.-C., *et al.*, *Enhanced electrocaloric effect for refrigeration in lead-free polymer composite films with an optimal filler loading.* Applied Physics Letters, **2019**. 114(23): p. 233901.

97. Qian, J., *et al.*, *Interfacial Coupling Boosts Giant Electrocaloric Effects in Relaxor Polymer Nanocomposites: In Situ Characterization and Phase-Field Simulation.* Advanced Materials, **2019**. 31(5): p. 1801949.

98. Tsangaris, G.M., *et al.*, *Electric modulus and interfacial polarization in composite polymeric systems.* Journal of Materials Science, **1998**. 33(8): p. 2027-2037.

99. Zhang, G., *et al.*, *Nanoconfinement-Induced Giant Electrocaloric Effect in Ferroelectric Polymer Nanowire Array Integrated with Aluminum Oxide Membrane to Exhibit Record Cooling Power Density.* Advanced Materials, **2019**. 31(8): p. 1806642.

100. Liu, Y., *et al.*, *High cyclic stability of electrocaloric effect in relaxor poly(vinylidene fluoride-trifluoroethylene-chlorofluoroethylene) terpolymers in the absence of ferroelectric phase transition.* Journal of Applied Physics, **2019**. 126(23): p. 234102.

101. Aziguli, H., *et al.*, *Tuning the electrocaloric reversibility in ferroelectric copolymers by a blend approach.* EPL (Europhysics Letters), **2019**. 125(5): p. 57001.

102.   Wu, M._, et al._, *Remarkably Enhanced Negative Electrocaloric Effect in PbZrO3 Thin Film by Interface Engineering.* ACS Applied Materials & Interfaces, **2019**. 11(40): p. 36863-36870.

103.   Gavrilov, G.A._, et al._, *Interrelation of electrocaloric and concomitant effects in lead magnesium niobate based ceramics.* Journal of Materials Science, **2020**. 55(16): p. 6783-6793.

104.   Zhao, C._, et al._, *Broad-temperature-span and large electrocaloric effect in lead-free ceramics utilizing successive and metastable phase transitions.* Journal of Materials Chemistry A, **2019**. 7(44): p. 25526-25536.

105.   Wu, M._, et al._, *Electrocaloric effect in ferroelectric ceramics with point defects.* Applied Physics Letters, **2019**. 114(14): p. 142901.

106.   Hou, Y._, et al._, *Interfacial coupling modulation to the electrocaloric effect of Ba(Zr, Ti)O3 multilayered thick films.* Journal of Applied Physics, **2019**. 125(21): p. 214105.

107.   Zhong, K._, et al._, *Polymer Nanocomposites for Dielectrics*. Vol. 1. **2017**, Singapore: Pan Stanford Publishing Pte. Ltd: CRC Press. 208.

108.   Thakur, P._, et al._, *Enhancement of beta phase crystallization and dielectric behavior of kaolinite/halloysite modified poly(vinylidene fluoride) thin films.* Applied Clay Science, **2014**. 99: p. 149-159.

109.   Thakur, P._, et al._, *Effect of in situ synthesized Fe_2O_3 and Co_3O_4 nanoparticles on electroactive β phase crystallization and dielectric properties of poly(vinylidene fluoride) thin films.* Physical Chemistry Chemical Physics, **2015**. 17(2): p. 1368-1378.

110. Thakur, P.*, et al.*, *The role of cerium(iii)/yttrium(iii) nitrate hexahydrate salts on electroactive β phase nucleation and dielectric properties of poly(vinylidene fluoride) thin films*. RSC Advances, **2015**. 5(36): p. 28487-28496.

111. Sukwisute, P.*, et al.*, *Micropower energy harvesting using poly(vinylidene fluoride hexafluoropropylene)*. Applied Physics Letters, **2013**. 103(6): p. 063905.

112. He, Z.*, et al.*, *Gel electrolytes based on poly(vinylidenefluoride-co-hexafluoropropylene)/thermoplastic polyurethane/poly(methyl methacrylate) with in situ SiO_2 for polymer lithium batteries*. RSC Advances, **2017**. 7(6): p. 3240-3248.

113. Chen, J.*, et al.*, *Ultrahigh discharge efficiency and energy density achieved at low electric fields in sandwich-structured polymer films containing dielectric elastomers*. Journal of Materials Chemistry A, **2019**. 7(8): p. 3729-3736.

114. Gao, J.*, et al.*, *Enhanced antiferroelectric phase stability in La-doped $AgNbO_3$: perspectives from the microstructure to energy storage properties*. Journal of Materials Chemistry A, **2019**. 7(5): p. 2225-2232.

115. Yin, J.*, et al.*, *Enhanced energy storage properties of $\{Bi_{0.5}[(Na_{0.8}K_{0.2})_{1-z}Li_z]_{0.5}\}_{0.96}Sr_{0.04}(Ti_{1-x-y}Ta_xNb_y)O_3$ lead-free ceramics*. Ceramics International, **2017**. 43(16): p. 13541-13546.

116. Liang, Z.*, et al.*, *Flexible lead-free oxide film capacitors with ultrahigh energy storage performances in extremely wide operating temperature*. Nano Energy, **2019**. 57: p. 519-527.

117. Li, L.*, et al.*, *Studies on the transformation process of PVDF from α to β phase by stretching*. RSC Advances, **2014**. 4(8): p. 3938-3943.

118. Gregorio, J.R.*, et al.*, *Effect of crystallization temperature on the crystalline phase content and morphology of poly(vinylidene fluoride).* Journal of Polymer Science Part B: Polymer Physics, **1994**. 32(5): p. 859-870.

119. Martins, P.*, et al.*, *On the origin of the electroactive poly(vinylidene fluoride) β-phase nucleation by ferrite nanoparticles via surface electrostatic interactions.* CrystEngComm, **2012**. 14(8): p. 2807-2811.

120. Patro, T.U.*, et al.*, *Studies on poly(vinylidene fluoride)–clay nanocomposites: Effect of different clay modifiers.* Polymer, **2008**. 49(16): p. 3486-3499.

121. Scherrer, P., *Bestimmung der Größe und der inneren Struktur von Kolloidteilchen mittels Röntgenstrahlen.* Nachrichten von der Gesellschaft der Wissenschaften zu Göttingen, Mathematisch-Physikalische Klasse, **1918**. 1918: p. 98-100.

APPENDICES

APPENDIX A

Paper I [published]; "The microstructure of negative electrocaloric Polyvinylidene fluoride-hexafluoropropylene copolymer on graphene loading for eco-friendly cooling technology"

The microstructure of negative electrocaloric Polyvinylidene fluoride-hexafluoropropylene copolymer on graphene loading for eco-friendly cooling technology

Ahamad Salea, Suphita Chaipo, Ardian Agus Permana, Kunthisa Jehlaeh, Chatchai Putson[*]

Materials-Physics Laboratory, Physics Department, Faculty of Science, Prince of Songkla University, Songkhla, 90112, Thailand

A B S T R A C T

Extraordinarily negative electrocaloric materials are desirable for environment-friendly cooling applications. Stretched and unstretched Polyvinylidene fluoride-hexafluoropropylene thin films with suitable graphene contents have been studied in this work. The thin films were fabricated by solution casting method. Crystallinity was induced by stretching technique resulting a translucent film, with increasing dielectric constant, dielectric loss, conductivity and ferroelectric properties. By increasing the filler content, the maximum negative temperature change was intensified, and Curie temperature was decreased by 20 °C. However, a good electrocaloric effect was achieved without stretching, although stretching could stabilize Curie temperature to a smooth curve. The best performance in this work was found with graphene of 1 wt% (weight fraction of 0.01), which had an enhanced electrocaloric effect with a potential for electrocaloric cooling applications.

© 2019 Elsevier Ltd. All rights reserved.

1. Introduction

Cooling systems are very important in various applications to increase heat transfer rates. The conventional cooling systems used in refrigeration and air conditioning might be replaced by novel technologies. Electrocaloric cooling (ECC) is recently interesting as innovative cooling system with green technology that releases no CFC emissions (Goupil et al., 2012; Scott, 2011). It has high energy conversion efficiency that is better than conventional cooling (Pakhomov et al., 2010). ECC can be potentially applied in microelectronic circuits, integrated circuit (ICs), automobiles, air-conditioners and refrigerators. ECC is based on both electrocaloric and pyroelectric effects, stemming from the cross-coupling of temperature and polarization change in an insulating dielectric material. The mechanism of electrocaloric effect (ECE) is started with heat energy that can be released or absorbed by applied electric field. As the consequence, it can reorient the dipole moments on the material. On the other hand, the reversed way of that

phenomenon called pyroelectric effect that still obeying Maxwell relations (Lines and Glass, 1977). ECC has been found in insulating dielectric-ferroelectric materials. In ferroelectric materials, ECE can be observed in term of the changing of both entropy (ΔS) and temperature (ΔT) when applying external electric field (E). The highest ΔT is usually found near the phase transition temperature or Curie temperature (T_c). A large ΔT with comparatively small E is beneficial for ECE. Moreover, large dielectric constant (ε_r) with small dielectric loss ($\varepsilon_r^{"}$) are desired for ECE according to the Maxwell relations.

ECE materials have been extensively applied to the innovative electrocaloric cooling system in particular high electrocaloric efficiency regarded to the ferroelectric ceramic, namely positive ECE such as BaTiO$_3$ with $\Delta T = 1.6$ K (1 MV/m) (Bai et al., 2012), Pb$_{0.97}$La$_{0.02}$(Zr$_{0.66}$Sn$_{0.23}$Ti$_{0.11}$)O$_3$ with $\Delta T = 0.6$ K (30 MV/m) (Zhuo et al., 2017), and negative ECE such as (Pb$_{0.88}$Sr$_{0.08}$)[Nb$_{0.08}$(Zr$_{0.53}$Ti$_{0.47}$)$_{0.92}$]O$_3$ with $\Delta T = -0.38$ K (1.5 MV/m) (Chen et al., 2017), NBT with $\Delta T = -1.6$ K (7 MV/m) (Jiang et al., 2014), Pb$_{0.97}$La$_{0.02}$(Zr$_{0.80}$Sn$_{0.14}$Ti$_{0.06}$)O$_3$ with $\Delta T = -5.5$ K (11 MV/m) (Zhuo et al., 2018), etc. It found that most of ferroelectric ceramic have love electrical breakdown. This is the main disadvantages to consider on ferroelectric ceramic, requiring low ΔS and ΔT,

* Corresponding author.
  E-mail address: chatchai.p@psu.ac.th (C. Putson).

respectively. The brittle and heavyweight are also another disadvantages to fabricate thin film. Recently, the ceramics are replaced with polymers due to they are flexible, modifier shape, lightweight, easy to process and low cost. Importantly, the larger electrical breakdown of ferroelectric polymer is a key point to enlarge ΔT for electrocaloric performances, such as P(VDF-TrFE)55/45 with $\Delta T = 12.6$ K (209 MV/m) (Neese et al., 2008).

However, not many research to date has focused on the ferroelectric polymers (Neese et al., 2008), i.e. Polyvinylidene Fluoride (PVDF) ferroelectric polymers or PVDF family. PVDF is a semicrystalline polymer containing Fluorine (F), Hydrogen (H), and a Carbon (C) backbone in the units $-(C_2H_2F_2)_n-$. β phase (TTTT conformation) has the most dipoles in PVDF, giving large net dipole moment, polarization, and dielectric constant, and producing a large ECE (Lu et al., 2011). Polyvinylidene fluoride-hexafluoropropylene (PVDF-HFP) is also one of interesting PVDF family that possess some advantages such as good flexibility, chemically resistance, excellent electromechanical properties and low cost (He et al., 2005; Huan et al., 2007; Neese et al., 2007).

Many different approaches have been proposed to improve this performance. Tailored polarization by electron-beam or gamma irradiation (Bauer, 2010; Parangusan et al., 2018b; Zhang et al., 1998), self-rearranged polarization by electrospinning (Parangusan et al., 2018a; Tohluebaji et al., 2019), rearranged polarization by poling at given temperature (Sencadas et al., 2004), modified crystal structure by stretching technique at given temperature (Tan et al., 2013), combination of polar and charge distributions on polymer composite by adding filler (Choolaei et al., 2017), are examples. However, stretching technique and adding filler are the most convenient way to improve these properties without using advanced tools as gamma source and high voltage. The combination of stretching technique and polymer composite by adding filler are interesting to study.

Stretching is one of technique to improve the configuration of the dipoles (Salimi and Yousefi, 2003). It has improved on dielectric and ferroelectric properties. S. Tan and coworkers (Tan et al., 2013) studied the reduction of crystallite size on stretched films and his results agree with other author's finding in this area (He et al., 2016; Zhao et al., 2009). He provided an improving dielectric and ferroelectric properties of stretched PVDF-TrFE film. He highlighted that the stretched films reduce crystallite size, improve crystal orientation polarization and overall crystallinity. As a result, they exhibited a dramatic increased dielectric constant, slightly increased dielectric loss, and smaller remnant polarization (P_r) as slimmer ferroelectric loop with enhanced relaxation speed of crystal grains. So far researchers have only found innovative ways to relate crystallite size reduction with dielectric and ferroelectric properties, but in this paper make a further contribution by showing that crystallinity reduction improve electrocaloric behavior.

On the other hand, many researches have been occurred on PVDF polymer with nanofillers. V. Goodarzi and coworkers (Goodarzi et al., 2014) studied nanofiller effect on crystallization behavior on mechanical PVDF nanocomposites properties. They found that the nanocomposite has a small greater than the pure polymer. V. Goodarzi continuously confirmed the effect on semicrystalline PVDF-HFP structure by adding LDH nanoparticles filler (Shojaei et al., 2018). They proved that most of crystallite size on PVDF-HFP are decreased with LDH loading. As yet, a solution of crystallite size effect on ECE has not found, although ECE have been made. Furtherly, they investigated the crystallite sizes of PVDF-HFP copolymer filled by Graphene Oxide (GO) (Choolaei et al., 2017). As a result, the crystallite size on β phase decreased by increasing GO content. It seems that crystal growth in a particular crystallographic direction is against by GO nanoparticle.

Besides GO, Graphene nanoplatelets is one of graphene family materials that have electrical and thermal conductor. Some works about graphene nanoplatelets have been reported on fluid heat transfer system (Bahiraei and Heshmatian, 2019; Bahiraei and Mazaheri, 2018; Bahiraei et al., 2019). The graphene nanoplatelets is clearly improved heat transfer efficiency, showing at the highest graphene concentration on that graphene nanofluid system. Besides its excellent properties on heat transfer, it is also interesting to study graphene nanoplatelets effect on electrical properties. Since it is included as great electrical conductor, graphene family materials also have potential roles to induce electroactive phase on electroactive polymer with crystallite size reduction. As reported, electrical conductive filler of graphene are the most interesting for improving dielectric PVDF polymers compared with other fillers (Li et al., 2009, 2010; Yang et al., 2016)

The aim of the present work is to fabricate a stretched PVDF-HFP/graphene nanoplatelets by two techniques of stretching film and adding graphene nanofiller, and to find a new electrocaloric relation in the amount of crystallite size and crystallinity formed. PVDF-HFP was blended with graphene nanoplatelets by using solution casting technique. Appropriate graphene contents for ECE were sought. Saturation of the electrocaloric effect will determine the suitable filler content. Both unstretched and stretched samples are compared, assessing the PVDF-HFP microstructure effects. The results of the comparison between the effects of the two techniques (i.e., adding graphene and stretching) encourage and propose to relationship between the structure morphology, crystallinity (X_c), crystallite size, dielectric properties and electrocaloric behavior. This new relation will be able to design and predict the advanced capacitor and electrocaloric cooling system in future.

2. Materials and methods

Graphene nanoplatelets powder was purchased from Sigma-Aldrich Ltd, Singapore, having 12.01 g/mol (806633 ALDRICH), and was ultra-sonicated in 200 W N,N-dimethylformamide with $\geq$ 99% purity (DMF), from RCI Labscan Limited, Thailand, for 20 min to prevent formation of agglomerates. Then, it was mixed with Polyvinylidene fluoride-hexafluoropropylene P(VDF-HFP) powder from Solvay Solexis, Belgium with a 10 wt % HFP (Solef 11010/1001) and then stirred at 30 °C around 12 h to get homogeneous composites solution. Then, the composite solution was casted on glass plate with an adjustable film applicator (Sheen S/N 102503/2, Incl, Shims) before evaporating DMF by drying at 80 °C 12 h in the oven (Asset positively identifiable T410353 Binder). The thickness of each composites thin film was about 100 μm after peeled off from the glass plates. This step has to drop a few DI water when peeling the film out for preventing the crack formation on films. Afterwards, the thin films were observed before stretched with original length ratio (L/L_0) of four times, from 20 mm to 80 mm elongation length. The stretching rate of 2.5 mm/min was used by adjustable step motor at 100 °C to about 30 μm. A suitable stretching force and temperature could induce large X_c in this PVDF-HFP, as reported in a prior study (Sukwisute et al., 2013). The stretched composite thin films with graphene filler loadings of 1, 2, 3, 4 and 5 wt% (0.01, 0.02, 0.03, 0.04, and 0.05, respectively by weight fraction) in PVDF-HFP were labeled GPN1ST, GPN2ST, GPN3ST, GPN4ST, and GPN5ST, respectively. Similarly, GPN1NST, GPN2NST, GPN3NST, GPN4NST, and GPN5NST, by loading level, were the labels used for cast film samples of 30 μm thickness without stretching. Pure PVDF-HFP thin films, with and without stretching were labeled as pureST and pureNST, were compared as the control cases.

3. Results and discussion

3.1. Macroscopic structure

Surface Morphology. Graphene distribution on the surface of a composite thin film was detected by SEM (FEI Quanta 400, USA). As Fig. 1(a)-(b), stretching changed pure PVDF-HFP to translucent material. Possibly crystalline regions were formed by stretching (He et al., 2016; Tan et al., 2013). Fig. 1(c) presents the distribution of filler in PVDF-HFP in TEM images. The filler was well dispersed in the polymer. The white color represents the insulating PVDF-HFP polymer while the darker color regions are graphene particles in the sample of GPN1NST. The graphene filler was surrounded by semicrystalline PVDF-HFP, as seen in Fig. 1(d), having both crystalline and amorphous parts. Furthermore, graphene filler directly darkens the film in a manner dependent on graphene content.

XRD diffraction. Film composites were investigated by using an X-ray diffractometer (XRD, X'Pert MPD, Philips, Netherlands). The 2θ was scanned from 14° to 38° with 0.05° s^{-1} scaning rate by Cu–K radiation (wavelength 0.154 nm) under 40 kV voltage. The crystallite size (L) were calculated following Equation (1) by Scherrer (1918). Where λ, FWHM, and θ, are the X-ray wavelength (0.154 nm), the full width at half maximum for diffraction peaks, and the corresponding diffraction angle, respectively.

$$L_{2\theta}(nm) = \frac{0.91\lambda}{FWHM \cdot \cos\theta} \qquad (1)$$

An XRD patterns presents in Fig. 2(a). PureNST, pureST, GPN1ST, GPN2ST, GPN3ST, GPN4ST, and GPN5ST were investigated. The strongest diffraction on PVDF-HFP exhibits at 2θ = 20.5° of β phase with (110)/(200) crystallographic planes. Diffraction peak 2θ = 18.3° is associated with α phase (020) plane (Patro et al., 2008). The β phase (TTTT) produces the highest net polarization compared with α (TGTG′) and γ (TTTGTTTG′) phases.

XRD by filler loading. Graphene nanoplatelets diffraction at 2θ = 26.5° increased with graphene content. However, adding filler had not significantly observed crystallite size reduction in both 2θ of 18.3° and 20.5° (Fig. 2 (b)), while previous study reported crystallite size reduction by adding filler (Choolaei et al., 2017). In this work, a few interval of graphene content has not enough to significantly differentiate on crystallite size. For 2θ = 20.5°, GPN5ST seemed the biggest crystallite size (0.123 nm) compared with pureST (0.087 nm), GPN1ST (0.094 nm), GPN2ST (0.082 nm), GPN3ST (0.091 nm), and GPN4ST (0.081 nm) due to excessive filler. In fact, crystallite size can be reduced with modified PVDF fillers (Choolaei et al., 2017) and stretching (Tan et al., 2013).

XRD by stretched case. It is seen that stretching significantly decrease crystallite size for 2θ = 18.3°, as in Fig. 2(b). After stretching film, the crystallite size was considerably decreased from 0.507 nm of pureNST to 0.042 nm of pureST. The stretching force have possibly energy to cut crystallite size into smaller pieces. This tendency is matched with prior study (Tan et al., 2013). They explained that crystallite size is reduced after stretching PVDF

polymer with increasing crystallinity.

DSC analysis. To characterize the samples for thermal stability, Differential Scanning Calorimeter (DSC, Simultaneous Thermal Analyzer, STA8000, PerkinElmer, USA) was used. The heat was applied to the samples from 120 °C to 180 °C at 10.00 °C/min in ambient atmospheric air. This experiment can determine the melting temperature (T_m) around 160 °C. The thermal stability was observed from the area under the endothermic peak, i.e., the melting enthalpy (ΔH_m). The crystallinity (X_c) was calculated from Equation (2), where ∅ is the filler's weight fraction in the composites. ΔH_m and ΔH_m^0 are the observed enthalpy of melting and that for 100% crystalline PVDF-HFP, which equals 104.6 J g^{-1} (He et al., 2017).

$$X_c(\%) = \frac{\Delta H_m}{(1-\varnothing)\Delta H_m^0} \times 100 \qquad (2)$$

DSC by filler loading. Fig. 3(a-b) exhibits the DSC results, including X_c (Fig. 3(c)) and T_m (Fig. 3(d)). It is seen that X_c and T_m increase with graphene content until they reach a peak in 2–3 wt%. Afterwards they gradually decreased at 4–5 wt%, because excessive filler decreased X_c along with T_m. In addition, X_c of GPN5ST suddenly dropped to 44.91%, whereas crystallite size on 2θ = 20.5° increased, seen in XRD result. It can seem that excessive filler of GPN5ST decreases X_c and increases crystallite size.

DSC by stretched case. It seems that the stretched films produce higher X_c, seen in Fig. 3(c). Stretching possibly changes the amorphous to crystalline phase in polymer causing unstable crystalline phase, matching translucent in Fig. 1(a–b). T_m seemly decreased after stretching. It is possibly that stretching force induced overall X_c and reduced the crystallite size, resulting to increase X_c and decrease T_m, respectively. The result is in agreement with a prior study (Fatou, 1971; Sukwisute et al., 2013; Tan et al., 2013). After stretching, X_c reduction on 5 wt% graphene is possibly the maximum limit in this work.

3.2. Dielectric properties

The samples were measured for dielectric properties across frequencies from 1 to 10^5 Hz by using an IM 3533 LCR meter (HIOKI, Japan) by setting the voltage across sample of 1 V ac, with 5 mm diameter electrodes and 30 μm sample thickness. The capacitance (C), loss tangent or dielectric loss ($\varepsilon_r^{"}$), and electrical conductivity (σ_{ac}) were recorded at room temperature. Subsequently, dielectric constant (ε_r) and σ_{ac} were calculated from Equations (3) and (4), respectively. Here d refers to the thickness, A refers to the electrode area, f refers to the ac frequency in Hz, and ε_0 refers to free space permittivity equaling 8.853 × 10^{-12} F m^{-1} (Thakur et al., 2015). The ε_r, $\varepsilon_r^{"}$, and σ_{ac} for unstretched and stretched samples are shown in Fig. 4(a-c), (d-f), and (g-i), respectively.

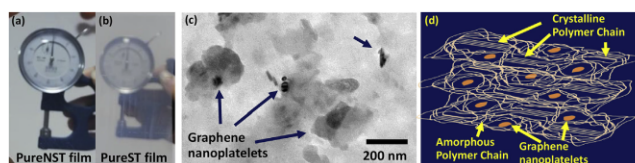$$\varepsilon_r = Cd/\varepsilon_0 A \qquad (3)$$

Fig. 1. Appearances of a pure PVDF-HFP film when (a) unstretched and (b) stretched. The composite film structure in (c) TEM image of the GPN1NST, (d) schematic idealization.
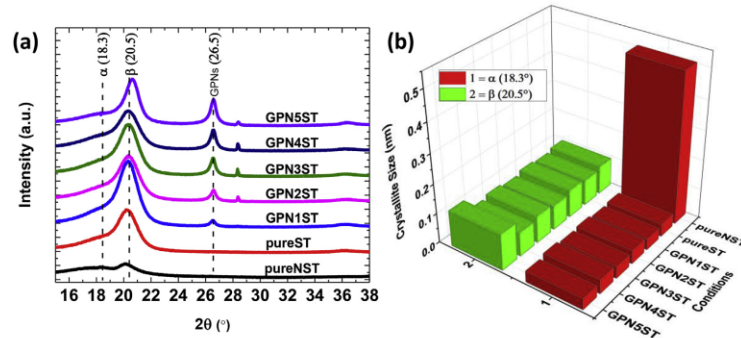
Fig. 2. (a) XRD diffraction at $2\theta = 15°-38°$ of pureNST, pureST, GPN1ST, GPN2ST, GPN3ST, GPN4ST, and GPN5ST, (b) crystallite size of PVDF-HFP at $2\theta = 18.3°$ and $20.5°$, referring to α and β phases.
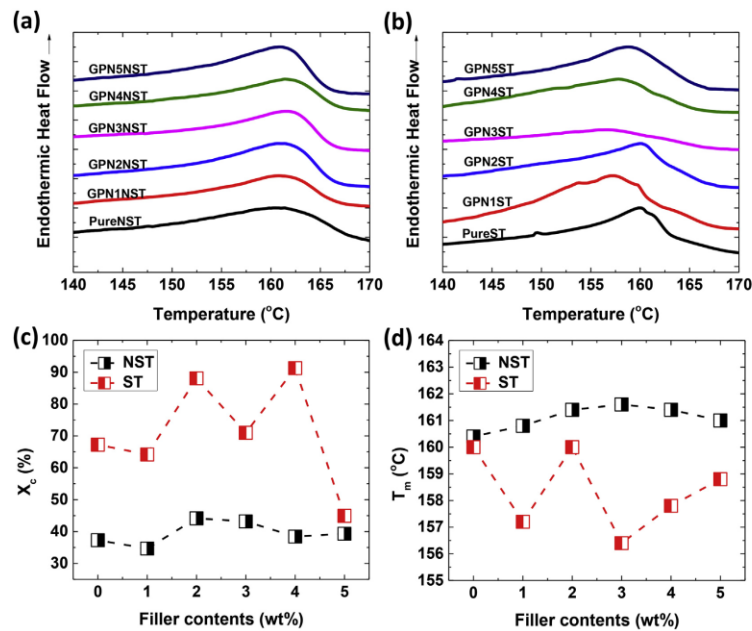
Fig. 3. DSC thermographs of (a) unstretched, and (b) stretched thin film composites, and dependence of (c) X_c, and (d) T_m on filler loading.

$$\sigma_{ac} = 2\pi f \varepsilon_0 \varepsilon_r \varepsilon_r^{''} \quad (4)$$

The ε_r at various frequencies is seen in Fig. 4(a)–(b) for unstretched and stretched cases with various filler contents. The orientational polarizability is represent by ε_r that generally decreases with frequency (Kasap, 2006). The dipoles could rapidly reorient following the alternating electric field at comparatively low frequencies, giving the maximum ε_r. In contrast, when the electric field changes too rapidly at high frequencies, the dipoles could not follow it. As a result, the ε_r decreased with frequency. The interfacial polarization effects is explained by the Maxwell-Wagner-Sillars (MWS) theory (Tsangaris et al., 1998). The ε_r at high graphene loadings of 3–5 wt% was increased at any frequency, while the films with 1 or 2 wt% graphene produce lower ε_r than pure PVDF-HFP at

Fig. 4. Dielectric properties of composite thin films with graphene filler in PVDF-HFP in unstretched and stretched cases. Dielectric constant against frequency for (a) unstretched films, and (b) stretched films, and (c) dielectric constant by filler loading at 1 Hz. (d)–(f) dielectric loss, (g)–(i) conductivity in similar plots.
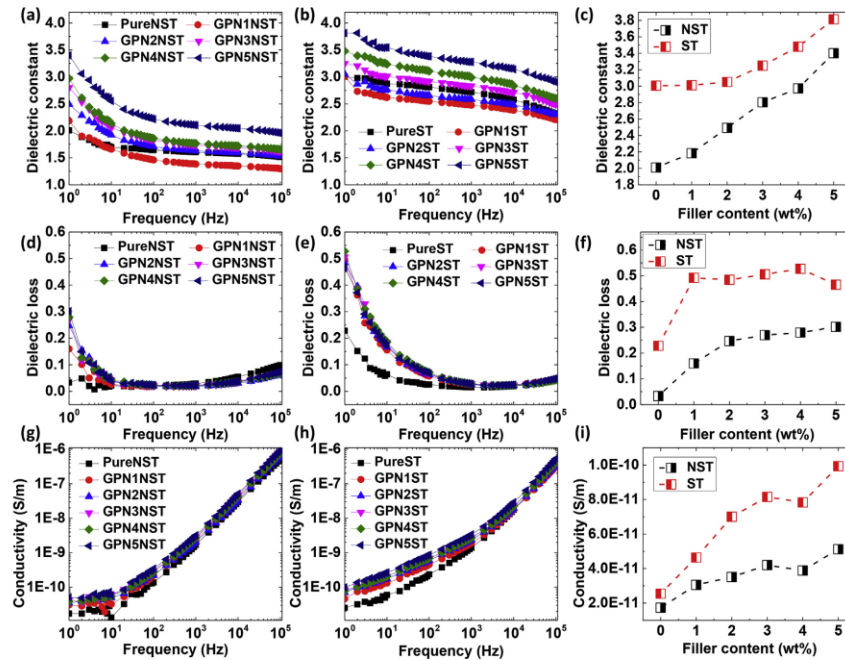
high frequencies. The largest ε_r (at 1 Hz) is shown in Fig. 4(c). According to these results, the ε_r increased with graphene content, likely because of enhanced interfacial polarization and improved the orientational polarizability of graphene charge, seen in Fig. 4. Moreover, excessive filler still increased ε_r although X_c decreased. The ε_r increase with conductive filler (Huang et al., 2009; Paik et al., 2015) is explained by the logarithmic law for heterogeneous phases (Lichtenecker, 1931). In addition, the $\varepsilon_r^{''}$ in Fig. 4(d−f) represents the energy loss as dipoles are oriented in an alternating electric field (Kasap, 2006). The $\varepsilon_r^{''}$ is decreased with frequency. Commonly the dipoles at low frequencies with an applied electric field give a high ε_r and $\varepsilon_r^{''}$ as well, while these both decrease with frequency. In Fig. 4(f), the $\varepsilon_r^{''}$ is increased with graphene content because of the effects on interfacial polarization, or MWS effect. The σ_{ac} was measured as shown in Fig. 4(g−i). It relates to the number of charge carriers, or electron mobility and electrical resistance in the heterogeneous dielectric material, which dissipates energy from the electric field to the heat. The σ_{ac} is increased with frequency and with graphene content. The lowest and highest σ_{ac} were observed for pure PVDF-HFP and 5 wt% filled case, respectively. The increase in σ_{ac} with frequency can be explained by hopping space-charges between the phases. The space charge mechanism is described by the MWS model (Tsangaris et al., 1998). When conductive graphene filler was added in PVDF-HFP, it generated a second phase in this material, making the composite heterogeneous and increasing σ_{ac}. This also increased the ε_r in a highly heterogeneous microstructure (Tsangaris et al., 1998). According to some prior studies (Ardimas

et al., 2018; Putson et al., 2012) adding a conductive filler into PU dielectric polymer increased the number of charge carries. In this current study, the 5 wt% loading, which produced the maximum σ_{ac}, was chosen for further experiments. In addition, stretching made a significant difference as seen in Fig. 4(e), (f), and (i). The stretched films have much larger ε_r, $\varepsilon_r^{''}$ and σ_{ac} than the unstretched films, caused by decreased crystallite size, improved the orientational polarizability of crystal domains (Tan et al., 2013), and increased overall X_c. As a result, the dielectric properties were improved.

The basic improvement of dielectric properties in both adding filler and stretching technique is crystallite size reduction. However, it seems that the majority influence of dielectric improvement on adding filler technique is conductive graphene loading.

3.3. Ferroelectric properties

The samples were measured for polarization and electric field measurements (P-E loop) using ferroelectric polarization loop and dielectric breakdown test system (PK-CPE1701, USA). The recoverable (U_e) and unrecoverable (U_l) energies are found from integrated areas of charge and discharge phases in Fig. 5. The energy storage efficiency of the materials can be evaluated from Equation (5). Remnant polarization (P_r, $\mu C/cm^2$) at 10 Hz frequency in 40 MV/m electric field was characterized using a Ferroelectric analyzer.

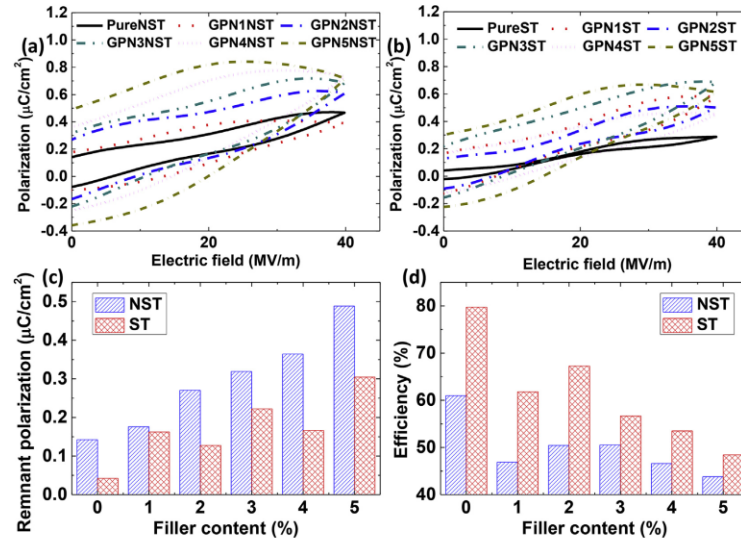$$Efficiency\ (\eta, \%) = U_e \times 100/(U_e + U_l) \tag{5}$$

Fig. 5. P–E loops (a) unstretched, and (b) stretched ferroelectric material composites with various filler contents. (c) Remnant polarization, and (d) efficiency.

Ferroelectric properties by filler loading. When the electric field is sufficiently high as 40 MV/m, P-E loops were occurred. P-E loops with various filler contents were showed by Fig. 5(a−b). The loops seem to be antiferroelectric being slim (Yang et al., 2013). Obviously the loop size changed to be bigger loop with graphene content, corresponding to give larger P_r as Fig. 5(c), give lesser U_e than U_l, and steadily produce low energy storage efficiency, η, as seen in Fig. 5(d). On the adding filler technique in PVDF-HFP ferroelectric polymer, the conductive graphene filler is seemly majority influences while the crystallite size reduction on adding filler is the minority influences, resulting in bigger loop from conductive filler instead of from crystallite size reduction. This reason is matched with the explanation of dielectric properties above. The disconnected initial-final P-E loop points were larger with graphene content. For example, at under zero external electric field (E = 0), the initial-final polarization is more disconnected because of the larger U_l from conductive graphene loading.

Ferroelectric properties of stretched samples. Comparing unstretched and stretched cases shows clear differences. The loops are totally seemed to be slimmer after stretching, correspond to smaller P_r, resulting greater U_e than U_l, and steadily produce high energy storage efficiency, η. On the stretching technique in PVDF-HFP ferroelectric polymer, the crystallite size reduction is seemly being main influences, resulting a narrower loop from crystallite size reduction. It was possible to describe that the crystallite size reduction is easy to switch the orientation polarization along the direction of the external electric field. It is causing the slimmer loops with enhanced relaxation speed of crystal grains, which is also corroborated by previous studies (He et al., 2016; Tan et al., 2013). This reason is matched with the explanation of dielectric properties above.

Basic improvement of slimmer ferroelectric loop in both adding filler and stretching technique is because of crystallite size reduction. However, it seems that the majority influence of bigger

ferroelectric loop on adding filler technique is the conductive graphene loading.

3.4. Electrocaloric properties

The P-E loops for each sample were recorded at temperatures from 30 to 140 °C in a controlled oven, to record P_r at 1 °C intervals. The slope at each point was calculated to obtain the adiabatic temperature change (ΔT) from Maxwell relations, according to Equations (6) and (7), where ΔS, P, T, ρ, C_E, and E are entropy change, polarization, temperature, density, specific heat capacity of PVDF-HFP (1600 J/kg/°C) and the electric field, respectively.

$$\Delta S = \int_{E_1}^{E_2} \left(\frac{\partial P}{\partial T}\right) dE \tag{6}$$

$$\Delta T = -\frac{1}{\rho C_E} \int_{E_1}^{E_2} T\left(\frac{\partial P}{\partial T}\right) dE \tag{7}$$

The loops became gradually larger with temperature as shown in supplementary material Fig. S1(a-b). The P_r then rapidly increased around 120 °C matching the T_c reported in a previous paper (Thetpraphi et al., 2015). Possibly, these samples show T_c from an anti-ferroelectric phase to normal loops of ferroelectric phase (Yang et al., 2013) resulting negative electrocaloric. The maximum ΔT (ΔT_max) is typically at T_c following Equations (6) and (7).

Electrocaloric properties by filler loading. Fig. 6(a-b) presents the relationship between ΔT and temperature with various filler contents. ΔT seems to be negatively electrocaloric effect. Practically, a negative ΔT_max directly intensified with graphene content at 1 wt%
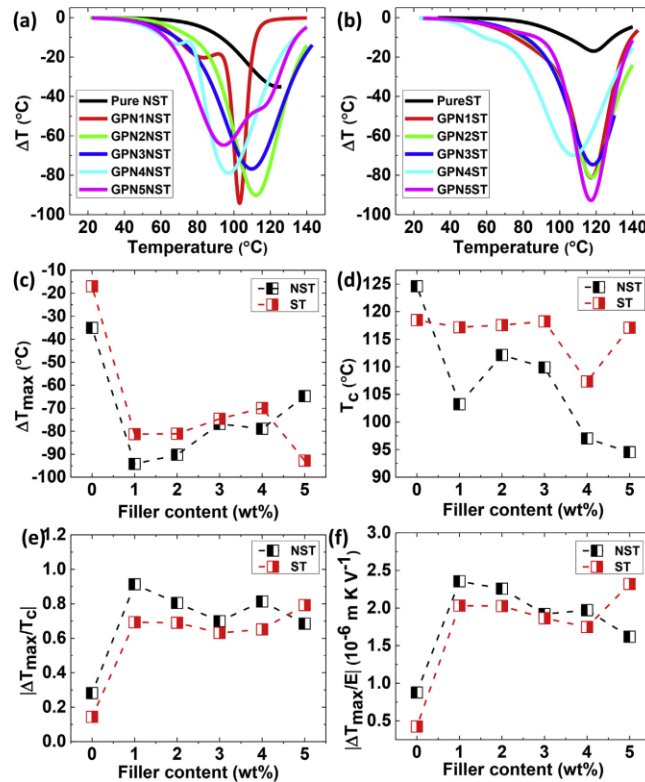
Fig. 6. Electrocaloric behavior with various graphene contents, (a)–(b) the negative ΔT of unstretched and stretched cases at various temperatures, (c) ΔT_{max}, (d) T_c, (e) $|\Delta T_{max}/T_c|$, and (f) $|\Delta T_{max}/E|$.

from -26 to -88 °C approximately and then slightly decreased to around -76 °C at 3 wt%, as seen in Fig. 6(c). The graphene fixed polymer chain to get a large net of dipole moment and made them easily following external E (free dipolar orientational polarizability). Consequently, they intensify negative ΔT_{max}. The T_c decreased with graphene content in Fig. 6(d), because graphene particle might able to slightly change anti-ferroelectric phase in PVDF-HFP to ferroelectric phase, in relation with a prior study (Zouari et al., 2018). Hence, T_c could be easily shifted at a lower temperature with increasing graphene content.

Electrocaloric properties of stretched cases. The unstretched and stretched cases differed in properties. Stretching was clearly effective in stabilizing T_c because of uniformity of dipolar orientational of polarizability that reducing the crystallite size and increasing the X_c. For example, the curves were smooth for 2, 4, and 5 wt% cases. The samples that producing maximum σ_{ac} that is larger than GPN5ST as Fig. 4(h), are unable to be measured because of easy to breakdown at high E (Chu et al., 2006). However, the negative ΔT_{max} reduced with stretching technique because of increased overall X_c for other filler contents, except 5 wt% as seen in

Fig. 6(c). The sample with 5 wt% graphene suddenly dropped overall X_c as in Fig. 3(c), giving a large negative ΔT_{max}. On the other hand, stretching slightly increased T_c because of larger overall X_c that hardly followed by E especially at the phase transition. Whereas, the unstretched cases had rapidly decreasing T_c in Fig. 6(d). The maximum of both absolute $|\Delta T_{max}/T_c|$ and $|\Delta T_{max}/E|$ were obtained especially with 1 wt% for both types of samples before the gradual decrease in Fig. 6(e)–(f). Excessive filler at 5 wt% with stretching eventually caused an improvement. For unstretched cases, less X_c had mostly better electrocaloric properties than the stretched cases. GPN1NST composites gave a large absolute $|\Delta T_{max}/E|$ value of about 2.36×10^{-6} m K V^{-1}, which is larger than that of ferroelectric ceramic $PbZr_{0.95}Ti_{0.05}O_3$ thin-film (0.25×10^{-6} m K V^{-1}) (Mischenko et al., 2006). However, L. Yang and colleagues (Yang et al., 2016) have reported the T_c of PVDF/graphene composite that is lesser than reported on this current study.

The improvement of electrocaloric properties in adding filler technique is mainly depended on the suitable of a few graphene loading as 1 wt% before it is gradually reducing with graphene

content. Too much graphene content will reduce ΔT_{max} and T_c, corresponding to decrease $|\Delta T_{max}/T_c|$ as well as $|\Delta T_{max}/E|$. It seems that the majority influence of electrocaloric improvement on stretching technique is caused by X_c reduction. The crystallite size reduction possibly has less influence on electrocaloric properties, resulting in no significant relation in both adding filler and stretching techniques.

4. Conclusion

Composite thin films of PVDF-HFP with various graphene filler contents (0-5 wt%) were fabricated by solution casting technique. The comparison of adding filler and stretching technique were considered. Well dispersed graphene in PVDF-HFP thin films were observed. Stretching induced crysrtallinity and made the film translucent. The crystalline enlargement was observed by DSC analysis. Adding filler to 2−3 wt% produced the maximum crystallinity before gradually decreased around 5 wt% due to excessive filler loading; while, stretching technique dramatically increased crystallinity. Both adding filler and stretching technique also induced crystallite size reduction as well. It resulting in great dielectric constant, dielectric loss, and conductivity. In stretching technique, smaller crystallite size produces slimmer ferroelectric loop, corresponding to lesser remnant polarization, smaller unre-coverable energy and larger recoverable energy and energy storage efficiency. The main influence on adding filler case is conductive graphene loading rather than crystallite size reduction that resulting in bigger ferroelectric loop, larger remnant polarization, higher unrecoverable energy and smaller recoverable energy and energy storage efficiency. The antiferroelectric was observed, giving maximum negative ΔT at T_c 120 °C. On the adding filler case, negative ΔT_{max} was intensified as well as T_c reduction to a lower temperature by 20 °C before electrocaloric properties as $|\Delta T_{max}/T_c|$ gradually decreased with graphene content due to agglomeration. For stretching technique, the electrocaloric properties are reduced with crystalline enlargement although the stretching technique could stabilize T_c to a smooth curve. Adding filler cases is attractive for dielectric and electrocaloric improvement but undesirable for ferroelectric properties; while, the stretching technique is attractive for improving dielectric and ferroelectric properties, but un-desirable for electrocaloric properties. Those two techniques facilitate for their adoption in advanced capacitor and electrocaloric refrigerators with suitable energy storage efficiency in the future.

Declaration of competing interest

The authors declare that they have no known competing financial interests or personal relationships that could have appeared to influence the work reported in this paper.

Acknowledgements

Appendix A. Supplementary data

Supplementary data to this article can be found online at https://doi.org/10.1016/j.jclepro.2019.119730.

References

Ardimas, Putson, C., Muensit, N., 2018. High electromechanical performance of modified electrostrictive polyurethane three-phase composites. Compos. Sci. Technol. 158, 164−174. https://doi.org/10.1016/j.compscitech.2018.02.012.

Bahiraei, M., Heshmatian, S., 2019. Graphene family nanofluids: a critical review and future research directions. Energy Convers. Manag. 196, 1222−1256. https://doi.org/10.1016/j.enconman.2019.06.076.

Bahiraei, M., Mazaheri, N., 2018. Application of a novel hybrid nanofluid containing graphene−platinum nanoparticles in a chaotic twisted geometry for utilization in miniature devices: thermal and energy efficiency considerations. Int. J. Mech. Sci. 138−139, 337−349. https://doi.org/10.1016/j.ijmecsci.2018.02.030.

Bahiraei, M., Mazaheri, N., Rizehvandi, A., 2019. Application of a hybrid nanofluid containing graphene nanoplatelet−platinum composite powder in a triple-tube heat exchanger equipped with inserted ribs. Appl. Therm. Eng. 149, 588−601. https://doi.org/10.1016/j.applthermaleng.2018.12.072.

Bai, Y., Ding, K., Zheng, G.-P., Shi, S.-Q., Qiao, L., 2012. Entropy-change measurement of electrocaloric effect of BaTiO$_3$ single crystal. Phys. Status Solidi A 209 (5), 941−944. https://doi.org/10.1002/pssa.201127695.

Bauer, F., 2010. Relaxor fluorinated polymers: novel applications and recent de-velopments. IEEE Trans. Dielectr. Electr. Insul. 17 (4), 1106−1112. https://doi.org/10.1109/TDEI.2010.5539681.

Chen, C., Liang, R., Liu, Z., Yan, S., Nie, X., Zhou, Z., Dong, X., 2017. Coexistence of negative and positive electrocaloric effect in Sr and Nb co-doped Pb(Zr,Ti)O$_3$ ferroelectric ceramics. Mater. Lett. 189, 303−306. https://doi.org/10.1016/j.matlet.2016.11.006.

Choolaei, M., Goodarzi, V., Khonakdar, H.A., Jafari, S.H., Seyfi, J., Saeb, M.R., Häußler, L., Boldt, R., 2017. Influence of graphene Oxide on crystallization behavior and chain folding surface free energy of poly(vinylidenefluoride-co-hexafluoropropylene). Macromol. Chem. Phys. 218 (19), 1700103 https://doi.org/10.1002/macp.201700103.

Chu, B., Zhou, X., Ren, K., Neese, B., Lin, M., Wang, Q., Bauer, F., Zhang, Q.M., 2006. A dielectric polymer with high electric energy density and fast discharge speed. Science 313 (5785), 334−336. https://doi.org/10.1126/science.1127798.

Fatou, J.G., 1971. Melting temperature and enthalpy of isotactic polypropylene. Eur. Polym. J. 7 (8), 1057−1064. https://doi.org/10.1016/0014-3057(71)90138-8.

Goodarzi, V., Kokabi, M., Razzaghi Kashani, M., Reza Bahramian, A., 2014. Prediction of long-term mechanical properties of PVDF/BaTiO$_3$ nanocomposite. J. Appl. Polym. Sci. 131 (16) https://doi.org/10.1002/app.40596.

Goupil, F.L., Berenov, A., Axelsson, A.-K., Valant, M., Alford, N.M., 2012. Direct and indirect electrocaloric measurements on (001)-PbMg$_{1/3}$Nb$_{2/3}$O$_3$-30PbTiO$_3$ sin-gle crystals. J. Appl. Phys. 111 (12), 124109 https://doi.org/10.1063/1.4730338.

He, F.-A., Lin, K., Shi, D.-L., Wu, H.-J., Huang, H.-K., Chen, J.-J., Chen, F., Lam, K.-H., 2016. Preparation of organosilicate/PVDF composites with enhanced piezo-electricity and pyroelectricity by stretching. Compos. Sci. Technol. 137, 138−147. https://doi.org/10.1016/j.compscitech.2016.10.031.

He, X.J., Yao, K., Gan, B.K., 2005. Phase transition and properties of a ferroelectric poly(vinylidene fluoride-hexafluoropropylene) copolymer. J. Appl. Phys. 97 (8), 084101 https://doi.org/10.1063/1.1862323.

He, Z., Cao, Q., Jing, B., Wang, X., Deng, Y., 2017. Gel electrolytes based on poly(vinylidenefluoride-co-hexafluoropropylene)/thermoplastic polyurethane/poly(methyl methacrylate) with in situ SiO$_2$ for polymer lithium batteries. RSC Adv. 7 (6), 3240−3248. https://doi.org/10.1039/C6RA25062A.

Huan, Y., Liu, Y., Yang, Y., 2007. Simultaneous stretching and static electric field poling of poly(vinylidene fluoride-hexafluoropropylene) copolymer films. Polym. Eng. Sci. 47 (10), 1630−1633. https://doi.org/10.1002/pen.20843.

Huang, X.Y., Jiang, P.K., Xie, L.Y., 2009. Ferroelectric polymer/silver nanocomposites with high dielectric constant and high thermal conductivity. Appl. Phys. Lett. 95 (24), 242901 https://doi.org/10.1063/1.3273368.

Jiang, X., Luo, L., Wang, B., Li, W., Chen, H., 2014. Electrocaloric effect based on the depolarization transition in (1−x)Bi$_{0.5}$Na$_{0.5}$TiO$_3$−xKNbO$_3$ lead-free ceramics. Ceram. Int. 40 (2), 2627−2634. https://doi.org/10.1016/j.ceramint.2013.10.066.

Kasap, S.O., 2006. Principles of Electronic Materials and Devices. McGraw-Hill, New York.

Li, J., Khanchaitit, P., Han, K., Wang, Q., 2010. New route toward high-energy-density nanocomposites based on chain-end functionalized ferroelectric polymers. Chem. Mater. 22 (18), 5350−5357. https://doi.org/10.1021/cm101614p.

Li, J., Seok, S.I., Chu, B., Dogan, F., Zhang, Q., Wang, Q., 2009. Nanocomposites of ferroelectric polymers with TiO$_2$ nanoparticles exhibiting significantly enhanced electrical energy density. Adv. Mater. 21 (2), 217−221. https://doi.org/10.1002/adma.200801106.

Lichtenecker, K., 1931. Die Herleitung des logarithmischen Mischungsgesetzes aus allgemeinen Prinzipien der Stationaren Stromung. Phys. Z. 32, 255−260.

Lines, M.E., Glass, A.M., 1977. Principles and Applications of Ferroelectrics and Related Materials. Oxford university press.

Lu, S.G., Zhang, Q.M., Kutnjak, Z., 2011. 15 − the electrocaloric effect (ECE) in ferroelectric polymer films. In: Cao, Z. (Ed.), Thin Film Growth. Woodhead Publishing, pp. 364−383.

Mischenko, A., Zhang, Q., Scott, J., Whatmore, R., Mathur, N., 2006. Giant electro-caloric effect in thin-film PbZr$_{0.95}$Ti$_{0.05}$O$_3$. Science 311 (5765), 1270−1271. https://doi.org/10.1126/science.1123811.

Neese, B., Chu, B., Lu, S.-G., Wang, Y., Furman, E., Zhang, Q.M., 2008. Large elec-trocaloric effect in ferroelectric polymers near room temperature. Science 321 (5890), 821−823. https://doi.org/10.1126/science.1159655.

Neese, B., Wang, Y., Chu, B., Ren, K., Liu, S., Zhang, Q.M., Huang, C., West, J., 2007. Piezoelectric responses in poly(vinylidene fluoride/hexafluoropropylene) co-polymers. Appl. Phys. Lett. 90 (24), 242917 https://doi.org/10.1063/1.2748076.

Paik, H., Choi, Y.Y., Hong, S., No, K., 2015. Effect of Ag nanoparticle concentration on the electrical and ferroelectric properties of Ag/P(VDF-TrFE) composite films. Sci. Rep. 5, 13209 https://doi.org/10.1038/srep13209.

Pakhomov, O.V., Karmanenko, S.F., Semenov, A.A., Starkov, A.S., Es'kov, A.V., 2010. Thermodynamic estimation of cooling efficiency using an electrocaloric solid-state line. Tech. Phys. 55 (8), 1155–1160. https://doi.org/10.1134/S106378421008013x.

Parangusan, H., Ponnamma, D., Al-Maadeed, M.A.A., 2018a. Stretchable electrospun PVDF-HFP/Co-ZnO nanofibers as piezoelectric nanogenerators. Sci. Rep. 8 (1), 754. https://doi.org/10.1038/s41598-017-19082-3.

Parangusan, H., Ponnamma, D., AlMaadeed, M.A.A., 2018b. Investigation on the effect of γ-irradiation on the dielectric and piezoelectric properties of stretch-able PVDF/Fe–ZnO nanocomposites for self-powering devices. Soft Matter 14 (43), 8803–8813. https://doi.org/10.1039/C8SM01655K.

Patro, T.U., Mhalgi, M.V., Khakhar, D.V., Misra, A., 2008. Studies on poly(vinylidene fluoride)–clay nanocomposites: effect of different clay modifiers. Polymer 49 (16), 3486–3499. https://doi.org/10.1016/j.polymer.2008.05.034.

Putson, C., Jaaoh, D., Meauma, N., Muensit, N., 2012. Effect of micro- and nano-particle fillers at low percolation threshold on the dielectric and mechanical properties of polyurethane/copper composites. J. Inorg. Organomet. Polym. Mater. 22 (6), 1300–1307. https://doi.org/10.1007/s10904-012-9755-z.

Salimi, A., Yousefi, A.A., 2003. Analysis Method: FTIR studies of β-phase crystal formation in stretched PVDF films. Polym. Test. 22 (6), 699–704. https://doi.org/10.1016/S0142-9418(03)00003-5.

Scherrer, P., 1918. Bestimmung der Größe und der inneren Struktur von Kolloid-teilchen mittels Röntgenstrahlen. Nachr. Ges. Wiss. Goettingen Math. Phys. Kl. 1918, 98–100.

Scott, J.F., 2011. Electrocaloric materials. Annu. Rev. Mater. Res. 41 (1), 229–240. https://doi.org/10.1146/annurev-matsci-062910-100341.

Sencadas, V., Lanceros-Méndez, S., Mano, J.F., 2004. Characterization of poled and non-poled β-PVDF films using thermal analysis techniques. Thermochim. Acta 424 (1), 201–207. https://doi.org/10.1016/j.tca.2004.06.006.

Shojaei, L., Goodarzi, V., Otadi, M., Khonakdar, H.A., Jafari, S.H., Asghari, G.h., Reuter, U., 2018. Temperature and frequency-dependent creep and recovery studies on PVDF-HFP/organo-modified layered double hydroxides nano-composites. J. Appl. Polym. Sci. 135 (23), 46352 https://doi.org/10.1002/app.46352.

Sukwisute, P., Muensit, N., Soontaranon, S., Rugmai, S., 2013. Micropower energy harvesting using poly(vinylidene fluoride hexafluoropropylene). Appl. Phys. Lett. 103 (6), 063905 https://doi.org/10.1063/1.4818339.

Tan, S., Hu, X., Ding, S., Zhang, Z., Li, H., Yang, L., 2013. Significantly improving dielectric and energy storage properties via uniaxially stretching crosslinked

P(VDF-co-TrFE) films. J. Mater. Chem. 1 (35), 10353–10361. https://doi.org/10.1039/C3TA11484H.

Thakur, P., Kool, A., Bagchi, B., Hoque, N.A., Das, S., Nandy, P., 2015. The role of cerium(iii)/yttrium(iii) nitrate hexahydrate salts on electroactive β phase nucleation and dielectric properties of poly(vinylidene fluoride) thin films. RSC Adv. 5 (36), 28487–28496. https://doi.org/10.1039/C5RA03524D.

Thetpraphi, K., Putson, C., Muensit, N., 2015. Dependence of mechanical and dielectric properties on temperature of poly(vinylidene fluoride-hexa-fluoropropylene). Appl. Mech. Mater. 749, 129–133. https://doi.org/10.4028/www.scientific.net/AMM.749.129.

Tohluebaji, N., Putson, C., Muensit, N., 2019. High electromechanical deformation based on structural beta-phase content and electrostrictive properties of elec-trospun poly(vinylidene fluoride- hexafluoropropylene) nanofibers. Polymers 11 (11), 1817. https://doi.org/10.3390/polym11111817.

Tsangaris, G.M., Psarras, G.C., Kouloumbi, N., 1998. Electric modulus and interfacial polarization in composite polymeric systems. J. Mater. Sci. 33 (8), 2027–2037. https://doi.org/10.1023/a:1004398514901.

Yang, L., Li, X., Allahyarov, E., Taylor, P.L., Zhang, Q.M., Zhu, L., 2013. Novel polymer ferroelectric behavior via crystal isomorphism and the nanoconfinement effect. Polymer 54 (7), 1709–1728. https://doi.org/10.1016/j.polymer.2013.01.035.

Yang, L., Qian, X., Koo, C., Hou, Y., Zhang, T., Zhou, Y., Lin, M., Qiu, J.-H., Zhang, Q.M., 2016. Graphene enabled percolative nanocomposites with large electrocaloric efficient under low electric fields over a broad temperature range. Nano Energy 22, 461–467. https://doi.org/10.1016/j.nanoen.2016.02.026.

Zhang, Q.M., Bharti, V., Zhao, X., 1998. Giant electrostriction and relaxor ferroelectric behavior in electron-irradiated poly(vinylidene fluoride-trifluoroethylene) copolymer. Science 280 (5372), 2101. https://doi.org/10.1126/science.280.5372.2101.

Zhao, C., Guo, M., Lu, Y., Wang, Q., 2009. Ferroelectric poly(vinylidene fluoride-trifluoroethylene-chlorotrifluoroethylene)s: effect of molecular weight on dielectric property. Macromol. Symp. 279 (1), 52–58. https://doi.org/10.1002/masy.200950508.

Zhuo, F., Li, Q., Gao, J., Ji, Y., Yan, Q., Zhang, Y., Wu, H.-H., Xi, X.-Q., Chu, X., Cao, W., 2018. Giant negative electrocaloric effect in (Pb,La)(Zr,Sn,Ti)O₃ antiferroelectrics near room temperature. ACS Appl. Mater. Interfaces 10 (14), 11747–11755. https://doi.org/10.1021/acsami.8b00744.

Zhuo, F., Li, Q., Gao, J., Yan, Q., Zhang, Y., Xi, X., Chu, X., 2017. Phase transformations, anisotropic pyroelectric energy harvesting and electrocaloric properties of (Pb,La)(Zr,Sn,Ti)O₃ single crystals. Phys. Chem. Chem. Phys. 19 (21), 13534–13546. https://doi.org/10.1039/C7CP01762F.

Zouari, I., Sassi, Z., Seveyrat, L., Abdelmoula, N., Lebrun, L., Khemakhem, H., 2018. Structural, dielectric, piezoelectric, ferroelectric and electro-caloric properties of Ba₁₋ₓCaₓTi₀.₉₇₅(Nb₀.₅Yb₀.₅)₀.₀₂₅O₃ lead-free ceramics. Ceram. Int. 44 (7), 8018–8025. https://doi.org/10.1016/j.ceramint.2018.01.242.

APPENDIX B

Paper III [under major revision]; "Effect of rare-earths Er and Dy on the Curie temperature and interfacial charge mobility of electrocaloric PVDF-HFP composites"

1

Effect of rare-earths Er and Dy on the Curie temperature and interfacial charge mobility of electrocaloric PVDF-HFP composites

Ahamad Salea [a], Kunthisa Jehlaeh [a], Jia-wei Zhang [b], and Chatchai Putson [a,*]

[a] Materials Physics Laboratory, Department of Physics, Faculty of Science, Prince of Songkla University (PSU) , Songkhla 90112, Thailand

[b] School of Electrical Engineering, Northeast Electric Power University, No.169, Changchun Road, Jilin City 132012, China

[1]Corresponding author: Asst. Prof. Dr. Chatchai Putson, Materials Physics Laboratory, Physics Department, Faculty of Science, Prince of Songkla University, Hatyai, Songkhla Thailand 90112, Tel. + 6674 288759; Fax + 667 55889 E- mail: chatchai.p@psu.ac.th

ABSTRACT

Nowadays ferroelectric polymer composites are applied in novel electrocaloric cooling technology. Ferroelectric poly(vinylidene fluoride-co-hexafluoropropylene) (PVDF-HFP) thin films with the different electronegativity (EN) rare earth fillers Erbium (Er) and Dysprosium (Dy) have been studied in this work. Solution casting was used to fabricate the thin films. The electroactive β phase on both crystalline and amorphous regions of PVDF-HFP was intensified by this filler. However, the stronger EN filler Er induced the β phase on crystalline region more strongly than Dy, resulting in total crystalline region reduction along with dielectric constant. On increasing the filler loading, the Curie temperature decreased dramatically by 40 °C with decreasing maximum negative temperature change (ΔT_{max}). The best performance in Curie temperature reduction

2

was found with 1 wt% Er filler. This reduced the Curie temperature and increased the dielectric constant related with micro-phase structure and interfacial charge mobility that are relevant to future electrocaloric cooling applications.

Keywords: Poly(vinylidene fluoride-co-hexafluoropropylene), Erbium, Dysprosium, Dielectric properties, Electrocaloric properties

1.INTRODUCTION

The electrocaloric effect (ECE) is an effect that can produce heating/cooling when an electric field is applied/removed, following the Maxwell relation [1]. This effect was discovered by Neese [2] and has a great cooling efficiency of around 70% [3] superior to a conventional cooling system. This type of cooling system is green in the sense of not releasing hazardous gases such as CFCs to the environment [4, 5]. In fact,

ECE is associated with the entropy change (ΔS) and temperature change (ΔT) in ferroelectric (FE) materials when an electric field (ΔE) is applied. The maximum ΔT (ΔT_{max}) is usually found at the ferroelectric phase transition or Curie temperature (T_c), which is another phase transform temperature below the melting temperature. Several studies have successfully improved the electrocaloric strength $|\Delta T_{max}/\Delta E|$ by several approaches [6-8]. However, an approach to reduce T_c [9] to near the room temperature is the main focus of this current research.

Microstructure phase tailoring is one of the many effective approaches for T_c reduction. For example, I. Zouari and coworkers [9] successfully reduced T_c from 100 °C to 91 °C in $BaTi_{0.975}(Nb_{0.5}Yb_{0.5})_{0.025}O_3$ lead-free ceramics by adding Ca filler. They indicated that T_c decreased with Ca content because the phase structure was changed by Ca. As a result, the large to 0.20×10^{-6} m K V^{-1}

3

electrocaloric strength $|\Delta T_{max} /\Delta E|$ was reported. Despite success with a ceramic, T_c reduction is not easy to achieve in PVDF polymer composites with graphene nanoplatelet powder. For example, Q Zhang and coworkers [7] have not significantly reduced T_c to a lower temperature, but it can greatly improve $|\Delta T_{max} /\Delta E|$ to 0.13×10^{-6} m K V^{-1}. Also C. Putson and colleagues [10] have improved $|\Delta T_{max} /\Delta E|$ to 2.36×10^{-6} m K V^{-1}, but the T_c remained about constant. It is possible that PVDF as a semi-crystalline polymer (having both crystalline and amorphous regions) is very challenging as regards T_c reduction.

In this challenging work, a special filler with stronger chemical bonding might be important for effective microstructural phase transformation of PVDF. According to the literature, many rare earth (RE) fillers have successfully affected the microstructure of PVDF by strong bonding interactions. For example, Lanthanide (La) powder was first reported as a RE filler for PVDF dielectric improvement [11]. However, the choice of RE powder form has also been changed to chloride salt [12] and nitrate hydrate [13]. Those forms were effective on PVDF molecules, and intensified the strongest electroactive β phases (TTTT conformation), which contribute the highest polarization [14]. It can be seen that the stronger chemical bonding of RE nitrate hydrate form can intensify PVDF dielectric properties. The two fluorine atoms of a PVDF repeating unit directly interacted with RE ions (RE^{3+}) by ion-dipole interactions [15]. As a result, the dielectric constant increased by 2,000 with dielectric loss unchanged, compared pure PVDF. This encourages further study on the interfacial charge mobility of RE filler and PVDF molecules in the context of electrocaloric behavior. This RE filler might effectively induce phase transition on PVDF molecules for Curie temperature reduction.

4

In this paper we report further work on microstructural PVDF-HFP composite films with two rare-earth fillers of different electronegativities (EN). Erbium (III) nitrate pentahydrate and Dysprosium (III) nitrate hydrate are the two candidate fillers tested. The PVDF-HFP thin film was fabricated by solution casting with various RE contents of 1, 5, 10, or 20 wt%. This work highlights the EN effects of Erbium and Dysprosium as fillers in PVDF-HFP. The β phase intensification, crystallinity reduction, interfacial charge mobility, dielectric properties, and electrocaloric performance are discussed.

2.   METHODS   AND CHARACTERIZATIONS

2.1 Materials and methods.

Rare earth filler was sonicated in solution of N, N-dimethylformamide (DMF, $\geq$ 99% purity, RCI Labscan, Thailand). Afterwards, the powder of Polyvinylidien

fluoride-hexafluoropropylene (PVDF-HFP, Solef 11010/1001, Solvay Solexis, Belgium) was gradually added and stirred for 12 hours at 30 °C, resulting in a uniform distribution. This homogeneous solution was cast on a glass plate, so the solution casting method was applied to make the films. Finally, about 100 μm thick composite films were peeled, after drying and evaporating the DMF at 80°C for 24 hours in an incubator. The cases with Erbium (III) nitrate pentahydrate ($Er(NO_3)_3 \cdot 5H_2O$ of 99.9% purity (298166 ALDRICH) at filler loadings 1, 5, 10 or 20 wt% in PVDF-HFP are here labeled as PEr1, PEr5, PEr10 and PEr20, respectively. Similarly, the cases with Dysprosium (III) nitrate hydrate $Dy(NO_3)_3 \cdot xH_2O$ at 99.9% purity (298158 ALDRICH) filler are labeled as PDy1, PDy5, PDy10 and PDy20, by loading level. These composite thin films were compared with neat PVDF-HFP as the baseline or control case.

5

2.2 Microstructural Characterization. Fourier Transform Infrared Spectroscopy (FTIR, ATR Vertex70, Bruker, Germany) determined the functional groups in the composite films. Spectra were recorded from 400 cm^{-1} to 1350 cm^{-1} as the wavenumber range, with a resolution of 4 cm^{-1}. The α phase is first detected from several peaks [16, 17], for example 484, 534, 613, 767, 795, 976, and 1210 cm^{-1}. The β phase is also identified from vibrational peaks [16, 17], for example at 511, 837, 1234, and 1275 cm^{-1}. The nucleation of β phase ($F(\beta)$) was estimated by using Lambert- Beer law in **Equation (1),** where A_α and A_β are the absorbances at 767 cm^{-1} and 837 cm^{-1}, respectively, and K_α (6.1 x 10^4 cm^2 mol^{-1}) and K_β (7.7 x 10^4 cm^2 mol^{-1}) are the coefficients of absorption at these wavenumbers [16].

$$F(\beta) = \frac{A_\beta}{\frac{K_\beta}{K_\alpha} A_\alpha + A_\beta} \qquad (1)$$

Moreover, an X- Ray diffractometer (XRD) , (PANalytical, Empyrean, Netherlands) , observed the material structure. The composite films were subjected to XRD from 10° to 40° range of 2θ, with 0.026° step size and 67.065 sec measurement per step in a scan, using 0.15406 nm wavelength Cu-Kα$_1$ radiation, at 40 kV, 30 mA. The electroactive β phase crystallinity ratio of I$_{20.5}$/I$_{18.3}$ was evaluated for β phase, where 2θ = 20.5° and 18.3 refer to β and α phases, respectively.

For Differential Scanning Calorimetry (DSC), the samples were heated from 140 °C to 178 °C with 10.00 °C/min heating rate by using DSC Thermal Analyzer (STA8000, Perkin Elmer, USA) in ambient atmospheric air. The area under the endothermic peak was evaluated as the enthalpy change (ΔH_m). The crystallinity (X_c) was estimated using equation (2), where Ø refers to the weight fraction of filler in the composite. ΔH_m and ΔH_m^0 are the melting

6

enthalpy observed and the melting enthalpy for 100% crystalline PVDF-HFP (104.6 J g^{-1} [18]), respectively. The temperature range 120-180 °C is related to X_c and content of the electroactive β phase.

$$X_c(\%) = \frac{\Delta H_m}{(1 - \emptyset)\Delta H_m^0} \times 100 \quad (2)$$

2.3 Dielectric and electrocaloric measurements. An LCR meter (IM 3533 HIOKI) measured the dielectric constant over the frequency range 1 Hz – 10^5 Hz. For example, the capacitance (C) and loss tangent or dielectric loss (ε_r') at RT were recorded by applying a 1 V ac electric field. The sample electrode was coated by using a Sputter Coater (SPI-MODULE, Structure Probe, Inc, West Chester, PA, USA). The two recorded components were converted to the relative permittivity or dielectric constant (ε_r) and the electrical conductivity (σ_{ac}), following equations (3) and (4), respectively. Here d is sample thickness (100 μm), A is the electrode area (5 mm diameter), f is the ac frequency in Hz, ε_r' is dielectric loss, and ε_0 is the free

space permittivity equaling 8.853 x 10^{-12} F m^{-1} [19].

$$\varepsilon_r = Cd/\varepsilon_0 A \quad (3)$$
$$\sigma_{ac} = 2\pi f \varepsilon_0 \varepsilon_r \varepsilon_r' \quad (4)$$

Moreover, a ferroelectric Polarization Loop Test System (PK-CPE1701, USA) measured the Polarization-electric field loop (P-E loop) across samples under 40 MV/m at 10 Hz. The area of charge and discharge curve of the PE loop can represent recoverable (U$_e$) and unrecoverable (U$_l$) energy, from which we can calculate the energy storage efficiency of the material as

$$\eta(\%) = U_e \times 100/(U_e + U_l)$$
$$(5)$$

This was recorded at 1 °C intervals in an oil-bath oven within 30 - 140 °C. The remnant polarization (P$_r$) was converted to entropy change (ΔS) and temperature change (ΔT) by using the Maxwell relations in Equations (6-7). Here polarization (P) and temperature (T) under electric field (E, 40 MV/m) are used along with density (ρ), and

7

the specific PVDF-HFP heat capacity (C_E, 1,600 J/kg/°C).

$$\Delta S = \int_{E_1}^{E_2} \left(\frac{\partial P}{\partial T} \right) dE$$ (6)

$$\Delta T = -\frac{1}{\rho C_E} \int_{E_1}^{E_2} T \left(\frac{\partial P}{\partial T} \right) dE$$ (7)

3. RESULTS AND DISCUSSION

3.1 Characterization of Er^{3+} and Dy^{3+} ions in PVDF-HFP Thin Films.

For basic structure confirmation, the thin films were analyzed by FTIR, XRD, and DSC techniques, which enable correlating β-phases and crystalline regions as shown in **Figure 1**. For these thin films, the two RE fillers Er^{3+} and Dy^{3+} were compared, as they differ by EN.

FTIR by filler loading. The FTIR technique observed whole amorphous and crystalline regions of PVDF-HFP polymer. In several electroactive phases, the β phases contribute the strongest polarization in PVDF

polymer. Figure 1 (a) shows several peaks of electroactive phases, such as β and α. It can be seen that most of the α vibrational peaks disappeared on adding RE. For example, 613, 767, 795, 976, and 1210 cm^{-1} peaks of α phases [20] decreased, while the β phase peaks at 837 and 1234 cm^{-1} obviously grew after adding RE, matching prior studies [21, 22]. This indicates that the RE filler can induce β phases in PVDF-HFP. The stronger β phase might arise from α phase and/or some other phase. The β phase intensification (F(β)) was evaluated according to Equation (1). Figure 1 (b) shows a sharp increase in F(β) with added RE, which though saturated at a higher RE content. For example, the F(β) increased from 55.12% for pure PVDF-HFP to 84.76% for PEr5 and 85.22% for PDy5. Further on, it slightly decreased at 10 wt% filler loading before saturation at 20 wt%. It is possible that the RE molecules were well dispersed in the polymer matrix, in amorphous and crystalline regions. The sharp

8

increase of β phase in PVDF-HFP was reviewed. In a prior study [15], the RE ions (X^{+3}) interacted with NO_3^- molecules and two F atoms on the PVDF polymer molecules, forming stronger chemical bonds by ion-dipole interactions.

FTIR by strength and loading of EN filler. The two RE fillers Dy and Er have different electronegativities (EN). In fact, the Er is stronger with EN at 1.24, while Dy has weaker EN at 1.22. In Figure 1 (b), it seems that F(β) would not significantly differ between Dy and Er. The F(β) with RE filler sharply increased from 55.02 % to around 83.17- 85.14 %, with the maxima similar to a prior study of pure PVDF-HFP fiber with ~ 85.90-89.65% F(β) [23]. It is possible that these RE ions interacted with PVDF-HFP by strong chemical bonds, effectively inducing conversion of PVDF-HFP to the stronger β phase form. By FTIR technique, it is not easy to differentiate between the two RE fillers. This is because FTIR observes the whole

semi-crystalline PVDF-HFP polymer including simultaneously both amorphous and crystalline regions.

XRD by filler loading. Figure 1 (c)-(d) present the crystallinity in semi-crystalline PVDF-HFP polymer. The outstanding XRD peak revealing crystallinity is at $2\theta = 20.5°$ for β phase and at $2\theta = 18.3°$ for α phase. These two peaks significantly decreased on adding filler loading. For example, the peak at $2\theta = 20.5°$ changed to a broad peak with filler loading. It is clear that the crystallinity was considerably reduced by the filler. These fillers have strong interactions and reduce crystallinity while inducing β phase formation in PVDF-HFP. Despite the loss of crystallinity, there is significant evidence that the RE fillers strongly induced PVDF-HFP conversion to β phase. In figure 1 (d), the electroactive β phase crystallinity ratio between the peaks at 20.5° and 18.3° was evaluated, indicating proportions of

9

crystalline β and α phases. This proportion increased from 1.36 to 1.47 at 1 wt% RE before saturating at 1.50 at 5 wt% loading. Afterwards, the ratio suddenly decreased at 10 wt% loading because of the crystallinity reduction effect. It fact, the crystalline regions gradually decreased since the small filler contents of 1 and 5 wt%, but the strong XRD peaks at 20.5° and 18.3° were clearly affected by the large filler contents of 10 and 20 wt%.

XRD by EN strength and filler loading. The XRD spectra effectively showed the dissimilarity on the two RE fillers, more so than the previous FTIR technique. This is because XRD is focused on the crystalline regions, while FTIR reflects the combination of crystalline and amorphous regions in the semi-crystalline PVDF-HFP polymer. Figure 1 (c) shows a broader XRD peak after adding filler. It is possible that the crystallinity of PVDF-HFP polymer gradually decreased with RE content. Considering to the gradual crystalline region reduction with RE content, the Er contributed to β phase ($2\theta = 20.5°$) more than Dy because of its stronger EN, as in Figure 1 (d). For example, the electroactive β phase crystallinity ratio with Er filler was 1.50 (5 wt%), 1.40 (10 wt%), and 1.38 (20 wt%) which are larger than with Dy that gave 1.49 (5 wt%), 1.35 (10 wt%), and 1.28 (20 wt%). The ratio is consistently larger than with Dy, which corroborates the argument that the stronger EN of Er helped induced PVDF-HFP conversion, and gradually decreased the crystallinity as well.

DSC by filler loading. Figure 1 (e-f) shows the DSC thermographs of neat PVDF-HFP and RE filled PVDF-HFP. In this work, the first DSC observation is the melting temperature. Initially the melting temperature slightly shifted upward with RE filler loading. However, the melting temperature then suddenly dropped after a maximum. For

10

example, increasing RE filler loading in PVDF-HFP shifted the melting temperature slightly upwards from 162.6 °C without filler to 163.4 °C (PEr10) and to 163.8 °C (PDy5); these were the maxima of T_m for each filler type. Further filler loading caused declines to 162 °C and to 161.8 °C, respectively, as shown in Figure 1 (e). The second determination was of crystallinity in PVDF-HFP. The crystallinity was estimated from measured melting enthalpy following Equation (2). It is clear that increasing RE content reduced crystallinity and crystalline regions were transformed to amorphous state. For example, the crystallinity of pure PVDF-HFP gradually decreased from 37.66% to 33.78% (5 wt%), 31.41% (10wt%), and 23.02% (20 wt%) with Dy filler. In Figure 1 (c) and (d), crystallinity gave broader XRD peaks with as RE loading increased. It seems that crystalline regions were replaced by amorphous regions as RE content increased. In a prior study, Thakur and colleagues [19]

found maximum X_c at a specific filler loading. However, Sie Chin Tjong and colleagues [24, 25] reported that X_c was decreasing with filler loading. This phenomenon was called "the competition between the nucleation effect and the blocking effect of the inorganic filler on the crystallization of polymer" [24, 26].

DSC by EN and filler loading. The two RE fillers have different EN, affecting the maximum melting temperature. The maximum melting temperature was observed at 10 wt% for Er and at 5 wt% for Dy. It is possible that the physical crystal size of Dy cluster was larger than that of Er at equal loading levels, as shown in Figure 2 (C). The larger cluster size of Dy had larger area for reaction to induce PVDF-HFP interactions, resulting in fast reaching of the maximum melting temperature at 163.8 °C with the smaller 5 wt% loading, while Er reached 163.4 °C with the larger 10 wt% loading. Figure 1 (f) shows the crystallinity reduction

11

with RE content, giving different slopes for the fillers. It is clear that the larger EN of Er made it stronger in reducing crystallinity of PVDF-HFP than Dy, as seen in Figure 1 (e-f). For example, the crystallinities 33.78% (5 wt%), 31.41% (10wt%), and 23.02% (20 wt%) with Dy are larger than with Er which gave 32.17% (5 wt%), 28.56% (10 wt%), and 19.19% (20 wt%). This argument of the stronger EN of Er is supported by the XRD results, in which Er affected the electroactive β phase crystallinity ratio more than Dy, while overall the crystallinity was reduced.

Figure 2 shows the conclusion of FTRI, XRD, and DSC results. This illustration shows the PVDF-HFP interacting with RE filler in a microstructural composite. The PVDF-HFP has F and H atoms bonding with the C backbone, as in Figure 2 (a). Increased order of the polymer chains is induced on adding RE filler, by the strong ion-dipole interactions, and self-induced by other PVDF-HFP molecules with weaker

bond (H-bonds) as dipole-dipole interactions. In a prior study [15], the RE ions (X^{+3}) interacted with one NO_3^- molecule and two F atoms on the polymer chains. As a result, the PVDF-HFP was polarized following the direction of RE filler with an opposite charge. The strong ion-dipole interactions can sharply increase the β phase, as indicated by Figure 1 (b). The filler was randomly dispersed in both crystalline and amorphous regions. It is clear that these fillers have two important roles to possibly affect PVDF-HFP. Firstly, these RE filler have the potential to improve β phase in whole regions of PVDF-HFP, by transforming the weaker α phase to in polarization stronger β phase, as explained in Figure 1 (a). Secondly, RE fillers gradually converted crystalline to amorphous regions, known as the crystalline-amorphous transformation, as in Figure 2 (b) with Figures 1 (c), (e), and (f). The melting enthalpy (ΔH_{m^*}) refers to pure PVDF-HFP with endothermic melting at a specific

12

temperature (T_m*). The ΔH_m* was lower (ΔH_m < ΔH_m*) with a small RE loading, while Tm slightly shifted upwards ($T_m \geq T_m*$). This behavior totally changed with high RE filler loadings that obviously reduced crystallinity of PVDF-HFP and decreased the melting temperature, so ΔH_m << ΔH_m* and T_m << T_m*. The melting temperature reduction (T_m << T_m*) occurred after it reached its maximum when RE content was further increased, as in Figure 1 (e). The RE contents giving the maxima were slightly different between Dy and Er, depending on cluster size as well as other factors. Figure 2 (c) confirms the different cluster sizes by SEM: larger for Dy than for Er at equal loading levels.

3.2 Dielectric properties. The ε_r, $\varepsilon_r^{'}$, and σ_{ac} are shown in **Figure 3** for the composite thin films along with pure PVDF-HFP.

Dielectric properties by frequency. Figure 3 (a) presents the relationship of dielectric constant with frequency for both PEr and PDy. The PVDF-HFP molecules were polarized in the direction of external electric field, and the internal rotation of dipoles caused dielectric losses. The results show that both dielectric constant and dielectric loss decreased with frequency. An electrical dipole has less time to align with the electric field alternating at a high frequency, while at a low frequency it can follow the direction of applied electric field [27]. As a result, the simple polarization at low frequencies produced a large dielectric constant and dielectric losses. Figure 3 (d) displays ac conductivity (σ_{ac}) against frequency. The highest conductivity was found at the highest frequency, and the lowest conductivity was found at the lowest frequency, according to Equation (4). The conductivity relates to the number of charge-carriers in the dielectric material that cause heating by the dissipation of electric power

13

[29]. The charge-carrier mobility increases with frequency of the electric field.

Dielectric properties by filler loading. According to Figure 3 (a)-(b), the dielectric constant and dielectric loss increased with RE content. The increase of filler-polymer interface follows a logarithmic law for heterogeneous phases [28]. The highest RE content of 20 wt% produced the highest dielectric constant and dielectric loss. These fillers can promote interfacial surface charges or interfacial polarization at phase boundaries in the polymer-filler composite, according to Maxwell-Wagner-Sillars (MWS) effect [29]. In previous studies [30, 31], it was found that the dielectric constant increased with filler content. The number of charge carriers increased with filler content in polyurethane. The increase of both dielectric constant and dielectric loss reportedly arises from the internal polarization of polymer molecules with filler

content [32], and it increases with interfacial area of polymer matrix with filler.

This confirms that the dipoles of PVDF-HFP molecules with RE filler were simply polarized in the direction of applied electric field. In addition, the conductivity increased with RE filler as in Figure 3 (d). This is because the RE filler also provided large quantities of free mobile electrons on the surfaces. In fact, the conductivity is related to dielectric constant and dielectric loss [27] according to Equation (4). As a result, the conductivity increased with RE content due to the charge-carrier mobility. This mechanism of interfacial polarization arises from the MWS effect of heterogeneous dielectric material composites. The dielectric properties suggest that there was less charge-carrier mobility at very low frequencies because the charge was trapped and accumulated at interfaces, resulting in larger interfacial polarization, dielectric constant, and dielectric loss.

14

Dielectric properties by EN strength of filler. On comparing the same loading level of the two RE fillers at 1,000 Hz, Figure 3 (b) shows the difference between the stronger EN of Er and weaker EN of Dy, which clearly differentiates them at larger contents. Matching with the DSC results in Figure 1 (f), the stronger EN of Er reduced PVDF-HFP crystallinity more, and the crystallinity decreased with RE content. As a result, there was less polarization on PVDF-HFP, lower electrical capacity, and lower dielectric constant. For example, the 20 wt% RE case produced the highest dielectric constants, 41.38 for Er and 42.05 for Dy (at 1 Hz), while the lowest dielectric constants were 7.87 for Er and 9.95 for Dy (at 10^5 Hz). These two examples show dielectric constants with Dy that are slightly greater than with Er. Therefore, the greater EN of Er gave lesser dielectric constants than the weaker EN filler Dy, due to the loss of crystallinity.

Compared with amorphous region, a crystalline region has boundaries that produce stronger polarization, resulting in a larger electrical storage capacity and dielectric constant. It can be concluded that the PVDF-HFP loss of crystallinity directly reduced the dielectric constant, and Er reduced PVDF-HFP crystallinity more effectively than Dy.

3.3 Electrocaloric properties. Figure 4 shows electrocaloric results for pure PVDF-HFP, and filled composites with 1 wt% and 5 wt% RE contents. The electrical breakdown strength had limited the electrocaloric measurement of 10 wt% and 20 wt% cases that had too high conductivity. Regarding the dielectric constant and dielectric loss of pure PVDF-HFP (Figure 4 (a)), the Curie temperature was at ~120 °C, which is at the ferroelectric phase transition, matching previous studies [10, 33]. The slim PE loop is shown in Figure S1 (a) in supplementary material. It was likely anti-

15

ferroelectric at 40 °C. Afterwards, the loop with P_r became gradually larger with temperature, and rapidly grew near the Curie temperature at ~118 °C followed by a slight increase above T_c, see Figure S1 (b). The storage energy efficiency (η) of pure PVDF-HFP of about 76.86 % was much greater than that of pure PVDF-TrFE-CTFE, which was 45.02 % [34], resulting in larger ΔT compared with the PVDF-TrFE-CTFE [35, 36].

Electrocaloric properties by filler loading. Figures 4 (b) and (c) show the relationship between ΔT and temperature, following Equation (7). The calculations are described in Supplementary data (Figure S1). The maximum negative ΔT (ΔT_{max}) coincided with the Curie temperature, Figure 4 (b) and (c). The ΔT_{max} gradually decreased with RE content. For example, there was a gradual decrease with Er from -16.99 °C for pure PVDF-HFP to -8.85 for 1 wt%, and -7.01 °C for 5 wt% loading. With Dy, the

ΔT_{max} decreased from -16.99 °C of pure PVDF-HFP to -11.29, and -7.99 °C at 1 and 5 wt% loadings, respectively. The decrease of ΔT_{max} with RE content is supported by the loss of crystallinity in the PVDF-HFP polymer. It is possible that these RE fillers with strong chemical bonding by ion-dipole interactions reduced crystallinity, transforming crystalline domains to amorphous state. The loss of crystallinity might reduce polarizability of PVDF-HFP under strong external electric fields. In fact, the electrocaloric polarizability of PVDF-HFP should be improved when adding graphene filler. However, the stronger ion-dipole interaction of these fillers reduced crystallinity in the beginning, resulting in decreased ΔT_{max}. The microstructure of PVDF-HFP suddenly changed when RE loading was increased. It is possible that ferroelectric phase transition or Curie temperature of PVDF-HFP changed also. Figure 4 (b) and (c) show the Curie

16

temperature decrease with RE content. For example, the Curie temperature with Er filler significantly decreased by 40 °C from 118.47 °C of pure PVDF-HFP to 77.38 °C with 1 wt% and 91.84 °C with 5 wt%. The largest drop in Curie temperature was with the lowest RE content of 1 wt%. In fact, many studies have tried to reduce the Curie temperature to near room temperature [9, 10]. For example, I. Zouari and coworkers [9] successfully reduced the Curie temperature from 100 °C to 91 °C of $BaTi_{0.975}(Nb_{0.5}Yb_{0.5})_{0.025}O_3$ lead-free ceramics by using Ca filler. In this work, the suitable RE filler loading of 1 wt% shifted downward the ferroelectric phase transition temperature of PVDF-HFP microstructure. It can be concluded that the strong ion-dipole interactions of this filler reduced crystallinity, resulting in decreases in ΔT_{max} and Curie temperature.

Electrocaloric properties by EN strength and filler loading. On comparison of the fillers by EN, it seems that the stronger EN of Er was better able to reduce ΔT_{max}, due to the larger loss of crystallinity confirmed in Figure 1 (f). For example, Er at 1 wt% had -8.85 °C while Dy gave -11.29 °C. Er at 5 wt% had -7.01 °C while Dy had -7.99 °C. The reduction of ΔT_{max} with the stronger EN filler was supported by loss of crystallinity. The stronger EN of Er effectively decreased crystallinity. Considering Curie temperature, it was significantly different with these two fillers, and Er successfully reduced the Curie temperature more than Dy. For example, Er at 1 wt% had 77.37 °C while Dy had 83.42 °C. Er at 5 wt% had 91.84 °C while Dy had 94.71 °C. The largest reduction in Curie temperature was found with the stronger EN filler, namely Er. It can be concluded that Er filler with stronger EN had more potential to reduce crystallinity, resulting in large ΔT_{max} and Curie temperature reduction.

Figure 4 (d) shows this electrocaloric performance in the form of absolute $|\Delta T_{max}$

17

/T$_c$|. This performance measure decreased with RE content, while the stronger EN of Er showed lower performance than Dy. This is because of crystallinity reduction in the filled PVDF-HFP polymer. In this work, a decrease of PVDFfa-HFP crystallinity caused by RE filler is the main reason for electrocaloric performance reduction. However, this work observed a large electrocaloric strength |ΔT$_{max}$ /ΔE| of about 0.22 × 10^{-6} m K V^{-1}, nearly of similar strength as ceramic materials (0.20 × 10^{-6} m K V^{-1} [9] and 0.27 × 10^{-6} m K V^{-1} [37]).

4. Conclusion

This paper demonstrated improved dielectric and electrocaloric properties, showing potential for applications in electrocaloric cooling. RE filler loadings of 1-20 wt% in PVDF-HFP positively induced β phase. The 5 wt% RE loading gave the most β phase in crystalline state, before decreases at 10 and 20 wt% loadings. The crystallinity clearly decreased with RE loading according to DSC measurements. The T$_m$ reduction from large RE loadings was obvious at 20 wt% filler, which is an excessive filler loading. The RE fillers were expected to improve the dielectric properties by contributing to polarizability. However, 1 wt% loadings were the best with the lowest T$_c$ near room temperature. The T$_c$ dramatically decreased by 40 °C, while the electrocaloric indicator ratio |ΔT/ T$_c$| decreased with filler content.

The greater EN of Er filler induced more conversion to β phase than Dy. The Er filler also was stronger in gradually reducing X_c along with ΔH_m, and T$_m$. The β intensity of crystalline regions was clearly reduced when RE filler loadings reached 10-20 wt%. As a result, the lesser X_c from the stronger EN of Er produced weaker dielectric properties. Moreover, the Er with larger EN decreased T$_c$ of PVDF-HFP closer to room temperature than Dy filler. The Er gave

18

slightly poorer electrocaloric properties because of loss of crystallinity, compared with Dy. Overall, small RE loadings have ability to improve dielectric and electrocaloric properties, facilitating adoption of these composites in future electrocaloric refrigerators.

Conflict of interest: The authors declare no conflict of interest.

References

[1]   M. E. Lines, A. M. Glass, Principles and applications of ferroelectrics and related materials, (Oxford university press, 1977)

[2]   B. Neese, B. Chu, S.-G. Lu, Y. Wang, E. Furman, Q. M. Zhang, Science **321**, 821-23 (2008)

[3]   O. V. Pakhomov, S. F. Karmanenko, A. A. Semenov, A. S. Starkov, A. V. Es'kov, Tech. Phys. **55**, 1155-60 (2010)

[4]   J. F. Scott, Annual Review of Materials Research **41**, 229-40 (2011)

[5]   F. L. Goupil, A. Berenov, A.-K. Axelsson, M. Valant, N. M. Alford, J. Appl. Phys. **111**, 124109 (2012)

[6]   Y. Bai, X. Han, L. Qiao, Applied Physics Letters **102**, 252904 (2013)

[7]   L. Yang, X. Qian, C. Koo, Y. Hou, T. Zhang, Y. Zhou, M. Lin, J.-H. Qiu, Q. M. Zhang, Nano Energy **22**, 461-67 (2016)

19

[8]   X.-S. Qian, H.-J. Ye, Y.-T. Zhang, H. Gu, X. Li, C. A. Randall, Q. M. Zhang, Adv. Funct. Mater. **24**, 1300-05 (2014)

[9]   I. Zouari, Z. Sassi, L. Seveyrat, N. Abdelmoula, L. Lebrun, H. Khemakhem, Ceram. Int. **44**, 8018-25 (2018)

[10]   A. Salea, S. Chaipo, A. A. Permana, K. Jehlaeh, C. Putson, J. Cleaner. Prod. **251**, 119730 (2020)

[11]   A. Hassen, T. Hanafy, S. El-Sayed, A. Himanshu, J. Appl. Phys. **110**, 114119 (2011)

[12]   S. El-Sayed, T. A. Abdel-Baset, A. Hassen, AIP Adv. **4**, 037114 (2014)

[13]   P. Thakur, A. Kool, B. Bagchi, N. A. Hoque, S. Das, P. Nandy, RSC Adv. **5**, 28487-96 (2015)

[14]   S. G. Lu, Q. M. Zhang, Z. Kutnjak in Thin film growth, ed. By Z. Cao Z (Woodhead Publishing, 2011), p. 364-83

[15]   M. C. Silva, A. S. S. de Camargo, L. A. O. Nunes, R. A. Silva, A. Marletta, J. Non-Cryst. Solids **354**, 5496-503 (2008)

[16]   L. Li, M. Zhang, M. Rong, W. Ruan, RSC Adv. **4**, 3938-43 (2014)

[17]   H. Parangusan, D. Ponnamma, M. A. A. Al-Maadeed, Sci. Rep. **8**, 754 (2018)

[18]   Z. He, Q. Cao, B. Jing, X. Wang, Y. Deng, RSC Advances 7, 3240-48 (2017)

[19]   P. Thakur, A. Kool, B. Bagchi, N. A. Hoque, S. Das, P. Nandy, RSC Adv. **5**, 28487-96 (2015)

[20]   X. Cai, T. Lei, D. Sun, L. Lin, RSC Advances 7, 15382-89 (2017)

[21]   P. Sukwisute, J. Yuennan, N. Muensit, Integr. Ferroelectr. **195**, 230-39 (2019)

[22]   J. Yuennan, P. Sukwisute, N. Muensit, Mater. Res. Express **5**, 055702 (2018)

20

[23] N. Tohluebaji, C. Putson, N. Muensit, Polymers **11**, 1817 (2019)

[24] S. C. Tjong, S. P. Bao, J. Polym. Sci., Part B: Polym. Phys. **42**, 2878-91 (2004)

[25] Y. Li, D. Zhang, S. Wang, Y. Zhan, J. Yin, X. Tao, X. Ge, S. C. Tjong, H.-Y. Liu, Y. W. Mai, Compos. Sci. Technol. **171**, 152-61 (2019)

[26] Y.-J. Wang, D. Kim, Electrochim. Acta **52**, 3181-89 (2007)

[27] S. O. Kasap, Principles of electronic materials and devices, (McGraw-Hill New York, 2006)

[28] K. Lichtenecker, Phys. Z **32**, 255-60 (1931)

[29] G. M. Tsangaris, G. C. Psarras, N. Kouloumbi, J. Mater. Sci. **33**, 2027-37 (1998)

[30] Ardimas, C. Putson, N. Muensit, Compos. Sci. Technol. **158**, 164-74 (2018)

[31] C. Putson, D. Jaaoh, N. Meauma, N. Muensit, J. Inorg. Organomet. Polym. Mater. **22**, 1300-07 (2012)

[32] H. Paik, Y.-Y. Choi, S. Hong, K. No, Sci. Rep. **5**, 13209 (2015)

[33] K. Thetpraphi, C. Putson, N. Muensit, Appl. Mech. Mater. **749**, 129-33 (2015)

[34] Prateek, V. K. Thakur, R. K. Gupta, Chem. Rev. **116**, 4260-317 (2016)

[35] B. Lu, X. Chen, T. Zhang, S. G. Lu, Q. M. Zhang, Appl. Phys. Lett. **113**, 153903 (2018)

[36] X. Li, X.-s. Qian, S. G. Lu, J. Cheng, Z. Fang, Q. M. Zhang, Appl. Phys. Lett. **99**, 052907 (2011)

[37] H. Kaddoussi, A. Lahmar, Y. Gagou, J. L. Dellis, H. Khemakhem, M. E. Marssi, Ceram. Int. **41**, 15103-10 (2015)
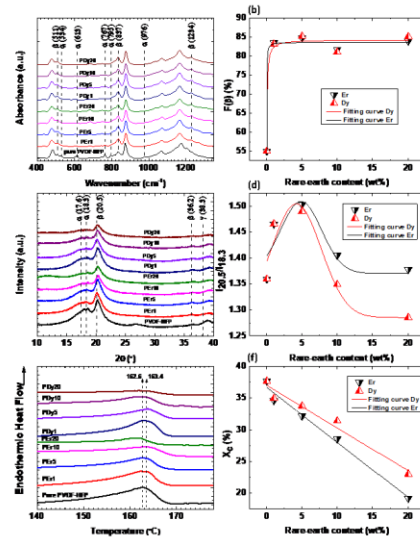
21

Figures:

Figure 1 FTIR spectra and β phase (a-b), XRD patterns and β phase (c-d), and DSC thermograph and dependence of X_c (e-f), on Er and Dy filler loadings in thin-film composites.

Figure 2 (a) Schematic illustration of the PVDF-HFP chain conformations with rare-earth filler (Rare^{3+}), (b) ΔH_m and T$_m$ related to filler loading level, and (c) SEM images with Er and Dy fillers at 20 wt%.

Figure 3 Comparison between the rare earth fillers Er and Dy in PVDF-HFP. (a) Dielectric constant versus frequency, (b) dielectric constant versus filler loading at 1k Hz, (c) dielectric loss versus frequency, and (d) conductivities.

Figure 4 (a) Dielectric constant and dielectric loss at various temperatures from ambient to 140 °C for pure PVDF-HFP, (b) electrocaloric behaviors with Er and Dy fillers, the negative ΔT at 1 wt%, and (c) at 5

wt% at various temperatures, and (d) electrocaloric performance indicator |ΔT $_{max}$ /T$_c$| with Er and Dy fillers.

Figure 1 FTIR spectra and β phase (a-b), XRD patterns and β phase (c-d), and DSC thermograph and dependence of X_c (e-f), on Er and Dy filler loadings in thin-film composites.
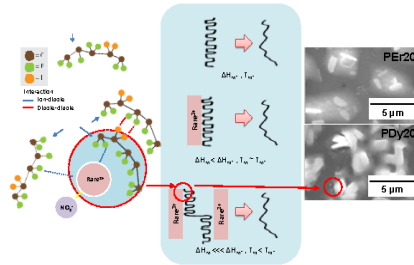
22

Figure 2 (a) Schematic illustration of the PVDF-HFP chain conformations with rare-earth filler (Rare^{3+}), (b) ΔH_m and T$_m$ related to filler loading level, and (c) SEM images with Er and Dy fillers at 20 wt%.
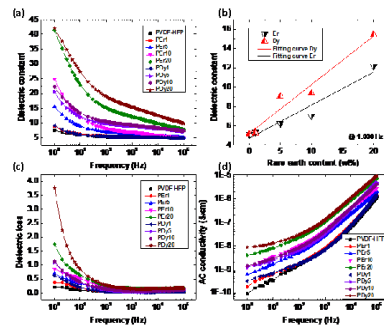

Figure 3 Comparison between the rare earth fillers Er and Dy in PVDF-HFP. (a) Dielectric constant versus frequency, (b) dielectric constant versus filler loading at 1k

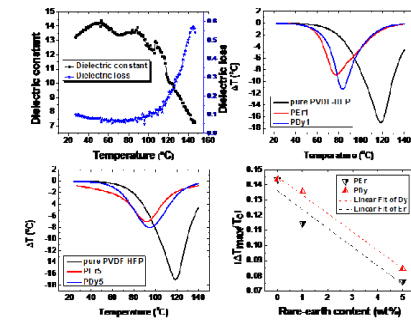Hz, (c) dielectric loss versus frequency, and (d) conductivities.

Figure 4 (a) Dielectric constant and dielectric loss at various temperatures from ambient to 140 °C for pure PVDF-HFP, (b) electrocaloric behaviors with Er and Dy fillers, the negative ΔT at 1 wt%, and (c) *at* 5 wt% at various temperatures, and (d) electrocaloric performance indicator |ΔT $_{max}$ /T$_c$| with Er and Dy fillers.

APPENDIX C

Paper I [Conference published]; "The enhancement of high dielectric properties for pure PVDF-HFP by using the suitable stirred temperature and time"

IOP Conference Series: Materials Science and Engineering

PAPER • OPEN ACCESS

The enhancement of high dielectric properties for pure PVDF-HFP by using the suitable stirred temperature and time

To cite this article: A Salea *et al* 2019 *IOP Conf. Ser.: Mater. Sci. Eng.* **625** 012011

View the article online for updates and enhancements.

Recent citations

- Preparation and Storage Energy Density Base on Dielectric Properties of P(VDF-HFP)/PU/BNKT Thin Films
K Jehlaeh *et al*

The enhancement of high dielectric properties for pure PVDF-HFP by using the suitable stirred temperature and time

A Salea[1], K Jehlaeh[1] and C Putson[1,*]

[1] Materials physics laboratory, Physics department, Faculty of Science, Prince of Songkla University, Songkhla, 90112, Thailand

*Email: chatchai.p@psu.ac.th

Abstract. A novel light-weight electronic device from the dielectric polymer is so remarkable as the actuators, sensors, energy storage device and energy conversion. For this work, the thin film electroactive polymer is fabricated by casting technique which PVDF-HFP dissolve in N,N-dimethylformamide (DMF). The three stirred temperatures (30, 55 and 80 °C) and two stirred times (6 and 12 h) are completely considering. The highest polarization as the β phase is also considered for dielectric properties improvement. The FTIR, LCR and DSC equipment are used to measure the electroactive improvement. As a result, the 12 h stirred time with 30 °C stirred temperature is the best condition. The 0.25 g/ml concentration is also the suitable condition. The better dielectric properties are the requisite condition for a novel energy storage device in the future.

1. Introduction

The flexibility, light-weight, easy to process and high breakdown strength of dielectric polymer have to be the main reason to apply in such the novel applications as the energy storage, electrostriction, pyroelectric and electrocaloric [1, 2]. These advantages of the polymer are so interesting to improve dielectric properties as much as dielectric ceramic materials. Polyvinylidien fluoride-hexafluoropropylene (PVDF-HFP) is a semi-crystalline polymer which is one of high dielectric properties. The improvement of dielectric properties has to controllable PVDF-HFP chain structure to be the highest net-dipolemoment as called β phase. The β phases are -[CH_2-CF_2]- structure that arranged to the opposite site between two C-H and two C-F, which is bonding up and down perpendicular to carbon backbone causing to produce the highest net-dipolemoment per unit cell compared with another phases such as α, γ and δ [3, 4]. The stretching and poling techniques are able to response the β phases to enhance including dielectric properties [5]. The controllable PVDF-HFP structure is able to improve β phases according to 511, 837, 1234 and 1275 cm^{-1} vibrational peak in FTIR [6]. Several reported papers tried to improve dielectric properties by using composites powder for dispersion in the polymer matrix but they lack observed the suitable stirred temperature and stirred time especially in the pure PVDF-HFP polymer. The suitable stirred temperature and stirred time might able to create the higher β phase transformation causing to enlargeable dielectric properties.

2. Materials and method

Polyvinylidien fluoride-hexafluoropropylene (P(VDF-HFP) powder, purchased from Solvay Solexis, Belgium) is dissolved in 99% purity N,N-dimethylformamide (DMF, purchased from RCI Labscan Limited, Thailand). And it is then stirred 12 h in different temperatures (30, 55 and 80 °C) to be

homogeneous solution before cast on the smooth class plate. They are directly dried in the oven at 80 ℃ for 24 h to become 100 μm thin film as showed in **Figure 1 (a)**. Afterward, their electroactive β phase and dielectric properties are analysed by using FTIR technique and LCR meter in frequency from 1 to 10^5 Hz followed by using the equation (1) and (2), respectively. Moreover, it are suddenly confirmed the melting temperature by using DSC technique. In addition, the best condition is altered the stirred time to be 6 h (from 12 h). Finally, the best condition is observed the surface morphology by using SEM with EDX for observing the atomic distribution.

3. Results and discussion

3.1. The electroactive β phases transformation

Fourier Transform Infrared Spectra (FTIR), (Vertex70, Bruker, Germany), is scientific equipment that is able to classify PVDF-HFP structure. **Figure 1 (b-c)** represented to the electroactive β phase including with α and γ (figure 2 a). The transformation of β phases are confirmed in the growing β phase intensity by using Lambert-Beer law the equation (1) which is a ratio between α and β phase at the wavenumber of 767 and 837 cm^{-1} respectively.

$$F(\beta) = \frac{A_\beta}{\frac{K_\beta}{K_\alpha} A_\alpha + A_\beta} \tag{1}$$

Where, A_α is the absorbance at 767 cm^{-1} and A_β is the absorbance at 837 cm^{-1} and K_α (6.1 x 10^4 cm^2 mol^{-1}) and K_β (7.7 x 10^4 cm^2 mol^{-1}) are the absorption coefficients at respective wavenumber [7]. The absorbance of wavenumber around 830 - 840 cm^{-1} is able to obviously seem that the β phase decrease when they are increased the stirred temperature to 55 and 80 ℃, respectively. The highest β phase is showed at 30 ℃. The β phase is calculated and plotted in different stirred temperature as showed in figure 2 (b). The higher temperature might be the disturbing the β phase conformation to be another phases as α or γ.
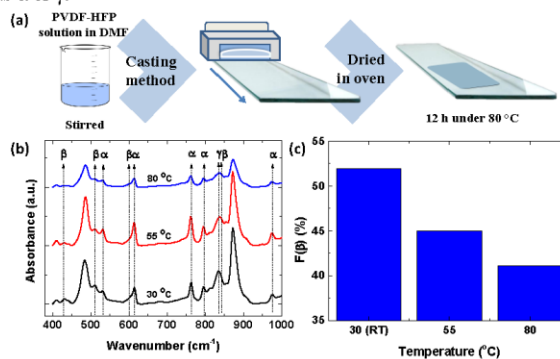

Figure 1 (a) film preparation by casting technique, (b) absorbance FTIR spectra (c) their absorbance β phase intensity of 30, 55 and 80 ℃ stirred temperatures in pure PVDF-HFP.

3.2. Dielectric properties and thermoanalytical analysis

The LCR meter (IM 3533 HIOKI) is dielectric measurement equipment to measure such dielectric properties as dielectric constant (ε_r) and dielectric loss (ε_r'') in various frequencies (1 - 10^5 Hz). The samples are applied 1 V ac voltage pass through the sample by two electrodes. And then they are measured surface charge (C, in F) and calculated to be ε_r as showed an Equation (2).

$$\varepsilon_r = Cd/\varepsilon_0 A \tag{2}$$

Where d is sample thickness (m), A is electrode area (m^2), and ε_0 is free space permittivity with value 8.853 x 10^{-12} F m^{-1}[8]. **Figure 2 (a-b)** showed the dielectric properties. The dielectric constant is decreased with increasing the frequency in any conditions as showed in figure 3 (a) which can be explained by Maxwell-Wagner-Sillars (MWS) interfacial polarization [9]. Moreover, as dielectric constant with different temperatures, the dielectric constant decreases when the temperature is increased because of the disturbing β phase from heat following FTIR result. In addition, the dielectric loss in figure 3 (b) is insignificantly different that the loss at the lowest frequency (1 Hz) produces unsteady transient because the lower frequency make easy to rearrange chain polarization or unsteady loss and it might fluctuate polarization.

Differential Scanning Calorimetry (DSC), Simultaneous Thermal Analyser, STA8000, Perkin Elmer, USA, is thermoanalytical technique to measure the absorbed heat energy of the sample from 30 °C (room temperature, RT) to 200 °C in the air atmosphere as showed **Figure 2 (c)**. The increasing stirred temperature is able to ship the melting temperature (T_m) referred to the changing of crystallinity to be lower temperature from 160.68 to 159.55 and 159.07 °C for 30, 55 and 80 °C, respectively. This result can also confirm the previous data that the hotter stirred temperature might able to destroy net polarization from the β phase to be another.

The stirred time of the best solution (RT) is decreased from 120 h to 6 h to find the minimum time for the suitable stirred time with measure dielectric properties as showed **Figure 2 (d-e)**. It can seem that the dielectric constant increase when the stirred time is increase from 6 to 12 h because it have time to rearrange and increase the β phase to be greater as well as their dielectric loss.
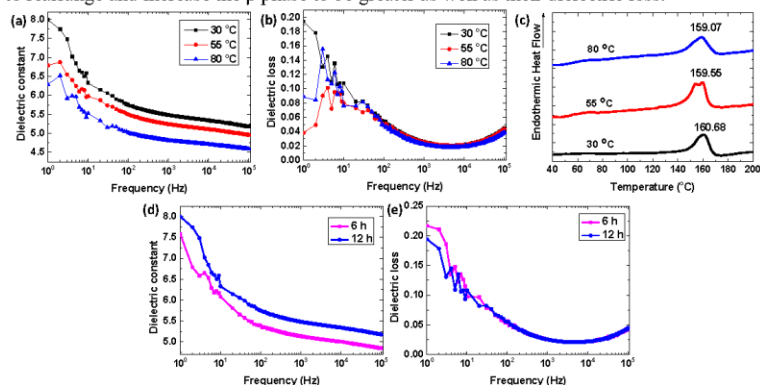

Figure 2 Dielectric constant (a), dielectric loss (b) and DSC-thermograph (c) of 30, 55 and 80 °C three stirred temperatures (d) dielectric constant and (f) dielectric loss of 6 and 12 h stirred times in pure PVDF-HFP

3.3. Surface morphology, atomic distribution and the thickness with various concentrations.
Scanning Electron Microscopy with Energy Dispersive X-ray spectroscopy (SEM-EDX), FEI, Quanta 400, SEM-Quanta, is electron microscope that not only produces the image by electron scattering but also detects several atomic elements which distribute on the sample surface as showed in **Figure 3 (a-d)**. The surface morphology of the sample is also slightly rough of porous which might come from the evaporated solvent as showed in figure 4(a). The carbon (C) and fluorine (F) atoms are detected for PVDF-HFP structure which distributed on that surface as showed in figure 4 (b-c). The structure of PVDF-HFP is shown in figure 4 (d) which related to the ratio of both two elements.

The PVDF-HFP with DMF is proportionated to 0.20, 0.25 and 0.30 g/ml as called concentration with measure thickness in various blade sizes (1.2, 1.4 and 1.6 mm) and figure out the relationship as showed in **Figure 3 (e)**. It can seem that the thickness size of samples is increased with

increasing concentration and blade sized because DMF are evaporated due to heat. The 0.25 g/ml concentration, 1.2 blade size and 100 μm thickness size is suitable for this work due to dissolvable and savable amount of DMF.
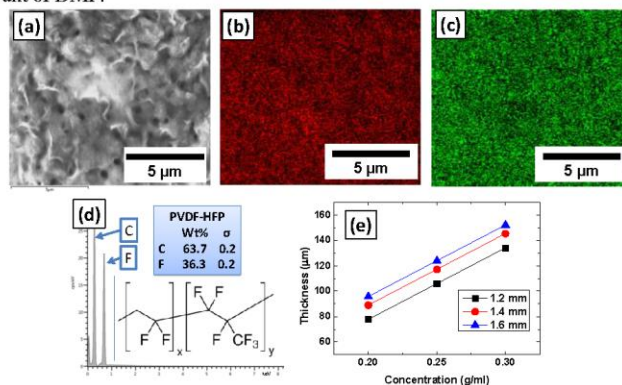

Figure 3 Surface morphology on pure PVDF-HFP; SEM image (a), with EDX signals of C (b) and F (c) elements, the percent atomic weight with PVDF-HFP structure, (d) relationship between thickness sizes with three concentrations in different blade sizes.

4. Conclusion
The 0.25 g/ml of PVDF-HFP in DMF is the suitable concentration for this work. It is cast on the smooth glass to adjust the thickness for characterization. The highest polarization as β phase is a critical dielectric properties term. The three stirred temperatures and two stirred time are considered. FTIR, Dielectric properties including with DSC are analysed. The best condition in this work is 12 h stirred time and 30 °C stirred temperature. The highest dielectric properties are applicable to be energy storage devices applications including a novel light-weight battery.

References
[1]   Lallart M, Thetpraphi K and Capsal J-F. 2018 *Phys. Lett. A* **382** 449-54
[2]   Yang L, Qian XS, Koo C, Hou Y, Zhang T, Zhou Y, Lin MR, Qiu JH and Zhang QM. 2016 *Nano Energy* **22** 461-7
[3]   Chen S, Yao K, Tay FEH and Liow CL. 2007 *J. Appl. Phys.* **102** 104108
[4]   Martins P, Costa CM, Benelmekki M, Botelho G and Lanceros-Mendez S. 2012 *CrystEngComm* **14** 2807-11
[5]   Kepler RG and Anderson RA. 1978 *J. Appl. Phys.* **49** 1232-5
[6]   Parangusan H, Ponnamma D and Al-Maadeed MAA. 2018 *Sci. Rep.* **8** 754
[7]   Thakur P, Kool A, Bagchi B, Das S and Nandy P. 2015 *Phys. Chem. Chem. Phys.* **17** 1368-78
[8]   Zhong K and Li B 2017 *Polymer Nanocomposites for Dielectrics* (Singapore: Pan Stanford Publishing Pte. Ltd) p 208
[9]   Tsangaris GM, Psarras GC and Kouloumbi N. 1998 *J. Mater. Sci.* **33** 2027-37

APPENDIX D

Paper V [Conference published]; "Enhanced interfacial dielectric polarization in PVDF-HFP copolymer with treating PPy by using silane coupling agent"

PAPER • OPEN ACCESS

Enhanced interfacial dielectric polarization in PVDF-HFP copolymer with treating PPy by using silane coupling agent

View the article online for updates and enhancements.

Enhanced interfacial dielectric polarization in PVDF-HFP copolymer with treating PPy by using silane coupling agent

A Salea[1], R Saputra[1,2] and C Putson[1],*

[1] Materials physics laboratory, Physics department, Faculty of Science, Prince of Songkla University, Songkhla, 90112, Thailand
[2] Physics Department, Faculty of Science and Technology, UIN Sunan Kalijaga Marsda Adisucipto street, No 1, Yogyakarta, 55281, Indonesia

*Corresponding author: email: chatchai.p@psu.ac.th

Abstract. Dielectric materials are polar materials for energy storage applications such as capacitors, transformer, and other electrical devices. The great dielectric properties generally depend on easily switchable polarization and higher-order structure in a material. Filler composite in the flexible dielectric polymer is then considered to rearrange polymer chain. However, the filler becomes agglomeration easily at high loading content in polymer, resulting in high energy loss and low electrical breakdown. This work presents the treated Polypyrrole (PPy) filler by 3-Aminopropyltriethoxysilane for avoiding agglomeration in PVDF-HFP thin film. These 30 μm PVDF-HFP film thickness is fabricated by tape casting method with *N,N*-dimethylformamide (DMF) solvent. The distributions of PPy filler on PVDF-HFP are observed by SEM image. Dielectric constant, dielectric loss, and conductivity are analyzed. As a result, the maximum silane content was found on 1 wt% for 1 wt% PPy/PVDF-HFP to maximized dielectric constant and reduce dielectric loss and conductivity. The conductive of PPy filler was lowered by covering with electrical insulating silane, resulting in decreased dielectric loss and conductivity. Then, polymer chain with silane bonding easily polarized under the electric field, resulting in an intensification of dielectric constant around 2.5 times compared with non-silane. Afterward, this dielectric constant clearly decreased when it reached to exceeded silane content as 5-20 wt%. Treated PPy with the suitable silane content in PVDF-HFP performs good dielectric properties for advanced energy storage in this work.

1. Introduction

A dielectric polymer is a flexible polar material that produces a large net dipole moment under an electric field. High dielectric properties, high chemical resistance, and low cost are key features to consider for dielectric polymer matrix in this field such as Polyvinylidene fluoride-hexafluoropropylene (P(VDF-HFP)). Conductive filler in dielectric polymer has been one of the other techniques to improve these properties. However, the large amount of this filler easily agglomerates, resulting in failure from energy loss heat. For example, Putson and colleagues found that dielectric loss of PVDF-HFP was increased with conductive filler [1]. This problem can be solved by using a Silane coupling agent to connect between filler and polymer on PVDF composite [2, 3]. An electrical insulator of Silane covered conductive fillers, bonding with polymer chain. The specific polymer has a specific silane along with filler content [4]. One of the high conductive fillers as Polypyrrole (PPy) is interesting to improve the dielectric properties of PVDF-HFP. There are no prior works to develop dielectric properties on PVDF-

HFP by using a silane coupling agent on PPy filler. In this work, the 3-Aminopropyltriethoxysilane coupling agent is considered for preventing agglomeration and aiming to achieve better dielectric performance.

2. Experimental

Composite film preparation, the polypyrrole (PPy) as 0.25, 0.50, 0.75, and 1.00 wt% is blended and stirred with Polyvinylidene fluoride-hexafluoropropylene (P(VDF-HFP)) (purchased from Solvay Solexis, Belgium) in 99% purity N,N-dimethylformamide (DMF) (purchased from RCI Labscan Limited, Thailand) before cast on the smooth glass by tape casting method. The suitable PPy content in PVDF-HFP is observed.

For the silane coupling agent process, the PPy is treated by Hydrogen peroxide 30% (H_2O_2) to get OH group on the surface by sonicating 30 min (250W) and drying 12 h (100°C). Afterward, the 3-Aminopropyltriethoxysilane (silane) is hydrolyzed by DI water and Ethanol (50 ml: 50 ml) for 20 min to open the functional group. The silane contents are considered as 1, 5, 10, and 20 % of PPy filler. These solutions are completely stirred with the suitable PPy content for 24 h. Resulting, treated PPy is obtained by removing the exceeding silane by DI water (5 times centrifuges). The treated PPy is completely dried 100°C (12 h). The treated PPy powder with several silane content is finally prepared to fabricate composite films as mentioned in the previous step.

For characterization, morphological PPy/PVDF-HFP image is observed by using the SEM (FEI Quanta 400, USA). Dielectric loss (ε_r'') and capacitance (C, in F) are recorded by applying 1 V ac voltage to the sample by two electrodes of LCR meter (IM 3533, HIOKI, Japan) in frequency from 1 to 10_5 Hz. Moreover, dielectric constant (ε_r) and conductivity (σ_{ac}, S/m) are calculated by using the equation (1) and (2), respectively. Here d is sample thickness (m), A is the area of the electrode (m_2), and ε_0 is free space permittivity (8.853 x 10_{-12} F m_{-1}), f is frequency (Hz).

$$\varepsilon_r = Cd/\varepsilon_0 A \qquad (1)$$
$$\sigma_{ac} = 2\pi f \varepsilon_0 \varepsilon_r \varepsilon_r'' \qquad (2)$$

3. Results and discussion

3.1. The PPy filler contents on PVDF-HFP transformation

Figure 1 shows the relationship between dielectric properties and frequency. The 0, 0.25, 0.5, 0.75, and 1 %PPy in PVDF-HFP is measured (Figure 1 (a)). The low frequency (10-10_3 Hz) provides the largest dielectric constant (ε_r) because interfacial polarization is mainly active and easily switchable explaining by the Maxwell-Wagner-Sillars (MWS) theory [5]. In PPy content, ε_r is increased with PPy content. For example, 0.75%PPy immediately increase ε_r from 5 (pure PVDF-HFP) to 76 at 10-10_3 Hz. The ε_r of 1 wt% PPy at low frequency is clearly disturbed by conductive filler loading to be unstable value, resulting in larger conductivity (σ_{ac}) and dielectric loss (ε_r'') as in Figure 1 (b) and (c), respectively. For an example of inthe crease σ_{ac} includes pure PVDF-HFP (10-10 S/m) to 1 wt% PPy (10-4 S/m) around 10_6 times. In addition, ε_r'' are clearly increased with PPy content. The fixed dipole with conductive filler is easily polarized under electric field, resulting in larger ε_r'' and σ_{ac} when adding conductive filler, as prior theory [5].
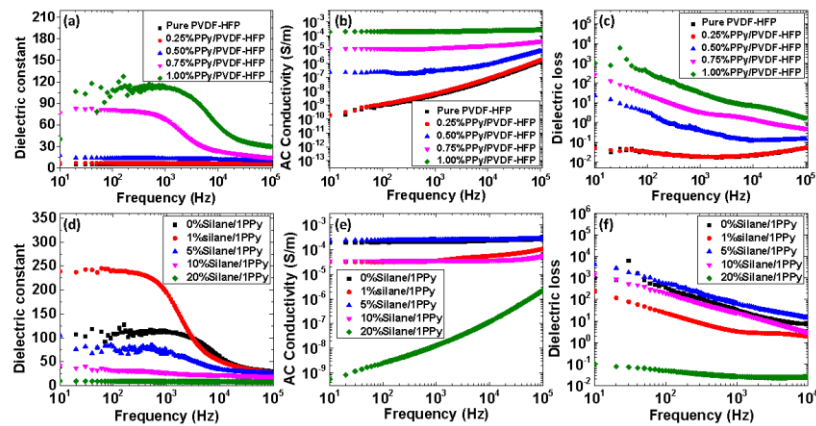
Figure 1 Dielectric constant (a), conductivity (b), and dielectric loss (c), for PPy content in PVDF-HFP. Dielectric constant (d), conductivity (e), and dielectric loss (f), for and for silane content on 1PPy/PVDF-HFP.

3.2. Silane effect on 1%PPy/PVDF-HFP dielectric properties

To enhance interfacial polarization, silane contents are considered. The 1, 5, 10, and 20% Silane on 1%PPy/PVDF-HFP are continuously prepared. As Figure 1 (d), dielectric constant at 10-10$_3$ Hz sharply increases from 111 (0%Silane/1PPy) to around 222 (1%Silane/1PPy), which seem 2 times differently. Dielectric constant, then, suddenly drops to 75 (5%Silane/1PPy), which is lower than the 0%Silane/1PPy. Afterward, there is a gradual decrease to 8.8 (20%Silane/1PPy) that is the lowest value. Surprisingly, this 1%Silane/1PPy can decrease their conductivity from 2.06×10^{-4} S/m of 0%Silane/1PPy to be 3.30×10^{-5} S/m. Afterward, the conductivity slightly increases at 5%Silane/1PPy before sharply decreased to 7.32×10^{-9} S/m at 20%Silane/1PPy. The trend of this conductivity is similar behavior with dielectric loss, matching with a prior study [2].

The larger insulating silane that covers on PPy has the ability to reduce PVDF-HFP conductivity as well as dielectric loss. The silane head (Si-Si with OH group) is bonded with the OH group on PPy filler surface, and the silane tail (Amino group) is completely connected with the PVDF-HFP polymer chain. It seems that the 1%silane on PPy filler is the suitable silane content that performs a good connector between polymer chain and PPy filler, resulting in the easiest switchable polarization and the largest dielectric properties. Surprisingly, this silane has ability to reduce conductivity as well as dielectric loss. Compared with thicker silane content, the stronger chemical bonding in thinner silane content is likely easier in switchable polarization, resulting in great dielectric properties [2].

3.3. Morphological PPy distribution and dispersion on treated PPy

Scanning Electron Microscopy (SEM), Hitachi TM 3030plus, is observed in the morphology on the sample surface. The PPy filler distribution is distinguishable between treated and untreated silane on 1%PPy in PVDF-HFP as showed in **Figure 2**. There are several big porosities on this sample by the DMF evaporation after drying. The PPy is noticeable as the small black dot. These dots have more noticeable and completely separated two phases on untreated PPy by silane (Figure 2 (a)). As a result, it seems a lot of PPy particles dispersing on PVDF-HFP. In contrast, when the treated PPy is connected to PVDF-HFP by silane, the separation between two phases is blurred. As a result, it seems less of PPy particles dispersing on PVDF-HFP.
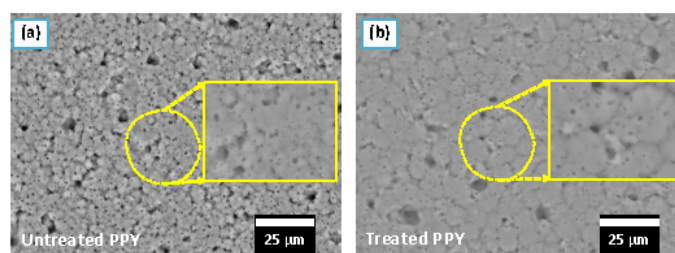
Figure 2 SEM images of untreated (a) and treated (b) PPy by a silane coupling agent.

4. Conclusion

The 0.25, 0.50, 0.75, and 1.00%PPy in PVDF-HFP polymer composites were fabricated by tape casting method. The dielectric constant, conductivity, and dielectric loss were increased with PPy content. Among them, the best dielectric constant was shown by 1.00%PPy in PVDF-HFP. Nevertheless, that condition also possessed the highest conductivity and dielectric loss. To reduce those two conductivity and dielectric loss, the 3-Aminopropyltriethoxysilane coupling agent was added into these composites. The silane content was varied of 1, 5, 10, and 20%. As a result, 1 % silane improved dielectric constant, and reduced both conductivity and dielectric losss. On the other hand, adding silane more than 1% could cover the filler to be thicker. As a consequence, the dipole moment is hard to polarize following the external electric field, resulting in decrease dielectric constant, conductivity along with dielectric loss. This silane content in this work has a potential role to increase dielectric properties for the advanced capacitor in the future.

5. References

[1.]   Salea, A., et al., *The microstructure of negative electrocaloric Polyvinylidene fluoride-hexafluoropropylene copolymer on graphene loading for eco-friendly cooling technology.* Journal of Cleaner Production, 2020. **251**: p. 119730.

[2.]   Zhang, Q., et al., *Enhanced dielectric tunability of Ba0.6Sr0.4TiO3/Poly(vinylidene fluoride) composites via interface modification by silane coupling agent.* Composites Science and Technology, 2016. **129**: p. 93-100.

[3.]   Tiwari, V.K., et al., *Thin and surface adhesive ferroelectric poly(vinylidene fluoride) films with β phase-inducing amino modified porous silica nanofillers.* Journal of Polymer Science Part B: Polymer Physics, 2016. **54**(23): p. 2401-2411.

[4.]   Xie, L., et al., *Core-shell Structured Hyperbranched Aromatic Polyamide/BaTiO3 Hybrid Filler for Poly(vinylidene fluoride-trifluoroethylene-chlorofluoroethylene) Nanocomposites with the Dielectric Constant Comparable to That of Percolative Composites.* ACS Applied Materials & Interfaces, 2013. **5**(5): p. 1747-1756.

[5.]   Tsangaris, G.M., G.C. Psarras, and N. Kouloumbi, *Electric modulus and interfacial polarization in composite polymeric systems.* Journal of Materials Science, 1998. **33**(8): p. 2027-2037.

Acknowledgment

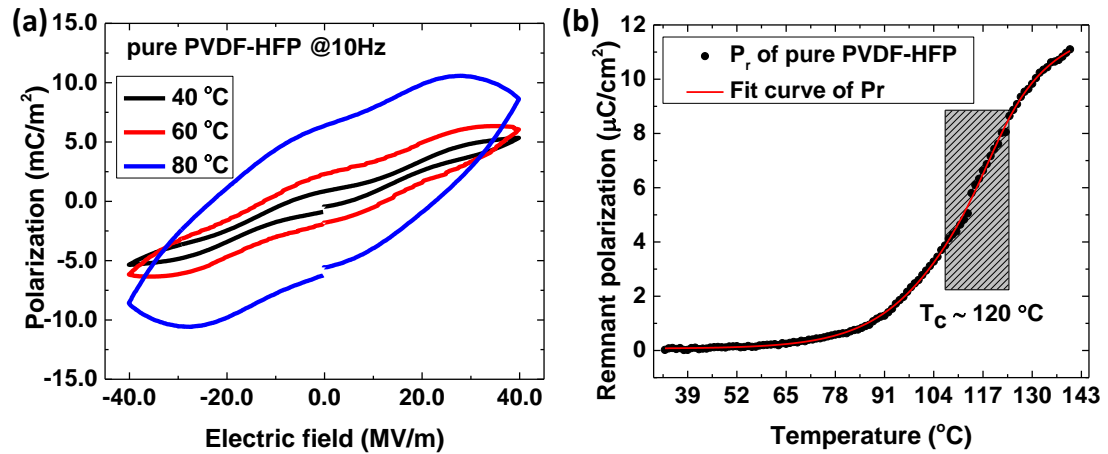**APPENDIX E**

Calculation of ∆T by Maxwell' relation

Figure S1 (a) P-E loops of pure PVDF-HFP ferroelectric in various three temperatures, (b) with Remnant polarization in various temperatures.

The loop at 40 °C was noticed as an antiferroelectric phase. The loop with P_r was then gradually larger with temperature from 0.091 µC/cm^2 at 40 °C to 0.639 µC/cm^2 at 80 °C, especially rapidly increase near T_c (6.804 µC/cm^2 at 118 °C) followed by a slight rise above T_c (11.051 µC/cm^2 at 140 °C) as figure S1 (b). The Pr data were plotted point to point. Afterward, they were fitted with mathematical model of BiDoseResp function to get more data for precisely calculating in Equation (24). The fitting data of Pr with small temperature interval was calculated as $\frac{\partial P}{\partial T}$ is the differentiate of ∂P and ∂T at each temperature (T) with 40MV/m of dE, 1,600 J/kg/°C of C_E, and 1.8 g/cm^3 of ρ, following Equation (24).

VITAE

Name   Mr. Ahamad Salea

Student ID   6010230026

Educational Attainment

Degree	Name of Institution	Year of Graduation
Master of Science (Materials Science and Engineering)	Mahidol University	2017
Bachelor of Science (Physics) (Second class honors)	Prince of Songkla University	2014

Scholarship Awards during Enrolment and Award

Science Achievement Scholarship of Thailand (SAST)

Best Presentation Award ICMENS 2019, March $26^{th} – 28^{th}$, Japan.

List of ISI Publications

Salea, A. Chaipo, S. Permana, A. A. Jehlaeh, K. and Putson, C. (2020) The microstructure of negative electrocaloric Polyvinylidene fluoride-hexafluoropropylene copolymer on graphene loading for eco-friendly cooling technology. Journal of Cleaner Production, 251, 119730.

Salea, A. Jehlaeh, K. Zhang, J. and Putson, C. (2020) Effect of rare-earths Er and Dy on the Curie temperature and interfacial charge mobility of electrocaloric PVDF-HFP composites. Journal of Materials Science: Materials in Electronics (revised).

Salea, A. Prathumwan, R. Junpha, J. and Subannajui, K. (2017) Metal Oxide Semiconductor 3D printing: Preparation of Copper (II) Oxide by Fused Deposition Modelling for Multi-functional Semiconducting Applications. Journal of Materials Chemistry C, 5, 4614-20.